STUDY ON THE INTERACTION BETWEEN PROTEINS AND NEW FLUORESCENT PROBES DERIVED FROM SYNTHETIC AND NATURAL PRODUCTS

14 พ.ย. 2562

DOCTORAL THESIS

BY

SUDARAT YENJAI

Presented in Partial Fulfillment of the Requirements for the

Doctor of Philosophy degree in Applied Chemistry

at Srinakharinwirot University

June 2018

Copyright of Srinakharinwirot University

A 437018

STUDY ON THE INTERACTION BETWEEN PROTEINS AND NEW FLUORESCENT PROBES DERIVED FROM SYNTHETIC AND NATURAL PRODUCTS

AN ABSTRACT
BY
SUDARAT YENJAI

Presented in Partial Fulfillment of the Requirements for the
Doctor of Philosophy degree in Applied Chemistry
at Srinakharinwirot University
June 2018

Sudarat Yenjai. (2018). *Study on the Interaction between Proteins and New Fluorescent Probes Derived from Synthetic and Natural Products.* Doctoral Thesis. Ph.D. (Applied Chemistry). Bangkok: Graduate School, Srinakharinwirot University. Advisor Committee: Assoc. Prof. Dr. Apinya Chaivisuthangkura, Assoc. Prof. Dr. Siritron Samosorn.

The interactions of a series of new fluorescent probes (PMA-1A, PMA-2A and PMA-3A) and natural products (berberine and piperine) were studied with proteins by spectroscopic methods, photocleavage and docking description. In this study, avidin and lysozyme were successfully cleaved with high specificity and efficiency after irradiation of the mixture solution of protein with the photochemical reagents (PMA-1A, PMA-2A, PMA-3A and berberine), in the presence of $Co(NH_3)_6Cl_3$ (CoHA) as an electron acceptor. However, the cleavage was not observed with piperine. *N*-terminal sequencing of the peptide fragments indicated a major cleavage site of avidin between Thr 77 and Val 78, and Trp108 and Val109 of lysozyme. Strong binding interaction was observed from binding studies using spectroscopic methods. Upon binding to the protein, spectral changes, such as hyperchromism and hypochromism were observed. The binding of a series of new fluorescent probes to both proteins (avidin and lysozyme) resulted in observable hypochromism, while binding of berberine to both proteins resulted in observable hyperchromism of the absorption spectrum. Moreover, bathochromic shift of the absorption peak positions of PMA-3A were also observed with isosbestic points at 328, 333, and 344 nm. The binding constants (K_b) in the range of 10^5 M^{-1} were obtained for all photochemical reagents with avidin and lysozyme, indicating high binding affinity. The fluorescence quenching of a series of new fluorescent probes, in the absence and presence of the protein, by an electron acceptor ($Co(NH_3)_6Cl_3$) showed no significant changes in the K_{sv} values (Stern-Volmer quenching constant), indicating that the binding sites of the probes were near the hydrophilic sites on both proteins, which made the fluorophore accessible for CoHA to quench. Molecular docking study indicated that all photochemical reagents were bound with polar amino acid residues and nonpolar amino acid residues of both proteins by hydrogen bonding interaction with donor-acceptor within the distance of less than 5 Å in the minimum of binding free energy. Molecular docking results have supported the overall experimental results from photocleavage and spectroscopic studies.

The thesis titled

"Study on the Interaction between Proteins and New Fluorescent Probes Derived from Synthetic and Natural Products"

by

Sudarat Yenjai

has been approved by the Graduate School as partial fulfillment of the requirements for the Doctor of Philosophy degree in Applied Chemistry of Srinakharinwirot University.

C Ekpanyaskul ..... Dean of Graduate School

(Asst. Prof. Chatchai Ekpanyaskul, MD.)

Month 16 Date July Year 2019

Thesis Committee

..... Major-advisor

(Assoc. Prof. Dr. Apinya Chaivisuthangkura)

S. Samosorn ..... Co-advisor

(Assoc. Prof. Dr. Siritron Samosorn)

Oral Defense Committee

L. Lawtrakul ..... Chair

(Assoc. Prof. Dr. Luckhana Lawtrakul)

..... Committee

(Assoc. Prof. Dr. Apinya Chaivisuthangkura)

S. Samosorn ..... Committee

(Assoc. Prof. Dr. Siritron Samosorn)

..... Committee

(Assoc. Prof. Dr. Teerayuth Liwporncharoenvong)

In this research received financial support

from the Thailand Research Fund through the Royal Golden Jubilee Ph.D. Program (Grant No. PHD/0266/2553)

ACKNOWLEDGEMENT

The author is deeply grateful to thank Associate Professor Dr. Apinya Chaivisuthangkura, major-advisor, for her invaluable advice, supervision, her arranging a Ph.D. grant and her tolerant proofreading towards the completion of this study. The author would especially like to thank Co-advisor, Associate Professor Dr. Siritron Samosorn, the Head of Chemistry Department at Srinakharinwirot University, for her precious guidance and supporting for research in her laboratory.

Furthermore, the author sincerely thanks the financial support from the Thailand Research Fund through the Royal Golden Jubilee Ph.D. Program (Grant No. PHD/0266/2553) for a Ph.D. grant. According to the cooperation between Associate Professor Dr. Apinya Chaivisuthangkura, Srinakharinwirot University, and Professor Dr. Challa Vijaya Kumar, University of Connecticut, under the Royal Golden Jubilee Ph.D. Program, the author would like to extend our sincere thanks to Professor Dr. Challa Vijaya Kumar and his team for their invaluable guidance and supervision throughout half year research in his laboratory at the University of Connecticut, USA.

Special thanks to Associate Professor Dr. Teerayuth Liwporncharoenvong, Oral Defense Committee, and Assistant Professor Dr. Mayuso Kuno, poprosal Committee, for sacrificing their time on this study. Especially, Chair of Oral Defense Committee, Assoc. Prof. Dr. Luckhana Lawtrakul from Sirindhorn International Institute of Technology, Thammasat University, for assistance, valuable discussion and encouragement. Moreover, the author is greatly thankful to all of my teachers from the Chemistry Department, Srinakharinwirot University, for their invaluable educating to learner.

Additionally, the author would like to thank SWU staffs at faculty of Science for supporting use equipments in this study, and the Graduate School, Srinakharinwirot University, for supporting this thesis book making.

Big thanks to Yenjai family and Sirisawat family for supporting every feeling, inspiration and constant encouragement throughout the study. Unforgettably, the friends in Thailand and USA, who have made this work possible with happy moments.

Lastly, the author would like to thank those whose names are not mentioned here but have greatly inspired and encouraged until this study becomes to an excellent thesis end.

Sudarat Yenjai

TABLE OF CONTENTS

Chapter		Page
1	INTRODUCTION	
	Background	1
	Objectives of the study	2
	Significance of the study	3
	Scope of the study	3
2	THEORY AND RELATED RESEARCH	
	Amino acids	4
	Proteins	7
	Electrophoresis	9
	Amino acid sequencing analysis	17
	Spectroscopic methods	18
	UV-Vis spectroscopy	18
	Fluorescence spectroscopy	24
	Computational chemistry	27
	Related research	29
3	EXPERIMETAL	
	Equipments and chemical reagents	40
	Methods	42
	Synthesis of photochemical reagent	42
	Protein photocleavage	42
	Sodium dodecyl sulfate-polyacrylamide gel electrophoresis	43
	Western blot (protein transfer)	45
	Absorption titration and fluorescence titration	47
	Fluorescence quenching studies	47
	Docking studies	47

TABLE OF CONTENTS (continued)

Chapter		Page
4	RESULTS AND DISCUSSION	
	Photochemical reagents	48
	Synthesis and characterization of new photochemical reagents	48
	PMA-1A	48
	PMA-2A	51
	PMA-3A	53
	Protein photocleavage by new photochemical reagents	55
	Protein transfer by western blot for amino acid sequencing analysis	66
	The interactions of new photochemical reagents with proteins	68
	binding interaction	68
	fluorescence quenching studies	72
	Binding mechanism of new photochemical reagents with the proteins	74
	Natural products	83
	Protein photocleavage by natural products	83
	Protein transfer by western blot for amino acid sequencing analysis	86
	Binding interactions of natural products with proteins	87
	Binding mechanism of natural products with the proteins	90
5	CONCLUSION AND RECOMMENDATION	
	Photochemical reagents	98
	Natural products	101
APPENDIX		104
REFERENCES		145
CURRICULUM VITAE		150

LIST OF TABLES

Table		Page
1	Amino acid requirements in humans	7
2	The appropriate concentrations of polyacrylamide gel for separating the proteins	12
3	Compositions of the stacking gel and running gel in SDS-PAGE	16
4	Relationship between wavelength region and colors	20
5	Absorbance and fluorescence of the aromatic amino acids	23
6	Conditions of photocleavage reaction	43
7	Variation of irradiating time for photocleavage reaction	43
8	The successful of protein photocleavage reaction	55
9	The maximum photoproduct yields obtained from SDS-PAGE	59
10	The distances of standard proteins obtained from SDS-PAGE	60
11	The maximum photoproduct yields obtained from SDS-PAGE	65
12	The distances of standard proteins for calculation molecular weight of photoproducts obtained from lysozyme cleavage by photochemical reagents.	65
13	Binding constants and other binding properties of probe/avidin	69
14	Binding constant and other binding properties of probe/lysozyme	70
15	Stern-Volmer quenching constants (Ksv) of PMA-1A, PMA-2A and PMA-3A	72
16	Binding constant of probe/avidin from absorption titration studies and binding free energy from docking studies	75
17	The distances between the new photochemical reagents and amino acid residues at cleavage site of avidin	79
18	The successful of protein photocleavage reaction	83
19	The distances of standard proteins for calculation of molecular weight of photoproducts obtained from avidin cleavage by berberine	85
20	Binding constants and other binding properties of berberine/protein and berberine derivative/protein	90
21	Binding constant of berberine/avidin and its derivatives/avidin from absorption titration studies and binding free energy from docking studies	90

LIST OF TABLES (continued)

Table		Page
22	Binding constant of berberine/lysozyme and its derivatives/lysozyme from absorption titration studies and binding free energy from docking studies.....	94
23	Photocleavage sites of avidin.....	98
24	Binding constant (M-1) from absorption titration studies, Gibbs free energy from calculation and binding free energy (kcal/mol) from docking studies of probe/protein.....	100

LIST OF FIGURES

Figure		Page
1	Basic structure of Amino acid in un-ionized form	4
2	Amino acid ionization state as a function of pH	5
3	The twenty kinds of amino acid different side chains	6
4	D-form and L-form of amino acid	6
5	Peptide bond of amino acid	8
6	The 4 levels of protein structure	9
7	The movement of ion compounds to the electrode	10
8	The structure of acrylamide, *N,N'*-methylenebisacrylamide, TEMED	11
9	Polymerization reaction of polyacrylamide gel	11
10	(a) The chemical structure of sodium dodecyl sulfate (SDS), which both polar and non-polar groups. (b) The SDS molecules coat the protein with negative charges	13
11	The structures of 2-mercaptoethanol and dithiothreitol	13
12	The structures of tricine and glycine	14
13	(a) Tricine-SDS-PAGE and (b) Glycine-SDS-PAGE	14
14	Discontinuous system of SDS-PAGE	15
15	The movement of protein molecules through the porous gel	15
16	A linear standard curve	17
17	Edman degradation steps	18
18	Electric field and magnetic field	19
19	Schematic diagram of electromagnetic spectrum	20
20	Electronic transition	21
21	UV-spectra of tryptophan, tyrosine and phenylalanine	22
22	Absorption spectra of poly-L-lysine in an α-helix, β-sheet and random coil	23
23	Absorbance and Intensity shifts	24
24	Dynamic quenching and static quenching	26
25	Stern–Volmer plot	27
26	Schematic illustration of lock-and-key	28
27	Comparison of docking application and reverse docking application	28
28	The structure of anthracyl derivatives	29

LIST OF FIGURES (continued)

Figure		Page
29	The structure of 4(1-pyrenyl) butylamine chloride (PBAC).....	29
30	The structure of Py-L-Phe.....	30
31	Binding of reagents to globular proteins.....	30
32	The structure of Py-$(Gly)_n$-Phe (n = 0, 1, 2).....	31
33	The possible mechanisms of protein cleavage.....	32
34	The structure of Py-biotin.....	32
35	The structures of 1-pyrenebutyric acid and 1-pyrenemethylamine.....	33
36	The structure of succinic acid.....	33
37	Applications of succinic as a precursor of many industrially chemicals.....	34
38	The structure of PMA-succinic acid.....	34
39	The structure of PMA-1A, PMA-2A and PMA-3A.....	35
40	The structure of berberine.....	35
41	Effect of berberine chloride (30 μM) to the activity of telomerase.....	36
42	The activity of Plasmodium falciparum telomerase was inhibited by berberine.	37
43	The structure of piperine.....	37
44	Piperine (5–200 μM) inhibits of (a) LNCaP (b) PC-3 (c) 22RV1 (d) DU-145 in prostate cancer cells for 24 h. (blue line), 48 h. (red line) and 72 h. (green line).....	38
45	Western blotting analysis, PARP-1 of LNCaP and DU-145 in prostate cancer cells were cleaved by concentration of piperine 60 μM and 160 μM respectively for 24 h.....	39
46	The effects of piperine on cell proliferation in SKBR3 breast cancer cells at various concentration of piperine (0-50 μM) in a time-dependent manner.	39
47	Mini Trans-Blot Electrophoretic Transfer Cell.....	46
48	Characterization of PMA-1A by ^1H NMR.....	49

LIST OF FIGURES (continued)

Figure Page

49 (a) Absorption spectra of PMA-1A (10 μM) at maximum wavelength (342 nm). (b) The linear regression equation and linear dependent coefficient (R^2) of 2-20 μM PMA-1A having peak at 342 nm. (c) Fluorescence spectra of PMA-1A (0.5 μM) with excitation wavelength at 342 nm. All data are from the average of three experiments..... 50

50 Characterization of PMA-2A by ^1H NMR..... 51

51 (a) Absorption spectra of PMA-2A (10 μM) at maximum wavelength (342 nm). (b) The linear regression equation and linear dependent coefficient (R^2) of 2-20 μM PMA-2A having peak at 342 nm. (c) Fluorescence spectra of PMA-2A (0.5 μM) with excitation wavelength at 342 nm. All data are from the average of three experiments..... 52

52 Characterization of PMA-3A by ^1H NMR..... 53

53 (a) Absorption spectra of PMA-3A (10 μM) at maximum wavelength (342 nm). (b) The linear regression equation and linear dependent coefficient (R^2) of 2-20 μM PMA-3A having peak at 342 nm. (c) Fluorescence spectra of PMA-3A (0.5 μM) with excitation wavelength at 342 nm. All data are from the average of three experiments..... 54

54 Photocleavage of avidin obtained from the reaction with PMA-1A..... 56

55 Photocleavage of avidin obtained from the reaction with PMA-2A..... 56

56 Photocleavage of avidin obtained from the reaction with PMA-3A..... 57

57 SDS-PAGE of photoproducts obtained from the reaction of avidin with the photochemical reagents, (a) PMA-1A, (b) PMA-2A and (c) PMA-3A..... 58

58 Photoproduct yields obtained from the reaction of photocleavage of avidin with photochemical reagents, (a) PMA-1A, (b) PMA2A and (c) PMA-3A. 59

59 A standard curve of molecular weight markers for calculation of molecular weights of unknown protein the cleaved fragments..... 60

60 Photocleavage of lysozyme obtained from the reaction with PMA-1A..... 61

61 Photocleavage of lysozyme obtained from the reaction with PMA-2A..... 61

62 Photocleavage of lysozyme obtained from the reaction with PMA-3A..... 62

LIST OF FIGURES (continued)

Figure		Page
63	SDS-PAGE of photoproducts obtained from the reaction of lysozyme with the photochemical reagents, (a) PMA-1A, (b) PMA-2A and (c) PMA-3A.....	63
64	The product yields of photocleavage of lysozyme from the reaction with photochemical reagents, (a) PMA-1A, (b) PMA2A and (c) PMA-3A.....	64
65	A standard curve of molecular weight markers for calculation of molecular weights of the cleaved fragments.....	66
66	The major and minor cleavage sites of avidin from the reaction of PMA-1A (a), PMA-2A (b) and PMA-3A (c).....	67
67	The cleavage sites of lysozyme from the reaction with three photochemical reagents.	
68	Proposed mechanism of protein photocleavage by photochemical reagent.....	68
69	Absorption spectra of PMA-1A (10 μM) in the absence (blue) and presence (red) of avidin (0-20 μM).....	69
70	Absorption spectra of PMA-2A (10 μM) in the absence (blue) and presence (red) of avidin (0-20 μM).....	69
71	Absorption spectra of PMA-3A (10 μM) in the absence (blue) and presence (red) of avidin (0-20 μM).....	70
72	Absorption spectra of PMA-1A (10 μM) in the absence (blue) and presence (red) of lysozyme (0-20 μM).....	70
73	Absorption spectra of PMA-2A (10 μM) in the absence (blue) and presence (red) of lysozyme (0-20 μM).....	71
74	Absorption spectra of PMA-3A (10 μM) in the absence (blue) and presence (red) of lysozyme (0-20 μM).....	71
75	The Stern–Volmer plots of new photochemical reagents (0.5 μM) by titration of CoHA (0–1.0 mM), in the absence of protein (○), in the presence of avidin (10 μM) (○) and in the presence of lysozyme (10 μM) (○), the fluorescence quenching data of PMA-1A (a), PMA-2A (b) and PMA-3A (c).....	73
76	The structure of (a) anionic PMA-1A, (b) anionic PMA-2A, (c) anionic PMA-3A.....	74

LIST OF FIGURES (continued)

Figure Page

77 (a) The binding location of PMA-1A on the part of hydrophilic site and hydrophobic site of avidin. (b) The amino acid residues of avidin surrounding PMA-1A within the distance of less than 5 Å. (c) Three hydrogen bonding interactions of anionic PMA-1A with three amino acid residues of avidin (dotted green lines)..... 76

78 (a) The binding location of PMA-2A on the part of hydrophilic site and hydrophobic site of avidin. (b) The amino acid residues of avidin surrounding PMA-2A within the distance of less than 5 Å. (c) Five hydrogen bonding interactions of anionic PMA-2A with five amino acid residues of avidin (dotted green lines)..... 77

79 (a) The binding location of PMA-3A on the part of hydrophilic site and hydrophobic site of avidin. (b) The amino acid residues of avidin surrounding PMA-3A within the distance of less than 5 Å. (c) Three hydrogen bonding interactions of anionic PMA-3A with three amino acid residues of avidin (dotted green lines)..... 78

80 (a) The binding location of PMA-1A on the part of hydrophilic site and hydrophobic site of lysozyme. (b) The amino acid residues of lysozyme surrounding PMA-1A within the distance of less than 5 Å. (c) A hydrogen bonding interaction of anionic PMA-1A with an amino acid residue of lysozyme (dotted green lines)..... 80

81 (a) The binding location of PMA-2A on the part of hydrophilic site and hydrophobic site of lysozyme. (b) The amino acid residues of lysozyme surrounding PMA-2A within the distance of less than 5 Å. (c) Two hydrogen bonding interactions of anionic PMA-2A with two amino acid residues of lysozyme (dotted green lines)..... 81

LIST OF FIGURES (continued)

Figure		Page
82	(a) The binding location of PMA-3A on the part of hydrophilic site and hydrophobic site of lysozyme. (b) The amino acid residues of lysozyme surrounding PMA-3A within the distance of less than 5 Å. (c) Two hydrogen bonding interactions of anionic PMA-3A with two amino acid residues of lysozyme (dotted green lines)	82
83	The structures of berberine derivatives (a) SST-29 and (b) SST-31	84
84	Photocleavage of avidin obtained from the reaction with berberine	84
85	Photoproduct yields obtained from the reaction of photocleavage of avidin with berberine	85
86	A standard curve of molecular weight markers for calculation of molecular weights of the cleaved fragments	86
87	The cleavage sites of avidin from the reaction of berberine	87
88	Absorption spectra of berberine (10 μM) in the absence (blue) and presence (red) of avidin (0-10 μM)	87
89	Absorption spectra of SST-29 (10 μM) in the absence (blue) and presence (red) of avidin (0-10 μM)	88
90	Absorption spectra of SST-31 (10 μM) in the absence (blue) and presence (red) of avidin (0-10 μM)	88
91	Absorption spectra of berberine (10 μM) in the absence (blue) and presence (red) of lysozyme (0-10 μM)	87
92	Absorption spectra of SST-29 (10 μM) in the absence (blue) and presence (red) of lysozyme (0-10 μM)	89
93	Absorption spectra of SST-31 (10 μM) in the absence (blue) and presence (red) of avidin (0-10 μM)	89
94	(a) The binding location of berberine on the part of hydrophilic site and hydrophobic site of avidin. (b) The amino acid residues of avidin surrounding berberine within the distance of less than 5 Å. (c) Two hydrogen bonding interactions of anionic berberine with two amino acid residues of avidin (dotted green lines)	91

LIST OF FIGURES (continued)

Figure Page

95 (a) The binding location of SST-29 on the part of hydrophilic site and hydrophobic site of avidin. (b) The amino acid residues of avidin surrounding SST-29 within the distance of less than 5 Å. (c) A hydrogen bonding interaction of SST-29 with an amino acid residue of avidin (dotted green lines)..... 92

96 (a) The binding location of SST-31 on the part of hydrophilic site and hydrophobic site of avidin. (b) The amino acid residues of avidin surrounding SST-31 within the distance of less than 5 Å. (c) A hydrogen bonding interaction of SST-31 with an amino acid residue of avidin (dotted green lines)..... 93

97 (a) The binding location of berberine on the part of hydrophilic site and hydrophobic site of lysozyme. (b) The amino acid residues of avidin surrounding berberine within the distance of less than 5 Å. (c) Two hydrogen bonding interactions of anionic berberine with two amino acid residues of lysozyme (dotted green lines)..... 95

98 (a) The binding location of SST-29 on the part of hydrophilic site and hydrophobic site of lysozyme. (b) The amino acid residues of lysozyme surrounding SST-29 within the distance of less than 5 Å. (c) Three hydrogen bonding interactions of SST-29 with three amino acid residues of lysozyme (dotted green lines)..... 96

99 (a) The binding location of SST-31 on the part of hydrophilic site and hydrophobic site of lysozyme. (b) The amino acid residues of lysozyme surrounding SST-31 within the distance of less than 5 Å. (c) A hydrogen bonding interaction of SST-31 with an amino acid residue of lysozyme (dotted green lines)..... 97

100 Photocleavage of α-chymotrypsin obtained from the reaction with PMA-1A.. 105

101 Photocleavage of β-lactoglobulin B obtained from the reaction with PMA-1A. 105

102 Photocleavage of myoglobin obtained from the reaction with PMA-1A..... 106

103 Photocleavage of HSA obtained from the reaction with PMA-1A..... 107

104 Photocleavage of BSA obtained from the reaction with PMA-1A..... 107

LIST OF FIGURES (continued)

Figure		Page
105	Photocleavage of α-casein obtained from the reaction with PMA-1A	108
106	Photocleavage of pepsin obtained from the reaction with PMA-1A	108
107	Photocleavage of concanavalin A obtained from the reaction with PMA-1A	109
108	Photocleavage of β-glucosidase obtained from the reaction with PMA-1A	109
109	Photocleavage of α-chymotrypsin obtained from the reaction with PMA-2A	110
110	Photocleavage of β-lactoglobulin B obtained from the reaction with PMA-2A	110
111	Photocleavage of myoglobin obtained from the reaction with PMA-2A	111
112	Photocleavage of HSA obtained from the reaction with PMA-2A	112
113	Photocleavage of BSA obtained from the reaction with PMA-2A	112
114	Photocleavage of α-casein obtained from the reaction with PMA-2A	113
115	Photocleavage of pepsin obtained from the reaction with PMA-2A	113
116	Photocleavage of concanavalin A obtained from the reaction with PMA-2A	114
117	Photocleavage of β-glucosidase obtained from the reaction with PMA-2A	114
118	Photocleavage of α-chymotrypsin obtained from the reaction with PMA-3A	115
119	Photocleavage of β-lactoglobulin B obtained from the reaction with PMA-3A	115
120	Photocleavage of myoglobin obtained from the reaction with PMA-3A	116
121	Photocleavage of HSA obtained from the reaction with PMA-3A	116
122	Photocleavage of BSA obtained from the reaction with PMA-3A	117
123	Photocleavage of α-casein obtained from the reaction with PMA-3A	118
124	Photocleavage of pepsin obtained from the reaction with PMA-3A	118
125	Photocleavage of concanavalin A obtained from the reaction with PMA-3A	119
126	Photocleavage of β-glucosidase obtained from the reaction with PMA-3A	119
127	Photocleavage of lysozyme obtained from the reaction with berberine	120
128	Photocleavage of α-chymotrypsin obtained from the reaction with berberine	120
129	Photocleavage of β-lactoglobulin B obtained from the reaction with berberine	121
130	Photocleavage of myoglobin obtained from the reaction with berberine	122
131	Photocleavage of HSA obtained from the reaction with berberine	122
132	Photocleavage of BSA obtained from the reaction with berberine	123
133	Photocleavage of α-casein obtained from the reaction with berberine	123

LIST OF FIGURES (continued)

Figure		Page
134	Photocleavage of pepsin obtained from the reaction with berberine.....	124
135	Photocleavage of concanavalin A obtained from the reaction with berberine...	124
136	Photocleavage of β-glucosidase obtained from the reaction with berberine....	125
137	Photocleavage of avidin obtained from the reaction with SST-29.....	125
138	Photocleavage of lysozyme obtained from the reaction with SST-29.....	126
139	Photocleavage of α-chymotrypsin obtained from the reaction with SST-29...	126
140	Photocleavage of β-lactoglobulin B obtained from the reaction with SST-29.	127
141	Photocleavage of myoglobin obtained from the reaction with SST-29.....	128
142	Photocleavage of HSA obtained from the reaction with SST-29.....	128
143	Photocleavage of BSA obtained from the reaction with SST-29.....	129
144	Photocleavage of α-casein obtained from the reaction with SST-29.....	129
145	Photocleavage of pepsin obtained from the reaction with SST-29.....	130
146	Photocleavage of concanavalin A obtained from the reaction with SST-29....	130
147	Photocleavage of β-glucosidase obtained from the reaction with SST-29....	131
148	Photocleavage of avidin obtained from the reaction with SST-31.....	132
149	Photocleavage of lysozyme obtained from the reaction with SST-31.....	132
150	Photocleavage of α-chymotrypsin obtained from the reaction with SST-31...	133
151	Photocleavage of β-lactoglobulin B obtained from the reaction with SST-31.	133
152	Photocleavage of myoglobin obtained from the reaction with SST-31.....	134
153	Photocleavage of HSA obtained from the reaction with SST-31.....	134
154	Photocleavage of BSA obtained from the reaction with SST-31.....	135
155	Photocleavage of α-casein obtained from the reaction with SST-31.....	136
156	Photocleavage of pepsin obtained from the reaction with SST-31.....	136
157	Photocleavage of concanavalin A obtained from the reaction with SST-31...	137
158	Photocleavage of β-glucosidase obtained from the reaction with SST-31...	137
159	Photocleavage of avidin obtained from the reaction with piperine.....	138
160	Photocleavage of lysozyme obtained from the reaction with piperine.....	138
161	Photocleavage of α-chymotrypsin obtained from the reaction with piperine....	139
162	Photocleavage of β-lactoglobulin B obtained from the reaction with piperine..	140

LIST OF FIGURES (continued)

Figure		Page
163	Photocleavage of myoglobin obtained from the reaction with piperine.....	140
164	Photocleavage of HSA obtained from the reaction with piperine.....	141
165	Photocleavage of BSA obtained from the reaction with piperine.....	141
166	Photocleavage of α-casein obtained from the reaction with piperine.....	142
167	Photocleavage of pepsin obtained from the reaction with piperine.....	142
168	Photocleavage of concanavalin A obtained from the reaction with piperine.....	143
169	Photocleavage of β-glucosidase obtained from the reaction with piperine.....	144

CHAPTER 1

Introduction

Background

The development of photochemical reagents to cleave protein at specific site has been of interest in molecular biology. Because of the stability of the peptide bond, which uncatalyzed hydrolysis of peptide bonds is extremely slow (half-life of peptide bond about 350-600 years at room temperature and neutral pH (Radzicka; & Wolfenden. 1996: 6105-6109). These photochemical reagents can be useful for converting larger protein into smaller fragments that are amenable for amino acid sequencing, understanding protein-ligand interactions, structure-activity studies of protein and investigation of protein structural domains (Rana; & Meares. 1991: 1859-1861). In addition, these photochemical reagents may be of interest for investigating drug binding sites in proteins and design of novel therapeutic drugs (Hegg; et al. 1999: 2961-2968).

The reaction of protein cleavage can be activated by two types of reaction: photoreaction and thermalreaction. However, using light as an activator in the photoreaction has many advantages, such as convenient, inexpensive, easy to control and minimizing side reactions. Moreover, the visible light is nontoxic. In particular, UV light can be used to activate fluorescent probes at ground state to excited state and then generates free radicals by an electron acceptor. This process is called as photolysis. The generated free radicals can then result in breaking peptide bonds. Cobalt(III) hexammine chloride (CoHA) has been used as an electron acceptor in many researches for several reasons, such as high solubility in water, low affinity for binding to proteins and chemical stability.

Many researchers have taken the advantages of the properties of the fluorescent probes for the development of new synthesized photochemical reagents. For example, site-specific photocleavage of bovine serum albumin (BSA) (Leu346-Arg347) and chicken egg-white lysozyme (lysozyme) (Trp108-Val109) by *N*-(1-phenylalanine)-4(1-pyrene) butyramide (Py-Phe) (Kumar; et al. 1997: 2085) was achieved. This photochemical reagents bound to both proteins with high affinities ($2.2 \pm 0.3 \times 10^5$ M^{-1} with BSA and $6.5 \pm 0.4 \times 10^7$ M^{-1} with lysozyme) (Kumar; et al. 1998: 10361). Moreover, derivatives of Py-Phe, Py-$(Gly)_n$-Phe (n=0, 1, 2) (Kumar; et al. 1999: 4202), cleaved lysozyme at 2 positions: between Trp108-Val109 (major cleavage site) and between Ala110-Trp111

(minor cleavage site). The efficiency of photocleavage of lysozyme decreased when the linker length of Py-$(Gly)_n$-Phe increased. In addition, avidin was also cleaved (Thr77-Val78) by Py-biotin (Malaikeaw; et al. 2011: 251-255). The photocleavage of proteins was achieved upon irradiation of a mixture of protein, fluorescent probe and an electron acceptor (CoHA) at the maximum absorption (λ_{max}) of the fluorescent probe (340-350 nm). The cleavage of protein was not achieved in the absence of either fluorescent probe, an electron acceptor or light. The mechanism of protein cleavage was found to be quenching of the singlet excited state of the pyrenyl chromophore by CoHA resulting to pyrene cation radical. Therefore, this pyrene cation radical was responsible for the cleavage of the peptide backbone (Kumar; et. Al. 2002: 5810-5815).

In this study, we focus on the development of new synthetized photochemical reagents by coupling fluorescent probes with the ability of a recognition element to selectively bind to specific sites on proteins. Pyrene is chosen for this study due to its strong absorption bands in the near visible region with long lived (~100 ns) and high energy (~70 kcal/mol) singlet excited state, thus, making it convenient to initiate the photoreaction to occur. Moreover, pyrene is hydrophobic, thus it may have high binding affinity to hydrophobic sites of proteins. However, we also interest in using other compounds, such as natural products, for more friendly to environment.

Therefore, the development of new synthesized photochemical reagents and natural products were focused in this research. The interactions between proteins and these reagents were studied using UV-Vis, fluorescence, gel electrophoresis and docking methods.

Objectives of the study

1. To design and synthesize new photochemical reagents.
2. To study binding interaction between proteins and new photochemical reagents, derived from synthetic and natural products.
3. To study protein photocleavage by new photochemical reagents and natural products.
4. To optimize conditions for high efficiency protein cleavage.
5. To study the binding position of new photochemical reagents and natural products with the target protein by molecular docking.

Significance of the study

1. Know binding constants of new photochemical reagents and natural products to protein.
2. Know the appropriate conditions of photocleavage reaction.
3. Know the amino acid sequences derived from protein cleavage.
4. Know the binding positions on the protein.

Scope of the study

1. Synthesize new photochemical reagents.
2. Study the binding interaction and fluorescence quenching between proteins and new photochemical reagents, derived from synthetic and natural products by spectroscopic methods.
3. Study the protein photocleavage by sodium dodecyl sulfate-polyacrylamide gel electrophoresis (SDS-PAGE).
4. Find amino acid sequence derived from protein cleavage.
5. Study the binding positions of new photochemical reagents and natural products on the protein binding site by molecular docking.

CHAPTER 2

Theory and related research

In this study, photochemical reagents were designed for binding study of small molecules with proteins. The binding interactions were investigated using UV-Vis, fluorescence, gel electrophoresis and docking description. General information and related research on topics are listed as following:

1. Amino acids
2. Proteins
3. Electrophoresis
4. Amino acid sequencing analysis
5. Spectroscopic methods
   - 5.1 UV-Vis spectroscopy
   - 5.2 Fluorescence spectroscopy
6. Computational chemistry
7. Related research

1. Amino acid

Amino acids are the basic structure of the proteins which are important components in all organisms. An amino group ($-NH_2$), a carboxyl group (-COOH), a hydrogen (-H) and a side chain (-R). These groups are connected to a central carbon, called α-carbon. The side chain of the amino acid makes amino acid different from each other (Figure 1).

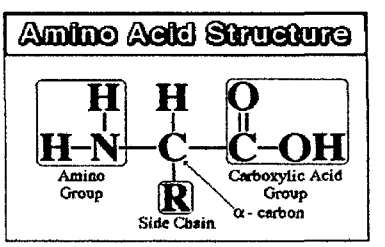


Figure 1 Basic structure of Amino acid in un-ionized form.

Source: Nelson, D.L.; & Cox, M.M. (2000). *Lehninger Principles of Biochemistry.*

If an amino acid is dissolved in a neutral pH solution, it will be in dipolar ions form (zwitterions) rather than in the unionized form. If an amino acid is dissolved in an acid solution at pH 2, the carboxylic group will be in un-ionized form (-COOH) and ionized form ($-COO^-$). If an amino acid is dissolved in an alkaline solution at pH 9, the amine group will be in unionized form ($-NH_2$) and ionized form ($-NH_3^+$) (Figure 2).

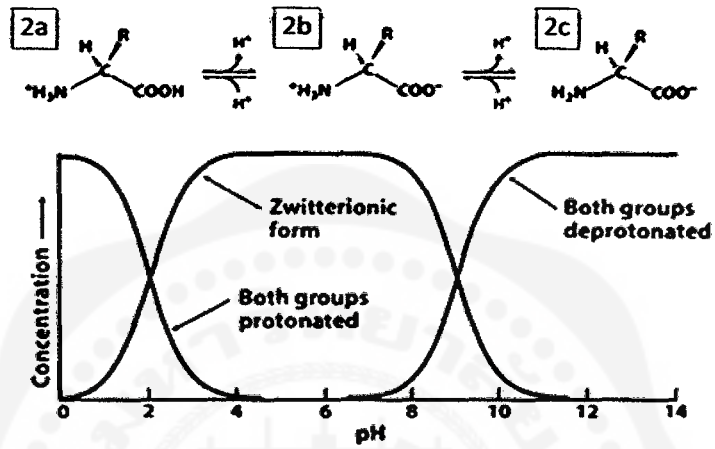


Figure 2 Amino acid ionization state as a function of pH.

Source: Berg, J.M.; Tymoczko, J.L.; & Stryer, L. (2012). *Biochemistry.*

There are twenty kinds of amino acid which can be divided to 4 types; polar uncharged amino acids, nonpolar amino acids, aromatic amino acids and electrically charged amino acids, each identified by the variable side chain (-R groups) bonded to the α-carbon.

1. Polar uncharged amino acids (serine, threonine, cysteine, asparagine, glutamine) are hydrophilic and can form hydrogen bonds (Figure 3a).

2. Nonpolar amino acids (glycine, alanine, proline, valine, leucine, isoleucine, methionine) are hydrophobic and usually found in the center of the protein (Figure 3b).

3. Aromatic amino acids (phenylalanine, tyrosine, tryptophan) contain aromatic rings and can absorb light that show the signals in the near-UV region (250-300 nm) (Figure 3c).

4. Electrically charged amino acids can be divided to 2 types; positively charged amino acids (lysine, arginine, and histidine) and negatively charged amino acids (aspartic acid, glutamic acid). Electrical properties of these amino acids can change depending on the pH of the solution (Figure 3d).

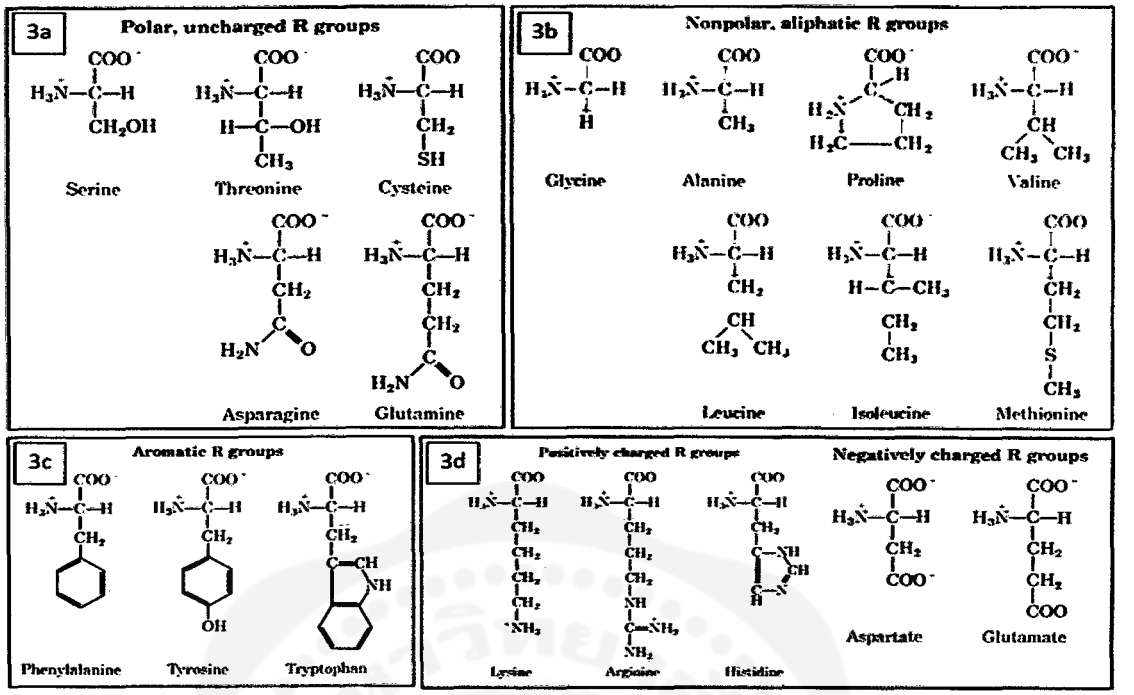


Figure 3 The twenty kinds of amino acid different side chains.

Source: Nelson, D.L.; & Cox, M.M. (2013). *Lehninger Principles of Biochemistry.*

The four groups attached to the chiral carbon center are chemically different for all amino acids, which can exist in two different forms (L-form or D-form), except glycine. Looking down the hydrogen atom away from the viewer, if the handle of the COOH to R to NH_2 groups around the chiral carbon atom is counter-clockwise, then it is the L-form. If the handle is clockwise, it is the D-form. Two mirror images of a chiral molecule are called enantiomers (Figure 4).

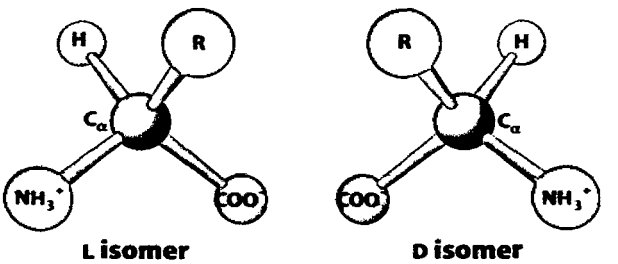


Figure 4 D-form and L-form of amino acid.

Source: Berg, J.M.; Tymoczko, J.L.; & Stryer, L. (2012). *Biochemistry.*

Essential amino acids are amino acids that cannot be synthesized by the organism. In human, the essential amino acids are phenylalanine, valine, threonine, tryptophan, methionine, leucine, isoleucine, lysine, arginine* and histidine* (*Essential for children, but not necessary for adults) (Table 1). These amino acids can be obtained from food.

Table 1 Amino acid requirements in humans.

Essential amino acid	Non-Essential amino acid
phenylalanine	alanine
valine	asparagine
threonine	aspartate
tryptophan	cysteine
methionine	glutamate
leucine	glutamine
isoleucine	glycine
lysine	proline
arginine*	serine
histidine*	tyrosine

Source: Young, V.R. (1994). *Adult Amino Acid Requirements: The Case for a Major Revision in Current Recommendations.* p. 1518S.

2. Protein

Each protein has unique amino acid sequence. An amino acid combines chemically with one another by a condensation reaction that bonds the carboxyl group (COOH) of one molecule to the amino group (NH_2) of another, causing the release of a molecule of water. The covalent carbon to nitrogen bond linking two amino acids is a peptide bond (Figure 5). The peptide can be divided to two types by the number of amino acids; oligopeptide and polypeptide. The oligopeptide is a peptide consisting of two to ten amino acids. The two joined amino acids are called a dipeptide. The polypeptide is a peptide that consists of more than 10 amino acids. A protein consists of one or more polypeptide chains. Each polypeptide has a free amino group or *N*-terminus at one end and a free carboxyl group or *C*-terminus at the opposite end.

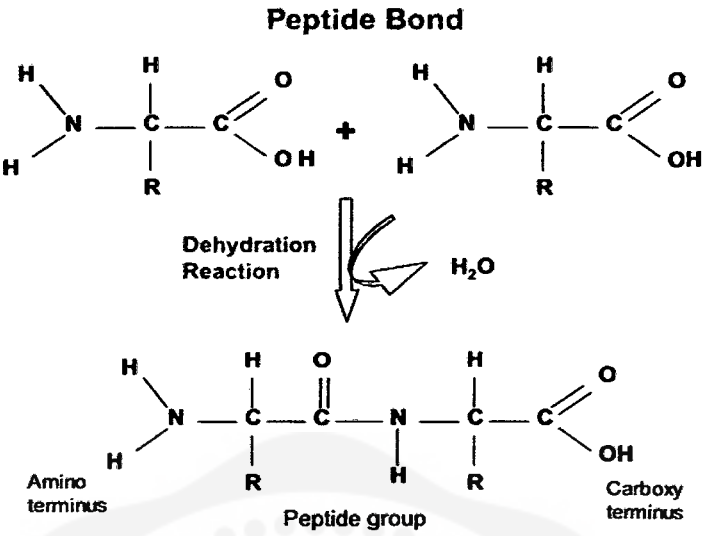


Figure 5 Peptide bond of amino acid.

Source: Moran, L.A.; et al. (2012). *Principles of Biochemistry*.

The principal roles of protein in the body are enzymes, muscle contraction, immunity, hormones, transport and energy. The protein structure is divided to 4 levels.

1. Primary structure is a linear sequence of amino acids in the polypeptide chain, consisting of 50 to 100 amino acids units (Figure 6a).

2. Secondary structure is highly regular. The two most common types of secondary structure are α-helix and β-pleated sheet. The helical structure is determined and maintained by the formation of intra-chain hydrogen bonds between a carboxyl group on peptide bond of an amino acid and the amino group on peptide bond of next 4 positions of amino acids in successive turns of the spiral coil. The R group of the amino acid is facing on the outside of the spiral. The α-helix is the most stable structure of a spiral structure. The hydrogen bonding in a β-pleated sheet takes place between a carboxyl group of an amino acid of a polypeptide chain and amino group of different polypeptide chain (Figure 6b).

3. Tertiary structure is the overall shape of a protein molecule. This 3D structure is determined by 4 main factors that involve interactions among R group belonging to the same polypeptide chain. These include both weak interactions, such as hydrogen bonds, ionic bonds, hydrophobic interactions, and strong covalent bonds (Figure 6c).

4. Quaternary structure is the resulting 3D structure of a protein with more than one polypeptide chain. The same types of interactions that produce secondary and tertiary structures also contribute to quaternary structure. For example, hemoglobin consists of 574 amino acids arranged in 4 polypeptide chains, 2 identical chains called α-chains and 2 identical chains called α-chains. (Figure 6d).

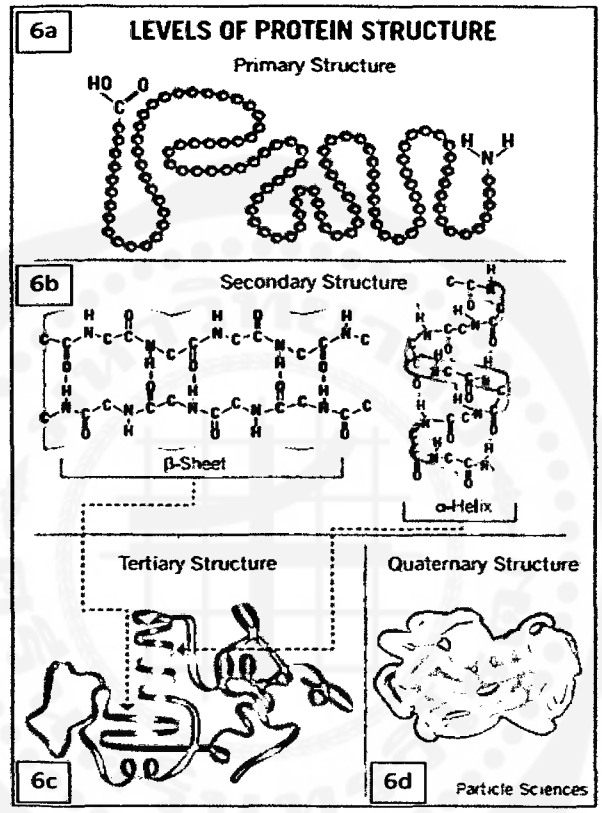


Figure 6 The 4 levels of protein structure.

Source: Protein Structure. (2009). (online).

3. Electrophoresis

Electrophoresis is a separation technique of biomolecules under an electric field. Proteins contain of many ionizable groups on the side chains, amino- and carboxyl-terminus of amino acids. Therefore, protein has a net charge that depends on the numbers and identities of the charged amino acids, and on the pH. Ion compounds will move to the opposite charge of the electrode with different speed based on the physical properties of

molecules (Figure 7). The speed of movement of the molecules (V, ms^{-1}) can be calculated by equation 1.

$$V = \frac{E \times Z}{f} \quad \text{—— [1]}$$

Where, E is the electric field (Volt m^{-1}).
Z is the net charge of the molecule.
f is the frictional coefficient (kg s^{-1}).

The frictional coefficient (f) can be calculated by equation 2. It depends on the size and shape of the molecule, with the radius of the sphere molecule (r) moving through a viscous medium (η).

$$f = 6\pi\eta r \quad \text{—— [2]}$$

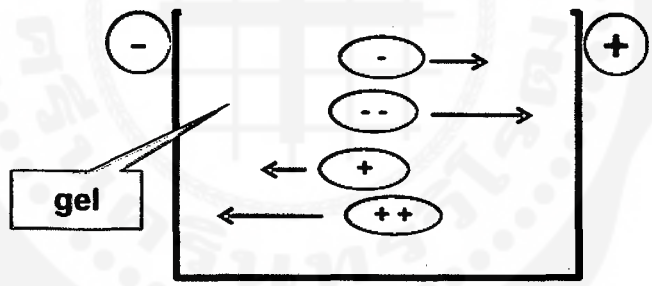


Figure 7 The movement of ion compounds to the electrode.

Separation of biomolecules by means of electrophoresis mainly uses an intermediate gel. The intermediate gel used to separate proteins is polyacrylamide gel. Polyacrylamide gel is prepared by polymerization reaction, resulting from the combination of acrylamide (Figure 8a) and *N,N'*-methylenebisacrylamide (Figure 8b). By using *N,N,N',N'*-tetramethylethylenediamine (TEMED) (Figure 8c) as catalyst, the sulfate radicals ($SO_4^{-\bullet}$) from ammonium persulfate ($(NH_4)_2S_2O_8$) will be generated in gel solution, causing to form a gel (Figure 9).

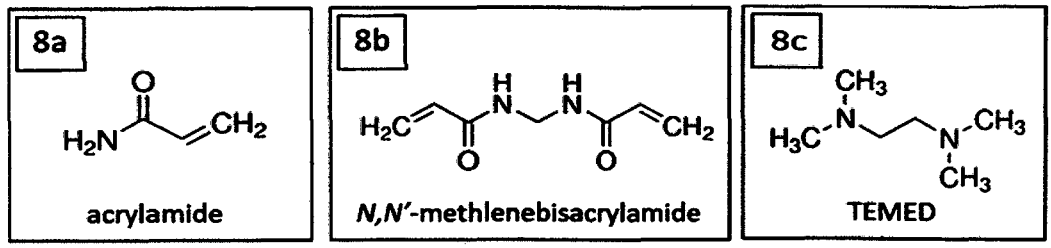


Figure 8 The structure of acrylamide, *N,N'*-methylenebisacrylamide, TEMED.

Source: The Chemical Structure of Acrylamide, *N,N'*-methylenebisacrylamide and *N,N,N',N'*-tetramethylethylenediamine. (2015). (online).

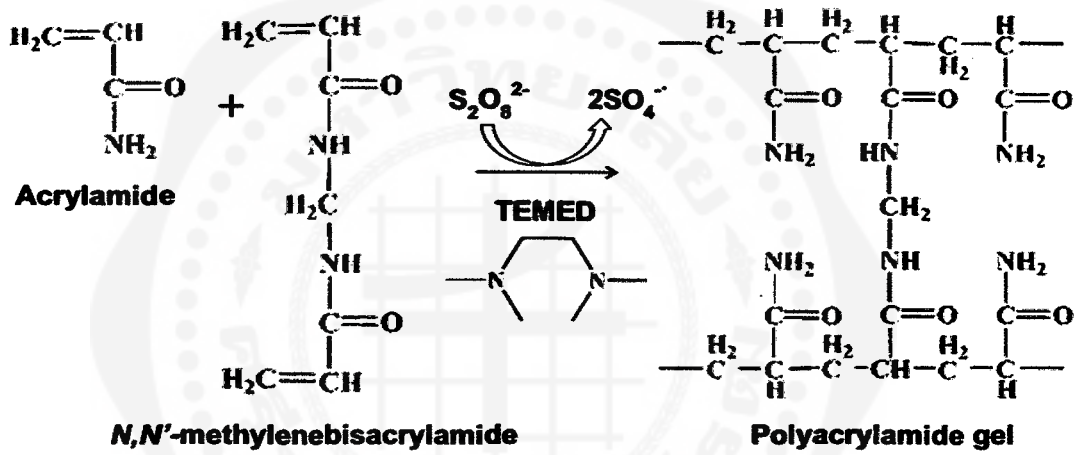


Figure 9 Polymerization reaction of polyacrylamide gel.

Source: Hames, B.D.; & Rickwood, D. (1990). *Gel Electrophoresis of Proteins: A Practical Approach*. pp. 3-5.

Separation of proteins by polyacrylamide gel depends on the pore size of the gel. The pore size of the gel is influenced by the total concentration of polyacrylamide in the polymerization mixture. If the concentration of polyacrylamide increases, pore size will decrease. The appropriate concentrations of polyacrylamide gel for separating the proteins are shown in Table 2. The composition of polyacrylamide gel is described by two parameters, %T and %C. The %T value is the total concentration of acrylamide plus *N,N'*-methylenebisacrylamide (%w/v). %C is the percentage of crosslinking agent (*N,N'*-methylenebisacrylamide) (%w/v). The both parameters can be calculated by equations 3 and 4.

$$\%T = \frac{(a + b) \times 100}{V} \quad \text{—— [3]}$$

$$\%C = \frac{b}{(a + b)} \times 100 \quad \text{—— [4]}$$

Where, a is the weight of acrylamide (g).

b is the weight of *N,N'*-methylenebisacrylamide (g).

V is the total volume of polyacrylamide mixture solution (ml).

Table 2 The appropriate concentrations of polyacrylamide gel for separating the proteins.

Concentrations of polyacrylamide gel (%w/v)	Molecular weights of proteins (kDa)
3.5	-
5.0	> 1000
8.0	300-1000
12.0	50-300
15.0	10-80
20.0	5-30

Source: Sheehan, D.; (2000). *Physical Biochemistry*.

The movement of protein in the gel when connecting to electrode depends on the different structures and net charges of proteins. Therefore, proteins must be denatured by sodium dodecyl sulfate (SDS) (Figure 10a) in loading buffer solution to unfold the protein structure. Sodium dodecyl sulfate contains both polar and non-polar groups. The non-polar group of SDS will bind with protein, in the ratio of one molecule of SDS to two amino acids. Tail of the SDS molecule is negative. These negative charges push themselves, resulting in the released structure of proteins (Figure 10b). The protein will have net negative charge after binding to SDS. Therefore, the separation will depend only on the size of the protein, and will not depend on the charge.

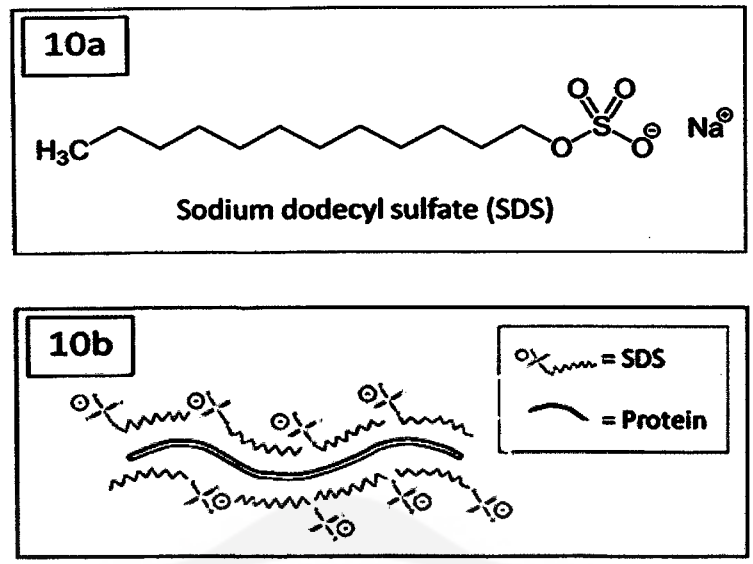


Figure 10 (a) The chemical structure of sodium dodecyl sulfate (SDS), which both polar and non-polar groups (b) The SDS molecules coat the protein with negative charges.

Source: Structure of Sodium Dodecyl Sulfate. (2015). (online).

In addition, the proteins mixture will be denatured by heating at 100°C for 3 min in loading buffer. The presence of excess SDS and reducing agent in loading buffer causes the cleavage of disulfide bonds (-RS-SR-) to sulfhydryl group (-RSH) in proteins, resulting in the released structure of proteins. The 2-mercaptoethanol (Figure 11a) and dithiothreitol (DTT) (Figure 11b) are widely used as reducing agents.

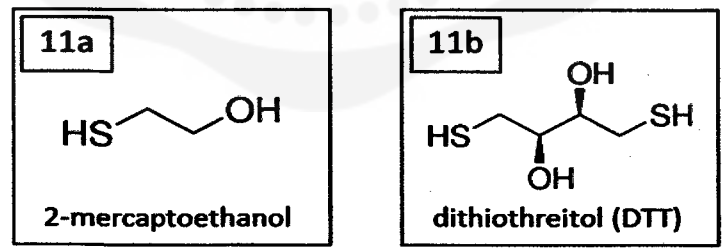


Figure 11 The structures of 2-mercaptoethanol and dithiothreitol.

Source: The structure of 2-mercaptoethanol and dithiothreitol (DTT). (2015). (online).

For separation of smaller proteins, tricine (Figure 12a) can be used instead of glycine (Figure 12b) to obtain better separation. This method is called Tricine-SDS-PAGE. The efficiency of separation by Tricine-SDS-PAGE is better than by Glycine-SDS-PAGE due to the differences of pK_a values and ionic strength (Figure 13).

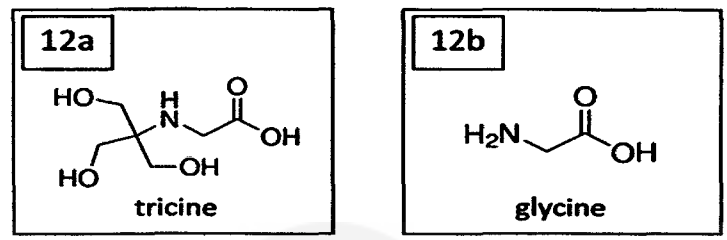


Figure 12 The structures of tricine and glycine.

Source: Good, N.E.; et al. (1966). *Hydrogen ion Buffers for Biological Research.* p. 467-477.

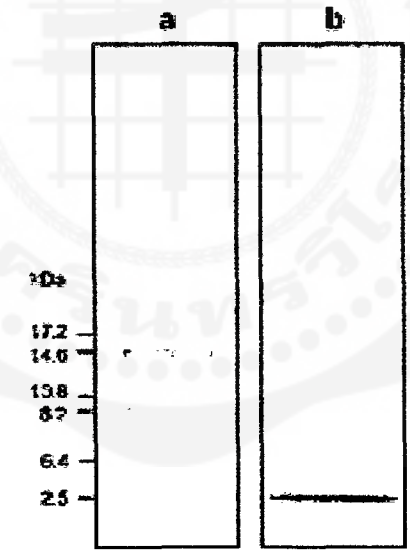


Figure 13 (a) Tricine-SDS-PAGE and (b) Glycine-SDS-PAGE.

Source: Shangger, H.; & Jagow, V.G. (1987). *Tricine-Sodium Dodecyl Sulfate-Polyacrylamide Gel Electrophoresis for the Separation of Proteins in the Range from 1 to 100 kDa.* pp. 368-370.

The gel in discontinuous system consists of 2 parts; stacking gel and running gel (Figure 14). Stacking gel has lower polyacrylamide concentration (4%), lower ionic strength and neutral pH (Tris-HCl buffer, pH 6.9) than running gel. Therefore, the proteins will move quickly as extremely narrow band in stacking gel zone prior to their separation in running gel. Running gel has higher polyacrylamide concentration (5-20%), higher ionic strength than stacking gel and pH > 8 (Tris-HCl buffer, pH 8-9). The pore size of running gel is smaller than that of stacking gel to increase the efficiency of separation. The proteins will move from negative electrode to positive electrode, and smaller proteins come out faster than larger proteins (Figure 15). The compositions of stacking gel and running gel for the separation of proteins (1-100 kDa) are shown in Table 3.

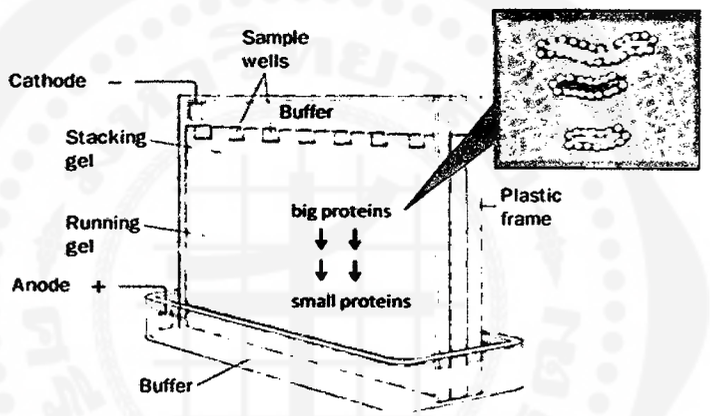


Figure 14 Discontinuous system of SDS-PAGE.

Source: Discontinuous Gel. (2005). (online).

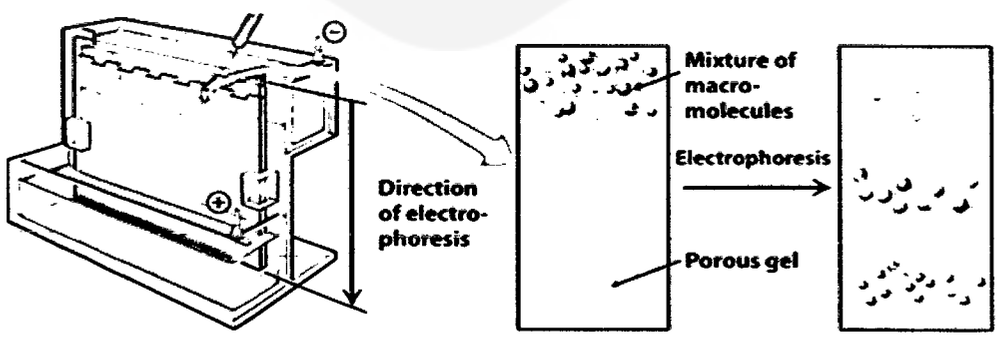


Figure 15 The movement of protein molecules through the porous gel.

Source: Berg, J.M.; Tyymoczko, J.L.; & Stryer, L. (2002). Biochemistry.

Table 3 Compositions of the stacking gel and running gel in SDS-PAGE.

The compositions of the stacking gel and running gel	Stacking gel (4%T, 3%C)	Running gel (10%T, 3%C)
acrylamide / bisacrylamide (49.5%T, 3%C)	0.125 ml	0.76 ml
gel buffer	0.39 ml	1.25 ml
deionized water	1.05 ml	1.11 ml
80% glycerol	-	0.625 ml
10% ammonium persulphate	13.75 µl	18.75 µl
TEMED	1.38 µl	1.88 µl

Source: Shangger, H.; & Jagow, V.G. (1987). *Tricine-Sodium Sodecyl Sulfate-Polyacrylamide Gel Electrophoresis for the Separation of Proteins in the Range from 1 to 100 kDa.* pp. 368-370.

Molecular weight of an unknown protein can be calculated using the relative mobility on the gel compared with the standard proteins. The mobility of a polypeptide chain can be correlated with the logarithm of molecular weight of protein (log M) (equation 5). A linearity standard curve between log M and distance of standard proteins (markers) can be created. Then, the molecular weight of an unknown protein can be calculated from the standard curve (Figure 16).

$$\text{Log M} = a - bx \qquad \text{—— [5]}$$

Where, a and b are constant value.

x is the speed of mobility of the polypeptide chain.

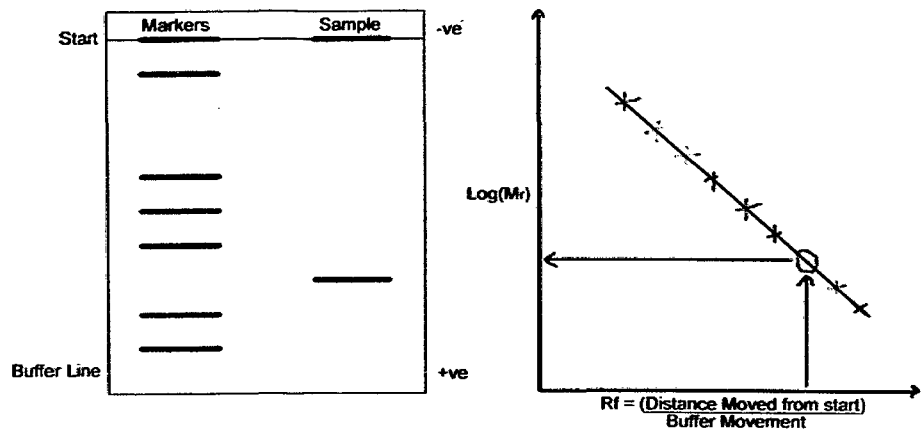


Figure 16 A linear standard curve.

Source: Protein Purification. (August 9, 2008). (online).

4. Amino acid sequencing analysis

The method used to find amino acid sequences was invented by Sanger in 1977. Later on, Edman degradation has been the most widely used sequencing method since it is the most convenient method. In this method, the amino acid at *N*-terminal residue is labeled by phenyl isothiocyanate, resulting to the phenylthiocarbamoyl derivative under acidic conditions. After hydrolysis of peptide bond the labeled amino acid will be released as thiazolinone amino acid, without disrupting the peptide bonds between other amino acid residues. The thiazolinone amino acid is then extracted into an organic solvent, and subjected to HPLC column, the amino acid can be identified by comparing with standard amino acids. The process will be repeated with the next amino acid (Figure 17).

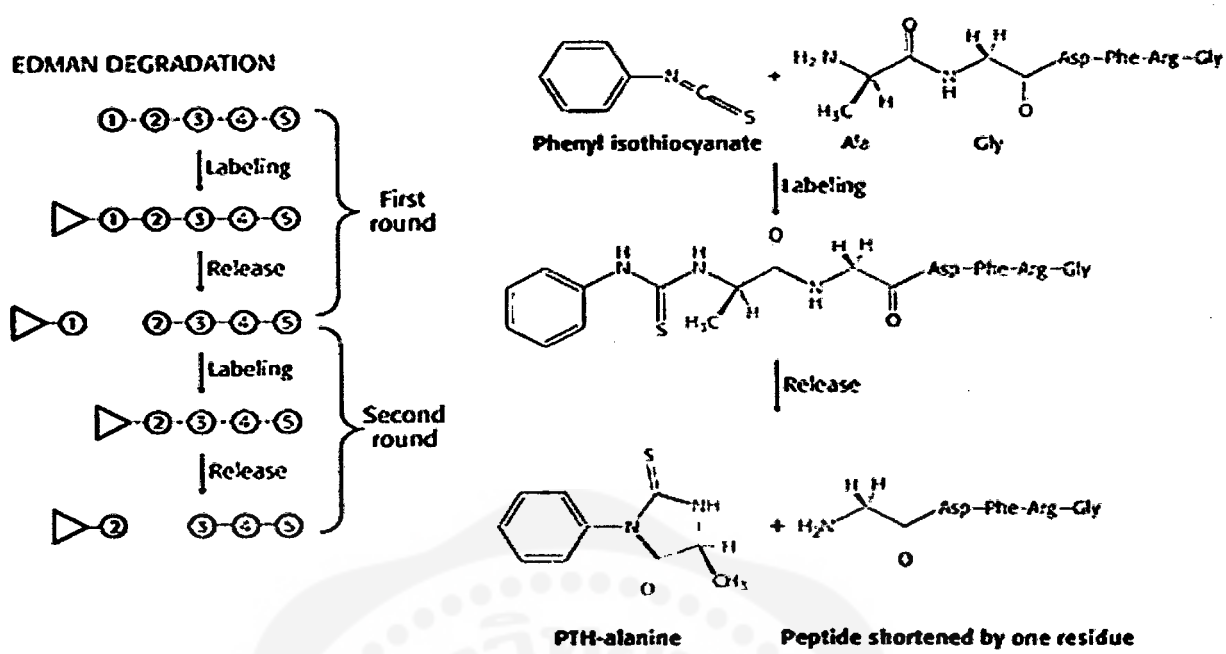


Figure 17 Edman degradation steps.

Source: Berg, J.M.; Tyymoczko, J.L.; & Stryer, L. (2002). *Biochemistry*.

5. Spectroscopic Methods

Spectroscopic techniques have been applied in all technical fields of science and technology. Spectroscopy is the study of the absorption and emission of light and other radiation by matter, as related to the dependence of these processes on the wavelength of the radiation. The physical properties of proteins can be analyzed by UV- Vis spectroscopy and fluorescence spectroscopy.

5.1 UV-Vis spectroscopy

Electromagnetic radiation consists of an electric field and a magnetic field that oscillate perpendicular to one another (Figure 18).

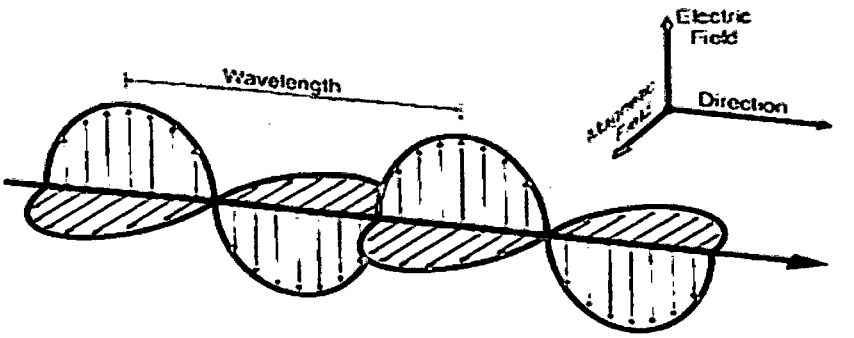


Figure 18 Electric field and magnetic field.

Source: Drago, R.S. (1992). *Physical Methods for Chemists.*

The absorption and the emission of energy in the electromagnetic spectrum occur in discrete photons. The relation between the energy of photon, the frequency and wavelength are shown in equations 6 and 7.

$$E = h\nu \quad \text{—— [6]}$$

$$\nu = \frac{c}{\lambda} \quad \text{—— [7]}$$

Where, E is energy.
h is Planck's constant (6.626×10^{-34} J s).
ν is frequency (s^{-1}).
c is the speed of light in a vacuum (2.9979×10^{8} m s^{-1}).
λ is wavelength (nm).

The various regions in the electromagnetic spectrum are displayed with the nature of the change brought about by the radiation (Figure 19). The ultraviolet region is in the range of 200-380 nm, while visible light is generally considered to extend from 380-780 nm (Table 4).

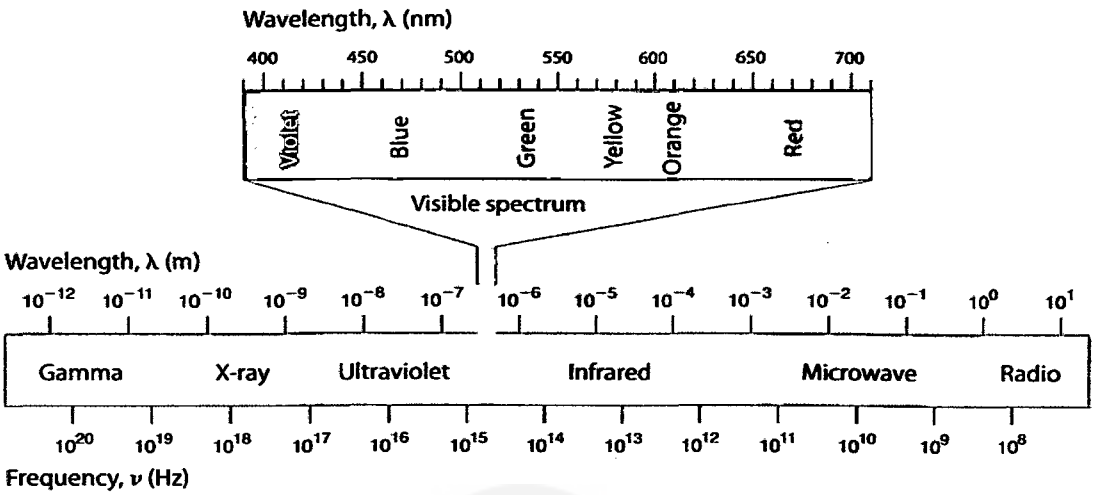


Figure 19 Schematic diagram of electromagnetic spectrum.

Source: Whittaker, A.G.; Mount, A.R.; & Heal, M.R. (2000). *Instant Notes: Physical Chemistry.*

Table 4 Relationship between wavelength region and colors.

Wavelength region (nm)	Transmitted color
< 380	Ultraviolet
380-435	Violet
435-480	Blue
480-490	Greenish blue
490-500	Bluish green
500-560	Green
560-580	Yellowish green
580-595	Yellow
595-650	Orange
650-780	Red
> 780	Near infrared

Source: Willard, H.H.; Merritt, L.L.; & Dean, J.A. (1974). *Instrumental Methods of Analysis.*

Absorbance is observed when light energy is used to promote electrons of molecule from the ground state to the excited state, while fluorescence emission is observed when the electrons at the excited state revert to the ground state. This phenomenon is called electronic transition (Figure 20).

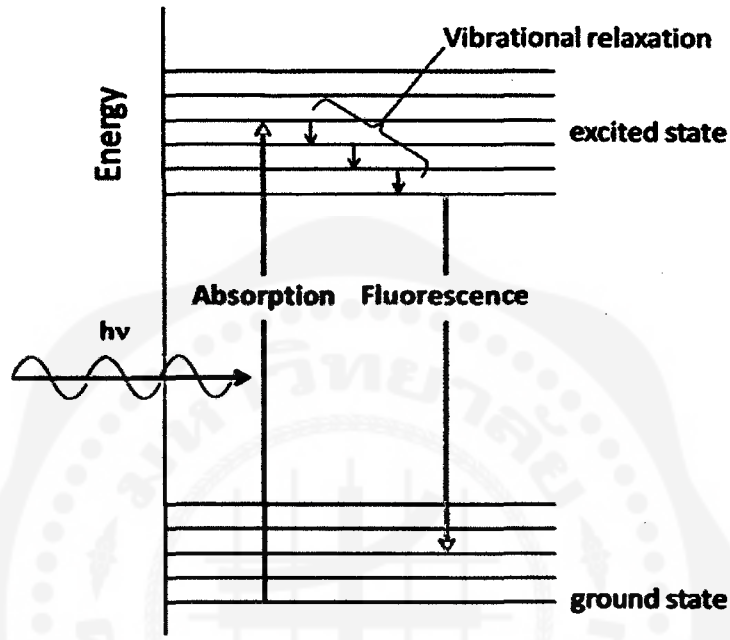


Figure 20 Electronic transition.

Source: Atkins, P.W. (2001). *The Elements of Physical Chemistry*.

Absorbance measurements are most commonly used to determine the concentration of biomolecules in a homogeneous solution. The absorbance is linearly related to the concentration by Beer-Lambert Law as shown in equation 8.

$$A = \varepsilon \times c \times l \qquad \text{—— [8]}$$

Where, A is the absorbance.

ε is the molar absorption coefficient ($\varepsilon=\alpha/2.303$) (M^{-1} cm^{-1}).

c is concentration of biomolecules (M).

l is the path length (cm).

In addition, binding constant (K_b) can be calculated by Scatchard equation (equation 9). K_b is obtained from the slope of the plot between r/C_f versus r.

$$r/C_f = K_b(n-r) \quad \text{—— [9]}$$

Where, C_f is concentration of free probe.

r is binding density.

K_b is binding constant.

n is the number of binding site.

Most proteins are colorless. However, they can absorb light and emit radiation in the UV range. Protein absorption spectrum can be considered by various factors. These factors are the absorbance of aromatic amino acids (tryptophan (Trp), tyrosine (Tyr), phenylalanine (Phe)) (Figure 21), protein backbone, secondary structure (α-helix, β-sheet, random coil) (Figure 22), bonding interaction and solvent. The absorbance and fluorescence of the aromatic amino acids in buffer (neutral pH) are shown in table 5.

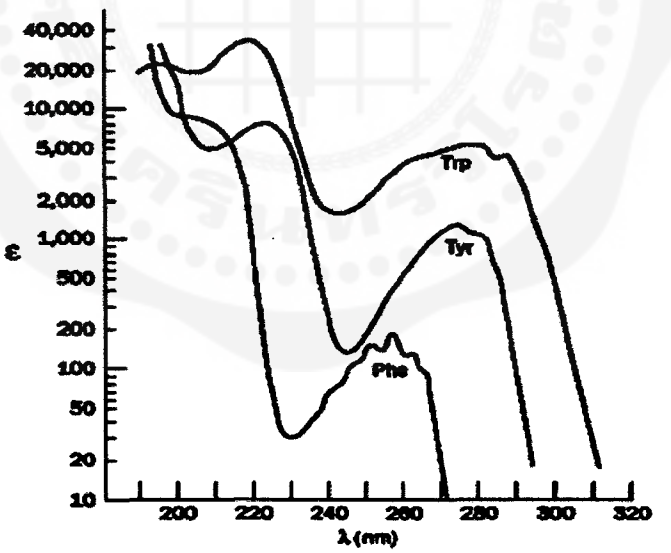


Figure 21 UV-spectra of tryptophan, tyrosine and phenylalanine.

Source: Tinoco, J.I.; et al. (2002). *Physical Chemistry: Principles and Applications in Biological Sciences.*

Table 5 Absorbance and fluorescence of the aromatic amino acids.

Compound	Absorbance	Fluorescence
	λ_{max} (nm)	λ_{max} (nm)
Tryptophan	280	348
Tyrosine	274	303
Phenylalanine	257	282

Source: Rickwood, D.; & Hames, B. D. (1990). *Protein Structure a Practical Approach.* p. 251-283.

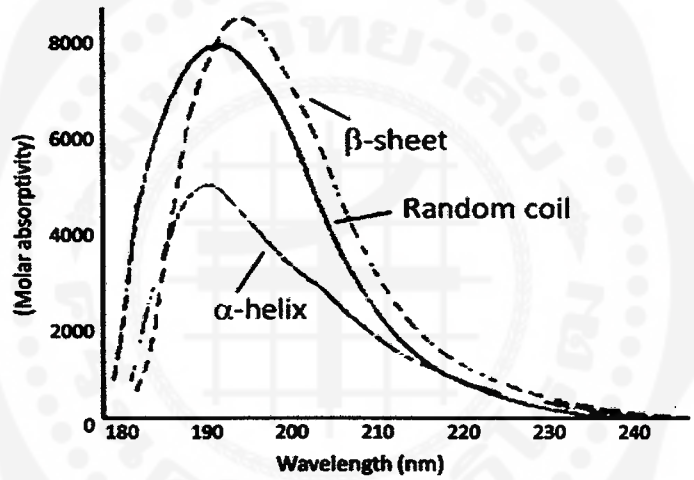


Figure 22 Absorption spectra of poly-L-lysine in an α-helix, β-sheet and random coil.

Source: Tinoco, J.I.; et al. (2002). *Physical Chemistry: Principles and Applications in Biological Sciences.*

The physical properties of a protein molecule depend on the environment surrounding the protein. The molecular environment can cause the protein conformational changes. The changes in the absorption spectrum can be classified to 4 types (Figure 23).

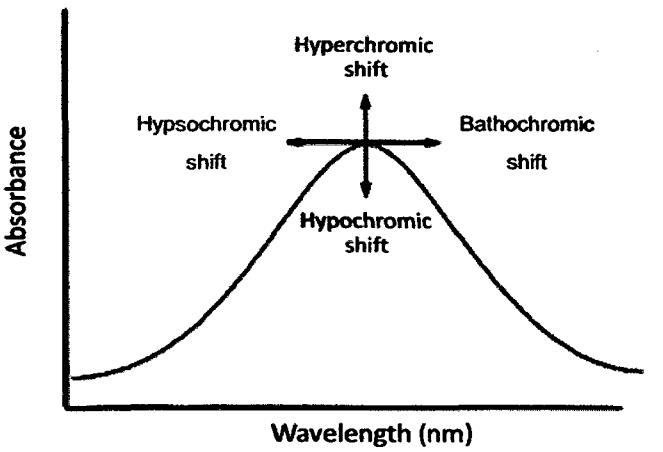


Figure 23 Absorbance and Intensity shifts.

5.2 Fluorescence spectroscopy

Fluorescence emission is caused by the transition of electrons from singlet electronic excited state (S_1) to singlet electronic ground state (S_0) in form of photons. Some energy is lost by vibrational transitions. The fluorescence lifetime is about 10^{-9} min.

The physical properties of a protein molecule depend on the environment of protein. Ligand-protein binding can make changes of the structure of the protein. Therefore, the fluorescence spectrum of the protein changes when the protein conformational changes. Changes are as follows: the increase or decrease of fluorescence intensities, the decrease of fluorescence lifetime in case of dynamic quenching and unaltered in case of static quenching. The fluorescence intensities of unfolded protein have energy less than folded protein. Moreover, the fluorescence quenching of protein by a quencher can show the ability of the quencher that can access to intrinsic fluorophore of protein.

The fluorescence quantum yield (Φ) is an indicator of occurring effective fluorescence, as shown in equation 10.

$$\Phi = \frac{\text{Fluorescence}}{\text{Absorbance}} \qquad \text{— [10]}$$

The fluorescence lifetime (τ) is inversely proportional to the decay rate constant (k_d), as shown in equation 11.

$$M \xrightarrow{h\nu} M^* \quad \text{(excitation)}$$

$$M^* \xrightarrow{k_d} M \quad \text{(fluorescence)}$$

$$\tau = \frac{1}{k_d} \qquad \text{— [11]}$$

The energy may be lost by thermal decomposition, photochemical reaction and quenching. Therefore, the decay rate constant can be expressed as shown in equation 12.

$$k_d = k_F + k_T + k_P + k_Q [Q] \qquad \text{— [12]}$$

Where,

k_F	is	rate constant of fluorescence.
k_T	is	rate constant of thermal decomposition.
k_P	is	rate constant of photochemical reaction.
k_Q	is	rate constant of quenching.
[Q]	is	the concentration of quencher.

The quenching molecule at excited state (M*) by the quencher can occur in 2 mechanisms; dynamic quenching and static quenching mechanisms (Figure 24). Dynamic quenching is caused by the collision of M* and Q. Then M* reverts to the ground state and losses the energy. When the temperature increases, the collision of M* and Q will increase due to the increase in the kinetic energy. Therefore, the quenching rate constant will also increase (equation 13). Static quenching is caused by the incorporation of M* at excited state with Q, producing the dark complex. When the temperature increases, the stability of the complex will decrease. Therefore, the quenching rate constant will decrease (equation 14).

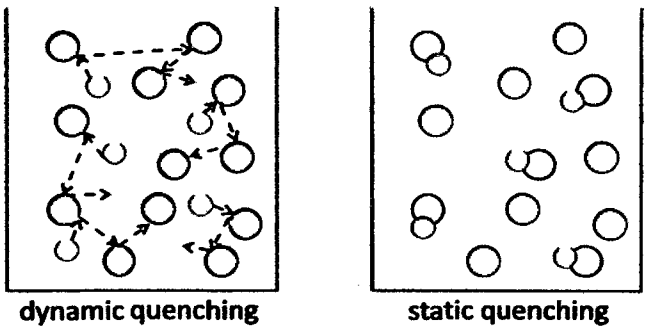


Figure 24 Dynamic quenching and static quenching.

Source: The Photochemistry Portal. (October 30, 2009). (online).

$$M + h\nu \longrightarrow M^* \quad \text{(excitation)}$$

$$M^* \xrightarrow{k_d} M \quad \text{(fluorescence)}$$

$$M^* + Q \xrightarrow{k_Q} M \quad \text{(dynamic quenching)} \quad \text{— [13]}$$

$$M^* + Q \xrightarrow{k_Q} MQ \quad \text{(static quenching)} \quad \text{— [14]}$$

Fluorescence quenching data can be analyzed using Stern–Volmer equation (equation 15). The Stern-Volmer quenching constant (K_{sv}) is obtained from the slope of the plot between I_0/I versus [Q] (Figure 25). Quenching rate constant (k_Q) can be calculated by equation 16.

$$\frac{I_0}{I} = 1 + K_{sv}[Q] \quad \text{— [15]}$$

$$K_{sv} = k_Q \times \tau_0 \quad \text{— [16]}$$

Where, I_0 is the fluorescence intensities in the absence of quencher.

I is the fluorescence intensities in the presence of quencher.

K_{sv} is the Stern-Volmer quenching constant.

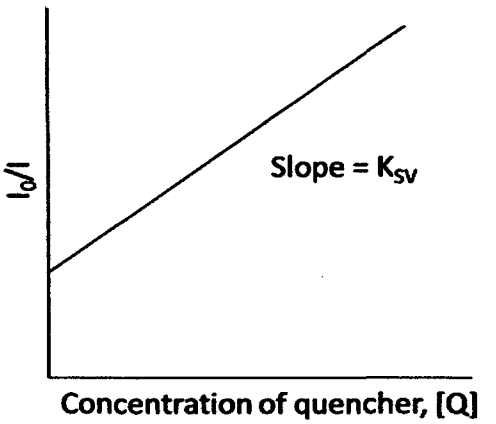


Figure 25 Stern–Volmer plot.

Source: Atkins, P.W. (2001). *The Elements of Physical Chemistry.*

6. Computational chemistry

Computational chemistry is a very useful method for investigating the molecular structure of biological molecules, binding affinity of small ligand to larger protein target (known three-dimensional structure) and drug design. The method can be used for virtual screening the efficiency of small molecule that can interact with protein target with decreasing time, cost and waste in experimental laboratory.

Molecular docking consists of two molecules; small ligand and a receptor. The three-dimensional structure of the ligand can be designed and optimized by Gaussian Chemdraw program. The receptor should include removal of the water molecules from the cavity, stabilizing charges, filling in the missing residues. After modification, the receptor should be biological active and stable. After the receptor is built (File.pdb), the active site within the receptor should be identified. The receptor may have many active sites. The efficiency of docking increases when the location of the binding site is known before docking processes. The crystal three-dimensional structure of protein (receptor) can be downloaded from the Protein Data Bank. Molecular docking can be used to study the binding position of small ligand on the protein, resulting to obtain the binding position on the protein binding site and binding energy. The ligand-receptor binding mechanism is the lock-and-key theory. Here, the protein can be thought of as the "lock" and the ligand can be thought of as a "key", in which the ligand has the best fit into the receptor (Figure 26).

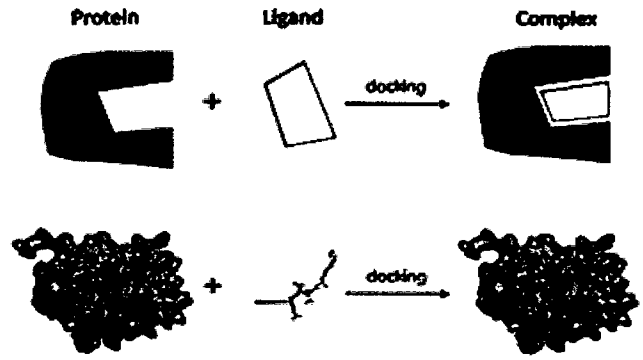


Figure 26 Schematic illustration of lock-and-key.

Source: Schematic illustration of docking. (December 14, 2015). (online).

Moreover, docking method is very useful for the study of selective ligand-protein interaction. However, reverse docking is another method which is opposite to the process of docking application. In this method, a small molecule of ligand is docked into the predefined binding sites of various protein structures from protein database to find suitable protein. The comparison of these two paradigms is shown in Figure 27.

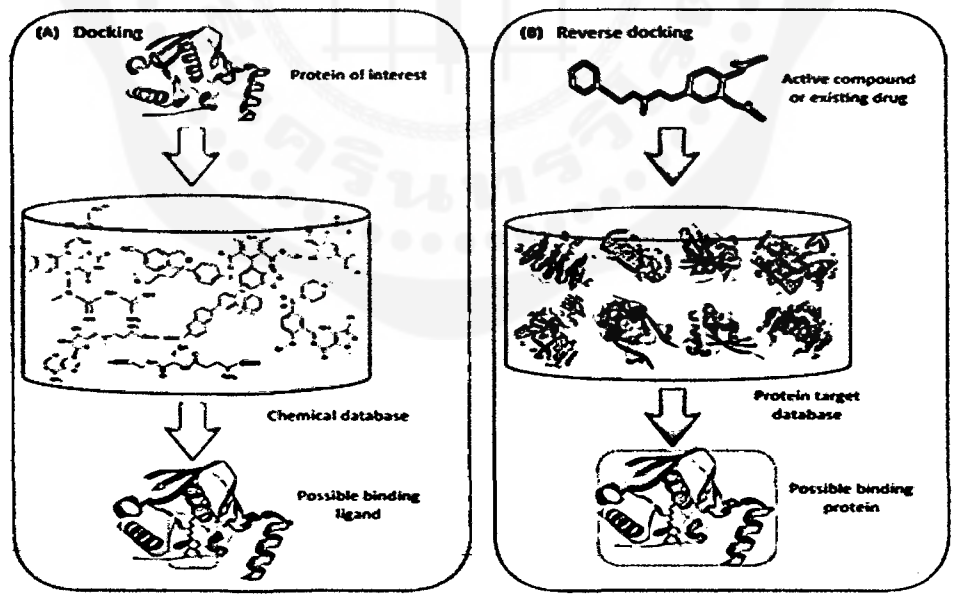


Figure 27 Comparison of docking application and reverse docking application.

Source: Zheng, M.; et al. (2013). Computational Methods for Drug Design and Discovery: Focus on China. *Trends in Pharmacological Sciences*. 34: pp. 549-559.

7. Related research

Many researchers have tried to develop new chemical reagents for selective binding to proteins since the peptide bond is unreactive towards hydrolysis with the half-life of 350-600 years at room temperature and neutral pH (Radzicka; & Wolfenden. 1996: 6105-6109). These chemical reagents can be useful for converting larger protein into smaller fragments, study on protein structure domains, understanding protein-ligand interactions and applying for the design of novel therapeutic drugs. Furthermore, these chemical reagents have also been used to selectively cleave proteins at ligand binding sites. The reaction of protein cleavage can be activated by 2 types of reaction: photo-reaction and thermal-reaction. However, using light as an activator in the photoreaction has many advantages, such as convenient, inexpensive, easy to control and minimizing side reactions. Moreover, the visible light can be nontoxic. The examples of photochemical reagents are anthracyl derivatives and pyrenyl derivatives.

In 1993, Kumar and Tolosa (Kumar; & Tolosa. 1993: 13914-13919) synthesized anthracyl derivatives; ((9-anthryl) methylamine hydrochloride (AMAC), 3-(9-anthryl) propylamine hydrochloride (APAC) and *N*-ethyl-(9-anthryl) methylamine hydrochloride (*N*-Et-AMAC)) (Figure 28) and pyrenyl derivative; (4(1-pyrenyl) butylamine chloride (PBAC)) (Figure 29) for study of binding interaction with proteins. The results showed that pyrenyl derivative bound to protein better than anthracyl derivative with higher binding constant.

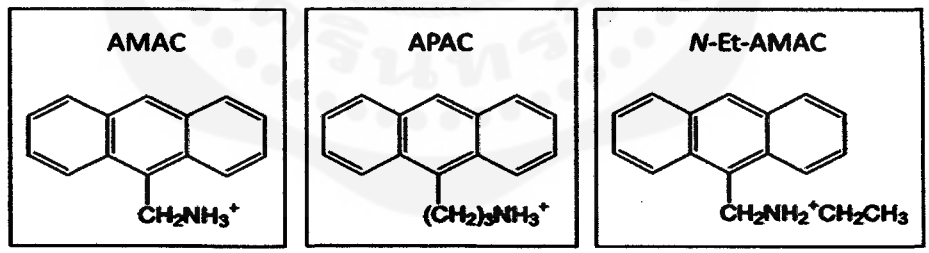


Figure 28 The structure of anthracyl derivatives.

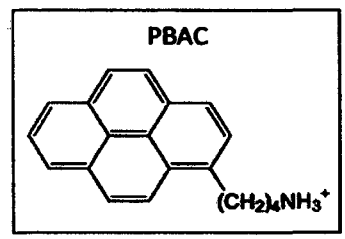


Figure 29 The structure of 4(1-pyrenyl) butylamine chloride (PBAC).

In 1997, Kumar and Buranaprapuk (Kumar; & Buranaprapuk. 1997: 2085-2087) designed and synthesized pyrenyl derivative by connecting L-phenylalannine to pyrenyl chromophore (*N*-(L-phenylalanine)-4(1-pyrene) butyramide (Py-L-Phe)) (Figure 30). Py-L-Phe was found to cleave BSA (between Leu346-Arg347) and chicken egg-white lysozyme (between Trp108-Val109) in the presence of an electron acceptor, Co(III)hexammine chloride (CoHA).

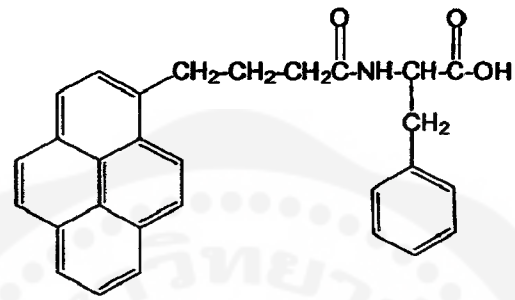


Figure 30 The structure of Py-L-Phe.

The design of Py-L-Phe has to be taken into consideration of protein structure. Most globular proteins display hydrophilic residues on the outside and hydrophobic residues at the inside. Therefore, Py-L-Phe consists of hydrophobic part, a suitable chromophore that can bind in the hydrophobic clefts of the protein (Py), and hydrophilic part with an ionic group (COOH) which can bind to the charged residues on the surface of the protein. This probe showed high binding affinities for binding to BSA ($2.2 \pm 0.3 \times 10^5$ M^{-1}) and lysozyme ($6.5 \pm 0.4 \times 10^7$ M^{-1}) (Kumar; et al. 1998: 10361-10366) (Figure 31).

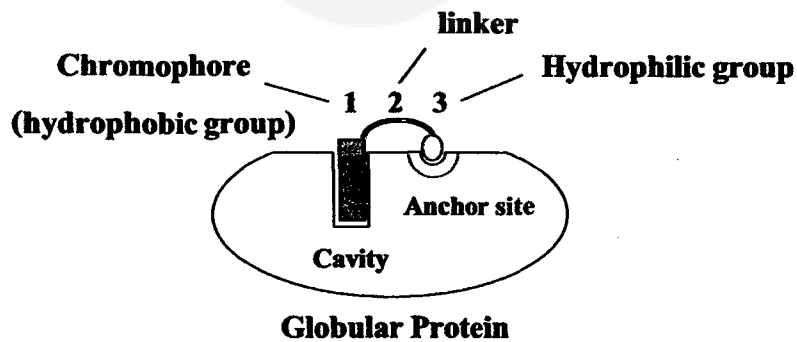


Figure 31 Binding of reagents to globular proteins.

In 1999, Kumar and Buranaprapuk (Kumar; & Buranaprapuk. 1999: 4262-4270) has studied the role of the distance between the hydrophobic chromophore and the hydrophilic group on the specificity of the protein photocleavage. Glycine residue was used to vary the linker length. These pyrenyl probes are Py-$(Gly)_n$-Phe (n = 0, 1, 2) (Figure 32). All of the pyrenyl probes (Py-$(Gly)_n$-Phe (n = 1, 2) cleaved lysozyme at 2 positions: between Trp108-Val109 (major cleavage site) and between Ala110-Trp111 (minor cleavage site).

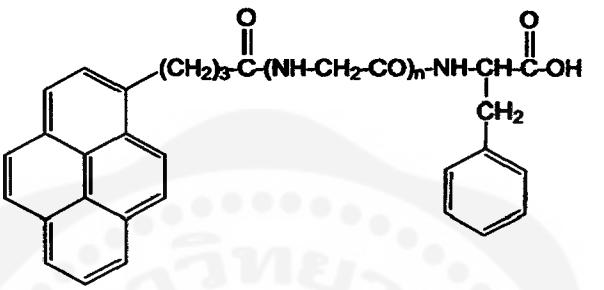


Figure 32 The structure of Py-$(Gly)_n$-Phe (n = 0, 1, 2).

In 2002, Kumar and coworkers (Kumar; et al. 2002: 5810-5815) investigated the cleavage mechanism by Laser flash photolysis. The study showed the absorption peak of pyrene cation radical (Py-L-$Phe^{+\bullet}$) at ~460 nm when Py-L-Phe was excited by light with CoHA as an electron acceptor (equation 24).

$$\text{Py-L-Phe} \xrightarrow{h\nu} \text{Py-L-Phe}^{*} \xrightarrow[-\text{CoHA}^{-\bullet}]{\text{CoHA}} \text{Py-L-Phe}^{+\bullet} \qquad \text{--- [24]}$$

The hydrogen atom at α-carbon on the peptide backbone was abstracted by Py-L-$Phe^{+\bullet}$ to produce α-carbon radical. Then, oxygen was attached to the α-carbon radical, resulting to hyperoxyl radical, followed by hydrolysis of the peptide backbone (Figure 33).

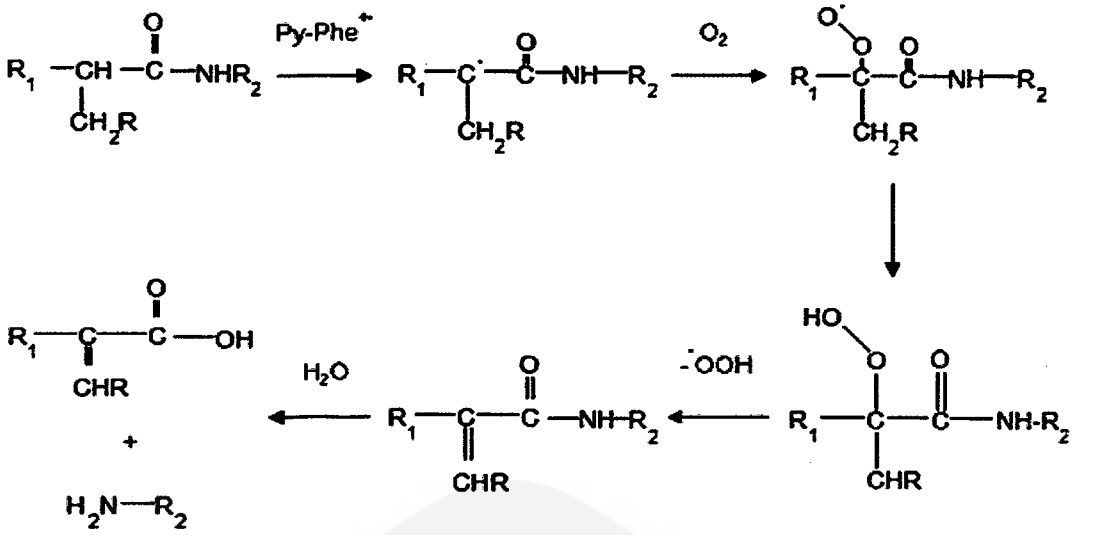


Figure 33 The possible mechanisms of protein cleavage.

In 2011, Malaikaew and coworkers (Malaikeaw; et al. 2011: 251-255) designed a new pyrenyl probe, (d-biotinyl-1(1-pyrene)methylamide (Py-biotin) (Figure 34), by coupling of d-biotin to 1(1-pyrene)methylamine hydrochloride. Binding of Py-biotin to the specific site of avidin was expected. When a mixture of avidin, Py-biotin and an electron acceptor, cobalt(III)hexamine chloride (CoHA), was irradiated at 342 nm, the photocleavage of avidin (between Thr77 and Val78) was achieved.

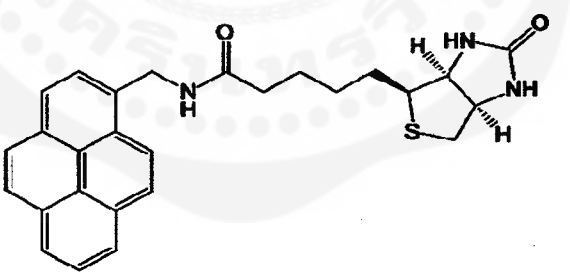
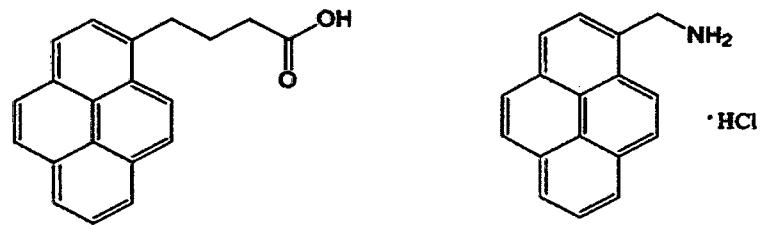


Figure 34 The structure of Py-biotin.

From the literatures, Pyrene (Figure 35) has been of interest since it has strong absorption bands in the near visible region with long lived singlet excited states that are convenient to initiate the photoreactions. Moreover, pyrene is hydrophobic, which can be expected to bind to hydrophobic sites of the protein.



1-Pyrenebutyric acid (PBA) 1-Pyrenemethylamine (PMA)

Figure 35 The structures of 1-pyrenebutyric acid (PBA) and 1-pyrenemethylamine (PMA).

In this research, succinic acid (Figure 36) is proposed to attach to the pyrenyl chromophore for specific binding to protein. Succinic acid is a common metabolite formed by plants, animals and microoganisms. It has been used in industries for producing food, polymers, flavours, surfactants and used as a precursor for many industrially important chemicals, such as adipic acid, 2-pyrrolidinone, 1,4-butanediol, which are used in the pharmacological industry.

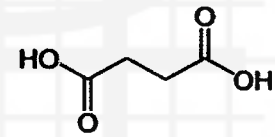


Figure 36 The structure of succinic acid.

In 1999, Zeikus and coworkers (Zeikus; et al. 1999: 545-552) reported map of the routes leading to succinic acid based products and specialty chemicals (Figure 37). The structure of succinic acid contains a linear saturated dicarboxylic acid, that can be used as an intermediate chemical and be converted to 1,4-butanediol, tetrahydrofuran, γ-butyrolactone and other four-carbon chemicals.

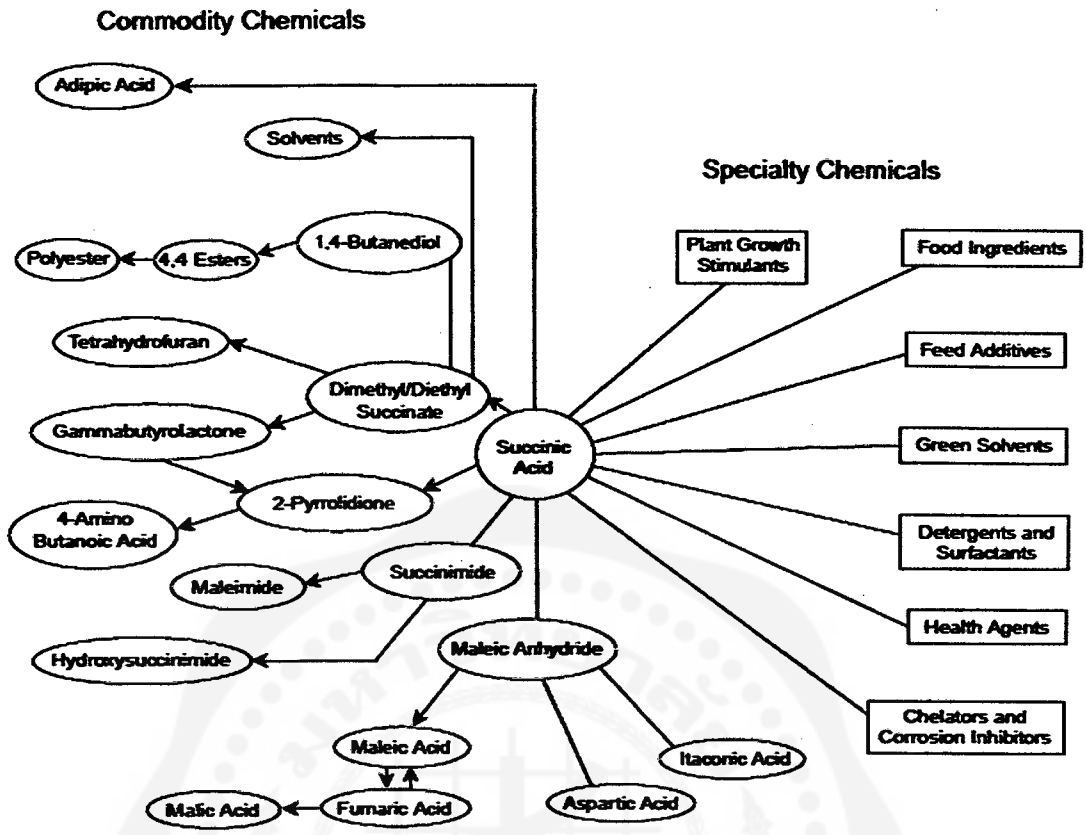


Figure 37 Applications of succinic as a precursor of many industrially chemicals.

Source: Zeikus, J. G.; et al. (1999). Biotechnology of Succinic Acid Production and Markets for Derived Industrial Products. *Applied Microbiology and Biotechnology.* 51: pp. 545-552.

Therefore, the new chemical reagents, such as PMA-succinic acid (Figure 38), have been designed and synthesized in this study. Binding to the protein and photocleavage of the protein by the new designed reagents were studied.

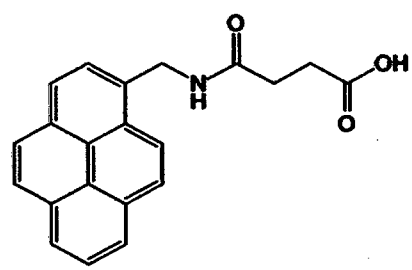


Figure 38 The structure of PMA-succinic acid.

Moreover, the new photochemical reagents were developed by tuning the side chain length with three or five-carbon spacers (PMA-1A and PMA-3A) (Figure 39). PMA-1A and PMA-3A were synthesized for comparison with PMA-2A (another name of PMA-succinic acid).

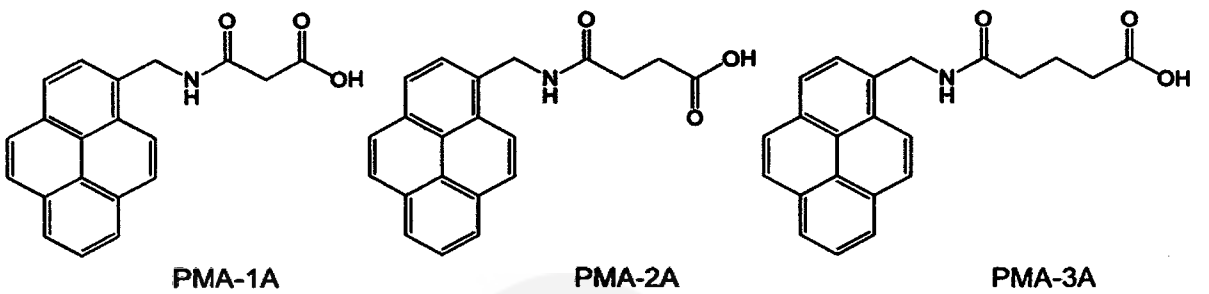


Figure 39 The structure of PMA-1A, PMA-2A and PMA-3A.

However, using another compound, such as natural products, instead of pyrene probe more friendly to the environment. Berberine, piperine and their derivatives are of interest in this study.

Berberine (Figure 40) is a quaternary ammonium salt, derived from the protoberberine group of isoquinoline alkaloid, which has various therapeutic potential. Berberine is usually found in the roots, rhizomes, stems, and bark of plants. The pharmacological activities of berberine as antihypertensive, anti-inflammatory, hepatoprotective, antioxidant and antidepressant have been demonstrated (Mohind; et al. 2017: 350-355).

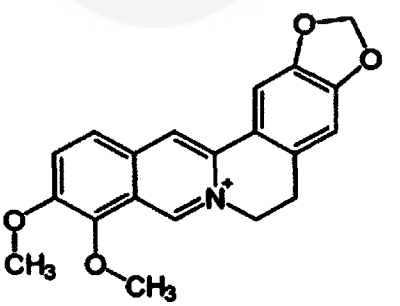


Figure 40 The structure of berberine.

In 1999, Naasani and coworkers (Naasani; et al. 1999: 4004–4011) reported berberine chloride, an alkaloid found in many plants, as a moderate inhibitor for telomerase with 50% inhibition at 30 μM (Figure 41) using the telomeric repeat amplification protocol (TRAP) assay with cellular lysates from a representative human cancer cell line.

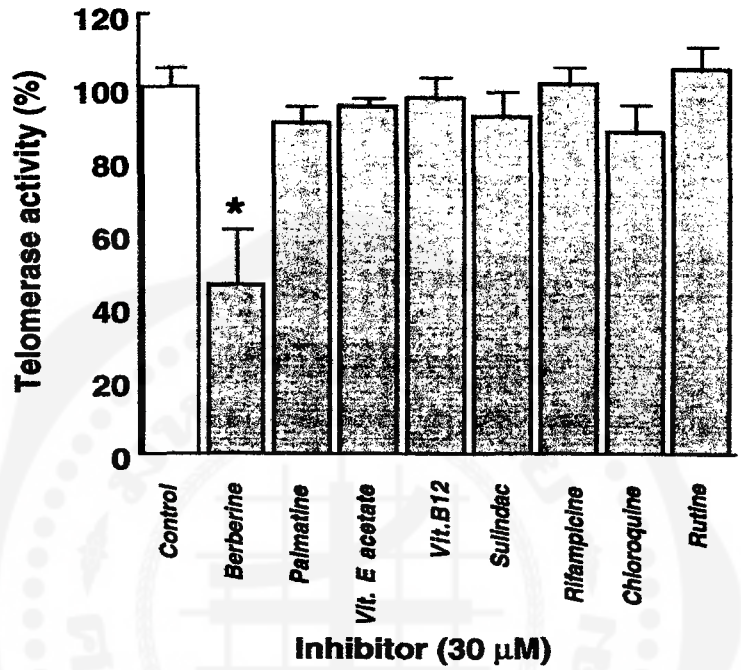


Figure 41 Effect of berberine chloride (30 μM) to the activity of telomerase.

Source: Naasani, I.; et al. (1999). FJ5002: A Potent Telomerase Inhibitor Identified by Exploiting the Disease-oriented Screening Program with COMPARE Analysis. *Cancer research.* 59: pp. 4004-4011.

In 2002, Sriwilaijareon and coworkers (Sriwilaijareon; et al. 2002: 99-103) confirmed inhibition of *Plasmodium falciparum* telomerase by the plant alkaloid, in a range of 30-300 μM berberine (Figure 42). *P. falciparum* telomerase activity was completely eliminated at 370 μM berberine. *P. falciparum* telomerase activity was studied using the TRAP assay.

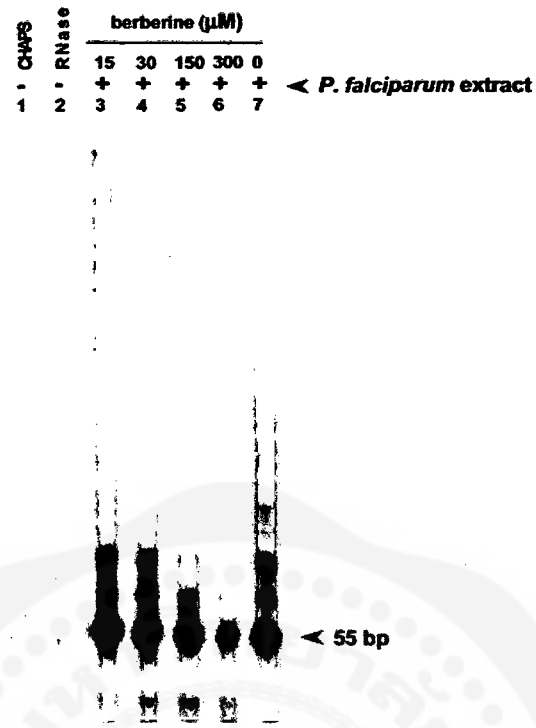


Figure 42 The activity of *P. falciparum* telomerase was inhibited by berberine.

Source: Sriwilaijareon, N.; et al. (2002). Stage Specificity of *P. falciparum* Telomerase and its Inhibition by Berberine. *Parasitology International.* 51: pp. 99-103.

Piperine (Figure 43) is one of the naturally alkaloid, a compound present in fruits of Piper nigrum and Piper longum, commonly known as 'Black pepper' and 'Long pepper', respectively. Piperine has variety of pharmacological activity including antidepressant, antipyretic, analgesic, hepatoprotective, antioxidant, and anti-inflammatory.

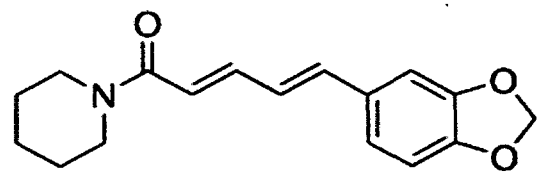


Figure 43 The structure of piperine.

In 2010, data collection of Jemal and coworkers (Jemal; et al. 2010: 277-300) demonstrated prostate cancer in men, with 32,050 deaths of this disease.

In 2013, Samykutty and coworkers (Samykutty; et al. 2013: e65889) investigated the anti-tumor mechanisms of piperine on androgen dependent (LNCaP) and androgen independent (PC-3, 22Rv1, DU-145) prostate cancer cells. All cells were treated with piperine (5–200 μM) for 24, 48 and 72 hours by MTT assay. Piperine inhibited both androgen dependent (AD) LNCaP and androgen independent (AI) PC-3, 22RV1, DU-145 prostate cancer cells (Figure 44).

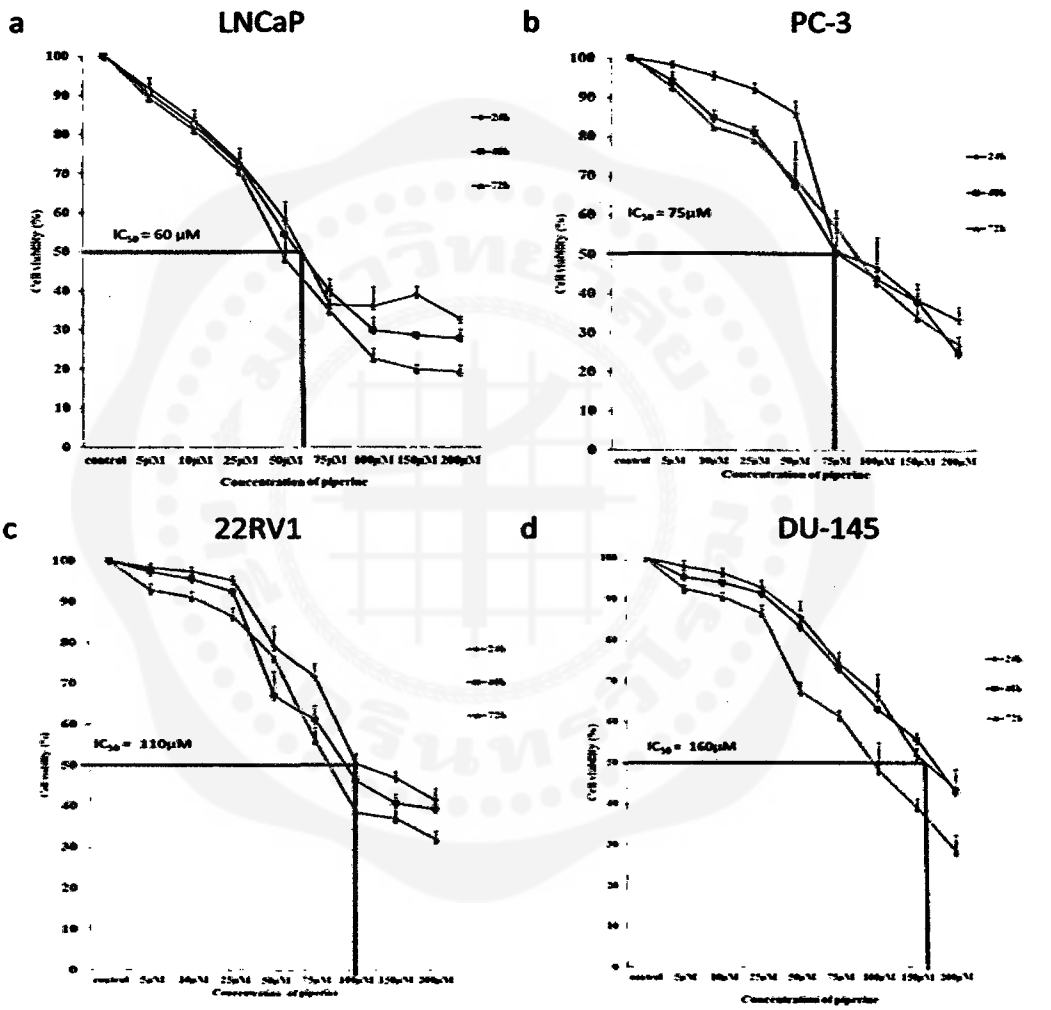


Figure 44 Piperine (5–200 μM) inhibits of (a) LNCaP (b) PC-3 (c) 22RV1 (d) DU-145 in prostate cancer cells for 24 h. (blue line), 48 h. (red line) and 72 h. (green line).

Source: Samykutty, A.; et al. (2013). Piperine, a Bioactive Component of Pepper Spice Exerts Therapeutic Effects on Androgen Dependent and Androgen Independent Prostate Cancer Cells. *PLoS ONE*. 8: pp. e65889.

The cleavage of poly-(ADP-Ribose) polymerase-1 (PARP-1) proteins in LNCaP and DU-145 prostate cancer cells were achieved. Control and cell treated with DMSO were demonstrated in Figure 45.

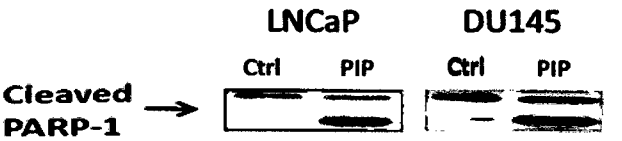


Figure 45 Western blotting analysis, PARP-1 of LNCaP and DU-145 in prostate cancer cells were cleaved by concentration of piperine 60 µM and 160 µM respectively for 24 h.

In 2013, Do and coworkers (Do; et al. 2013: 2591-2599) showed that piperine significantly inhibited proliferation in HER2-overexpressing SKBR3 human breast cancer cell line. SKBR3 were treated with piperine at various concentrations (0-50 µM) for 24 h, 48 h and 72 h (Figure 46). Cell proliferation decreased when increasing time and concentration of piperine.

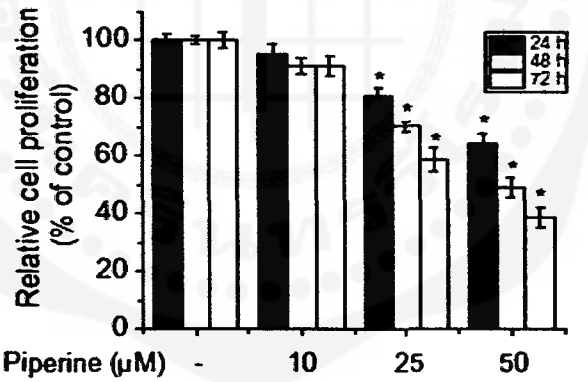


Figure 46 The effects of piperine on cell proliferation in SKBR3 breast cancer cells at various concentration of piperine (0-50 µM) in a time-dependent manner.

Source: Do, M. T.; et al. (2013). Antitumor efficacy of piperine in the treatment of human HER2-overexpressing breast cancer cells. *Food Chemistry.* 141: pp. 2591–2599.

Therefore, the development of new synthesized chemical reagents and natural products were focused in this research. Interaction of these reagents with proteins were studied using UV-Vis, fluorescence, gel electrophoresis and docking methods.

CHAPTER 3

Experimental

1. Equipments

- precision analytical balance digital scale, Mettler Toledo, code AB104-S
- magnetic stirrer, GEM, code MS-115
- TLC plate, Merck
- rotary evaporator, Buchi, code R-210
- melting point apparatus, Griffin
- micropipette (2, 10, 20, 100, 200 and 1000 µl), Gilson
- pH meter, Mettler Toledo
- cavitator ultrasonic cleaner, Mettler Electronics Corp.
- laboratory freeze dryer, Provac, code RFD-8
- blot filter paper, BIO-RAD
- Sequi-Blot™ PVDF membrane (2 µm), BIO-RAD
- Mini Trans-Blot® electrophoretic transfer cell, BIO-RAD
- SDS-PAGE apparatus, BIO-RAD
- UV-spectrophotometer, Shimadzu, code UV-2401 PC
- fluorescence spectrophotometer, Jasco, code FP-6200 PC
- Spectroline, Spectronics Corporation, code ENF-240C

2. Chemical reagents

- 1-pyrenemethylamine hydrochloride (PMA), Sigma-Aldrich
- succinic anhydride, 99%, Acros Organics
- ethyl malonyl chloride, 97%, TCI
- gutaric anhydride, 95%, Sigma-Aldrich
- sodium hydroxide (NaOH), Carlo Erbra
- *N,N*-dimethylformamide (DMF), Carlo Erbra
- hydrochloric acid (HCl), QRëC™ Quality Reagent Chemical
- acetic acid, Carlo Erbra
- acetonitrile (ACN), Merck

- acetone, Carlo Erbra
- dichloromethane (DCM), Carlo Erbra
- methanol, Carlo Erbra
- n-hexane, Carlo Erbra
- amino acids, Sigma-Aldrich
- proteins (avidin, lysozyme, α-chymotrypsin, β-lactoglobulin B, myoglobin, bovine serum albumin (BSA), Human serum albumin (HSA), α-casein, pepsin, concanacalin A and β-glucosidase), Sigma-Aldrich
- 1-butanol, Carlo Erbra
- berberine, Sigma-Aldrich
- piperine, Sigma-Aldrich
- acrylamide, Plusone
- methylenebisacrylamide, Plusone
- glycerol, Fluka
- ammonium persulfate, Sigma-Aldrich
- tetramethylethylenediamine (TEMED), Sigma-Aldrich
- cobalt(III)hexammine chloride (CoHA), Sigma-Aldrich
- Coomassie Blue R-250, Sigma-Aldrich
- cyclohexylaminopropane sulfonic acid (CAPS), Sigma-Aldrich
- Trizma® base, SAFC
- Trizma® hydrochloride, Sigma-Aldrich
- tricine, Sigma-Aldrich
- sodium dodecyl sulfate (SDS), Sigma-Aldrich
- Mark12™ MW standard, Invitrogen
- bromophenol blue, Plusone
- 2-mercaptoethanol, Merck
- pyridine, Carlo Erbra

3. Methods

3.1 Synthesis of photochemical reagents

Synthesis of PMA-1A: A mixture of 1(1-pyrene) methylamine hydrochloride (PMA) (50.1 mg) and a pellet of sodium hydroxide (NaOH) (104.2 mg) was dissolved by acetonitrile (ACN) 5 ml. After that, ethyl malonyl chloride ($C_5H_7ClO_3$) (45 µl) was added, and the mixture solution was stirred continuously for 3 hours at 40 °C. After heating, precipitate and salt (NaCl) occurred in the mixture solution. Water was then added and the solution was acidified to pH 1-2 by 5 M hydrochloric acid (HCl). The product was separated out by extraction using pure dichloromethane (DCM). The product solution was evaporated to dryness under vacuum and the residue was recovered to afford pure product (PMA-1A).

Synthesis of PMA-2A: PMA-2A was synthesized by coupling of PMA (100.0 mg) to succinic anhydride (56.0 mg), with addition of NaOH (101.5 mg) in *N,N*-dimethylformamide (DMF) 6 ml. The mixture was stirred at room temperature for 24 hours. The reaction progress was monitored by TLC. The mixture solution was acidified with 5 M HCl to pH 1-2. After cooling, the resulting precipitate was collected by filtration, dried and identified by spectroscopic techniques.

Synthesis of PMA-3A: PMA (30.4 mg) was dissolved in pyridine 3 ml until clear yellow solution was obtained. Gutaric anhydride (31.6 mg) was added to the solution, with continuous stirring at room temperature for 24 hours. Water was then added and the solution was acidified to pH 1-2 by 5 M HCl. The product was separated out by extraction using pure DCM.

3.2 Protein photocleavage

The mixture solution of protein (15 µM), photochemical reagent (15 µM), and CoHA (1 mM), in 50 mM Tris–HCl buffer, pH 7.0 (total volume 200 µl) was irradiated at room temperature for 20 min (342 nm; using a 150 W xenon lamp) (Table 6). The control solution was prepared under the same conditions, except that the solutions was protected from light. All irradiated samples were dried until dryness under vacuum using freeze dryer. Time of irradiation was optimized to obtain higher efficiency protein cleavage (Table 7).

Table 6 Conditions of photocleavage reaction.

order	probe	protein	CoHA	Tris-HCl buffer, pH 7.0	condition
1	✓	✓	✓	✓	control
2	✓	✓	✓	✓	Irradiation at 342 nm for 20 min
3	-	✓	-	✓	control
4	-	✓	-	✓	Irradiation at 342 nm for 20 min
5	-	✓	✓	✓	control
6	-	✓	✓	✓	Irradiation at 342 nm for 20 min
7	✓	✓	-	✓	control
8	✓	✓	-	✓	Irradiation at 342 nm for 20 min

Table 7 Variation of irradiating time for photocleavage reaction.

order	probe	protein	CoHA	Tris-HCl buffer, pH 7.0	condition
1	✓	✓	✓	✓	control
2	✓	✓	✓	✓	Irradiation at 342 nm for 1 min
3	✓	✓	✓	✓	Irradiation at 342 nm for 5 min
4	✓	✓	✓	✓	Irradiation at 342 nm for 10 min
5	✓	✓	✓	✓	Irradiation at 342 nm for 15 min
6	✓	✓	✓	✓	Irradiation at 342 nm for 20 min

3.3 Sodium dodecyl sulfate-polyacrylamide gel electrophoresis (SDS-PAGE)

All dried samples were redissolved in loading buffer (glycerol (1.2 ml), sodium dodecyl sulfate (7% w/v), Tris–HCl (50 mM, pH 6.8), bromophenol blue (0.01% w/v) and 2-mercaptoethanol (2%, v/v)). All solutions were heated for 3 min in loading buffer. The sample solutions (8 µl) were loaded to the gel. The gel was run by applying 60 V until the protein bands passed through the stacking gel, and then the voltage was increased to 110 V in running gel. After that, the gels were stained with Coomassie brilliant blue for 12 hours, and destained in acetic acid (10%, v/v) for 12 hours. The gels were scanned with an Epson scanner (TX220), and the product yields were quantitated using ImageJ program. Molecular

weight markers were loaded in each gel for calibration and molecular weight of each fragments could be estimated from their mobility by linear regression equation of this calibration curve.

3.3.1 Cathode buffer solution (5X), 500 ml

Trizma® base	6.05	g
tricine	8.96	g
SDS	0.50	g

Mixture of Trizma® base, tricine and SDS was dissolved in deionized water. Then, the volume of the mixture solution was adjusted to 500 ml with deionized water.

3.3.2 Anode buffer solution (5X), 500 ml

Trizma® base	12.20	g

Trizma® base was dissolved in deionized water. Then, the pH was adjusted to 8.9 by 5 M HCl. The volume of the solution was adjusted to 500 ml with deionized water.

3.3.3 Gel buffer solution, 50 ml

Trizma® base	36.32	g
SDS	0.30	g

Mixture of Trizma® base and SDS was dissolved in deionized water (40 ml) and the mixture was heated until all solid was dissolved. The pH of the solution was then adjusted to 8.45 by 5 M HCl. The volume of the solution was adjusted to 50 ml with deionized water.

3.3.4 Acrylamide/bisacrylamide solution, 50 ml

acrylamide	23.25	g
bisacrylamide	1.50	g

Mixture of acrylamide and bisacrylamide was dissolved in deionized water (40 ml) and the mixture was heated until solid all was dissolved. The volume of the mixture solution was then adjusted to 50 ml with deionized water.

3.3.5 Loading buffer solution, 100 ml

SDS	0.07	g
glycerol	40	µl
bromophenol blue	0.0001	g
50 mM Tris-HCl buffer, pH 6.8	960	µl
2-mercaptoethanol	20	µl

Mixture of SDS, glycerol, bromophenol blue and 2-mercaptoethanol was dissolved in 50 mM Tris-HCl buffer (pH 6.8).

3.3.6 Staining solution, 100 ml

0.5% coomassic blue	10	ml
methanol	50	ml
acetic acid	10	ml

Coomassie blue (0.5%), methanol and acetic acid and were mixed, and the volume was adjusted to 100 ml with deionized water.

3.4 Western blot (protein transfer)

For sequencing analysis, protein fragments on the gel were transferred to PVDF membrane by applying the electricity (60 mA) for 1.5 h using the Wet/Tank Blotting Systems (BIORAD). Blotting filter paper (2 sheets), fiber pad (2 sheets), a gel, and a polyvinylidene fluoride (PVDF) membrane were soaked in CAPS buffer, pH 10.5, for 10-15 min before setting equipment. The equipment was installed as shown in Figure 47. Blotting was performed by applying voltage of 60 V, 140 mA, for 90 min. After that, peptide fragments on PVDF membrane were stained with Coomassie brilliant blue for 5 min, and destained with 10% acetic acid for 1 min. PVDF membrane was then dried until dryness. The peptide fragments were sent to Midwest Analytical, Inc., MO, USA for amino acid sequence analysis.

3.4.1 CAPS buffer solution (100 mM, pH 10.5), 1000 ml

CAPS	22.13	g

CAPS was dissolved in deionized water. Then, the pH of the solution was adjusted to 11.0 by NaOH. The volume of the solution was adjusted to 1000 ml with deionized water.

3.4.2 Staining solution for polyvinylidene fluoride membrane, 100 ml

Coomassic blue	0.1	g
methanol	45	ml
acetic acid	10	ml

Coomassie blue, methanol and acetic acid were mixed in deionized water with stirring until all solid was dissolved. The volume was then adjusted to 100 ml with deionized water.

3.4.3 Destaining solution for polyvinylidene fluoride membrane, 100 ml

methanol	45	ml
acetic acid	10	ml

Methanol and acetic acid were mixed and the volume of the solution was adjusted to 100 ml with deionized water.

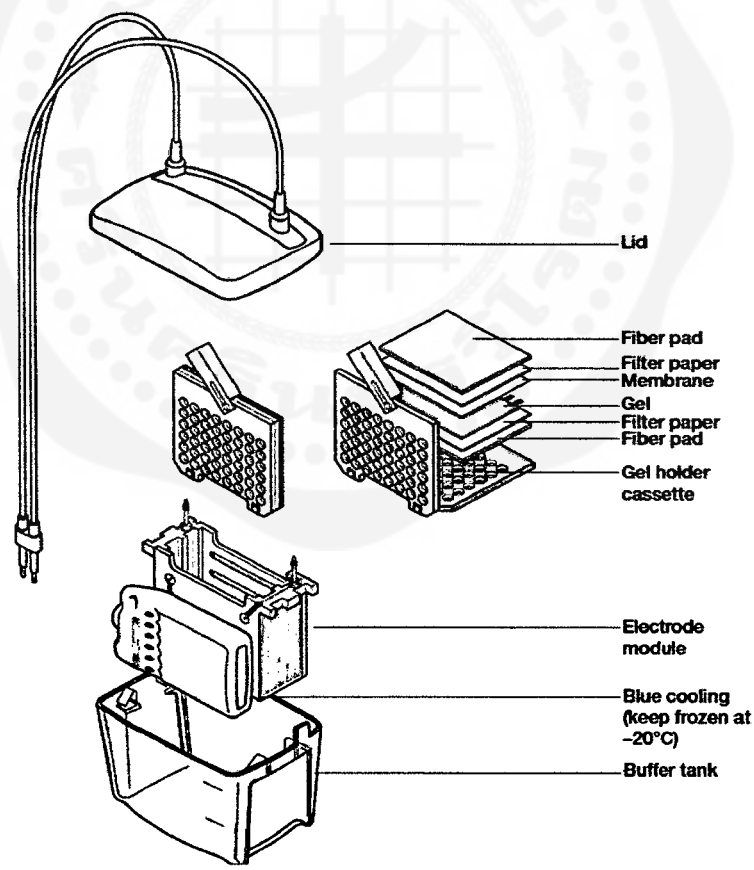


Figure 47 Mini Trans-Blot Electrophoretic Transfer Cell.

Source: BIO-RAD Instruction Manual. (2015). (online).

3.5 Absorption titration and fluorescence titration

The absorption spectra of new photochemical reagent (10 μM), with the presence of the protein (0-100 μM) in 50 mM Tris-HCl buffer, pH 7.0 were recorded in the range of 300-400 nm on a Shimadzu UV-2401 PC UV-VIS spectrophotometer. The binding constant was calculated by Scatchard equation (discussed in Chapter 2). In fluorescence spectroscopic measurements, new photochemical reagent concentration was fixed at 0.5 μM while the protein concentration was varied (1-20 μM). The fluorescence were monitored in the range of 350-550 nm on a Jasco FP-6200 spectrofluorometer. The fluorescence emission of new photochemical reagent was monitored at 375 nm with excitation wavelength at 342 nm.

3.6 Fluorescence quenching studies

The probe-protein mixtures (0.5 μM: 10 μM) were titrated with CoHA (0-1 mM), and the fluorescence intensities were monitored in the range of 350-550 nm with excitation at 342 nm, in 50 mM Tris–HCl buffer, pH 7.0. The data can be fitted to Stern–Volmer equation (discussed in Chapter 2) and the Stern-Volmer quenching constant (K_{sv}) could be obtained from the slope of the graph.

3.7 Docking studies

The crystal structures of avidin (1AVD.pdb) and lysozyme (4PHI.pbd) were downloaded from the Protein Data Bank. All of probe structures were optimized by Gaussian 03 at HF/3-21G level of calculation to obtain the most stable conformation of these probes with appropriate bond lengths and angles. The AutoDock 4.2 was used to calculate the interaction energy for searching a suitable location of photochemical reagent to the protein. The dimensional size of the docking box was set at 100 x 100 x 100 Å with the spacing of 0.375 Å. The center of grid box was located at the center of macromolecule with the coordination center (x, y and z) of 32.226, 13.557 and 26.976 in case of avidin, whereas in case of lysozyme, the center of grid box was located at the center on macromolecule with the coordination center (x, y and z) of -19.882, 1.023 and -0.562. The size of grid box was the defined area of the interaction between amino acid residues of protein with photochemical reagent. Therefore, protein was covered by the grid box for enhancing opportunity of interaction between photochemical reagent with the protein. The docking results were illustrated by Accelrys Discovery Studio Client 2.5 to visualize the three-dimensional structure of the protein with the bound photochemical reagent.

CHAPTER 4

Results and Discussion

In this research, we focus on the development of the new synthesized photochemical reagents and natural products for converting larger protein into smaller fragments, understanding protein-ligand interactions, structure-activity studies of protein, investigating drug binding sites in proteins and design of novel therapeutic drugs. The interactions of these photochemical reagents and natural products with proteins were investigated using UV-Vis, fluorescence, gel electrophoresis and docking techniques. The outline for the study is as following:

1. Photochemical reagents
    - 1.1 Synthesis and characterization of new photochemical reagents.
    - 1.2 Protein photocleavage by new photochemical reagents.
    - 1.3 Protein transfer by western blot for amino acid sequencing analysis.
    - 1.4 The interactions of new photochemical reagents with proteins.
        - binding interaction
        - fluorescence quenching studies
    - 1.5 Binding mechanism of new photochemical reagents with the proteins.
2. Natural products
    - 2.1 Protein photocleavage by natural products.
    - 2.2 Protein transfer by western blot for amino acid sequencing analysis.
    - 2.3 Binding interactions of natural products with proteins.
    - 2.4 Binding mechanism of natural products with the proteins.

1. Photochemical reagents

1.1 Synthesis and characterization of new photochemical reagents

Synthesis of PMA-1A

The product of PMA-1A is yellowish amorphous powder (48 mg, 80.10%) with m.p. of 160-163 °C. The product was identified using ^{1}H NMR and mass spectrometry. ^{1}H NMR (300 MHz; d_6-DMSO): 12.5 (1H, s, OH), 8.8 (1H, t, NH), 8.0–8.4 (9H, m, ArH), 5.00 (2H, d, $ArCH_2$), 3.4 (2H, s, $COCH_2$) (Figure 48); MS (ES): m/z (%) 318.1 (100) $[M+H]^+$.

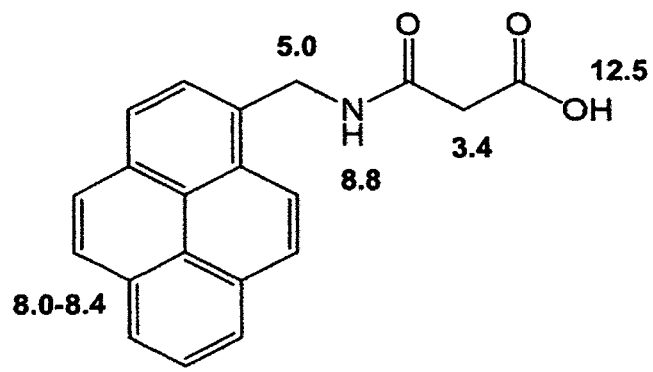
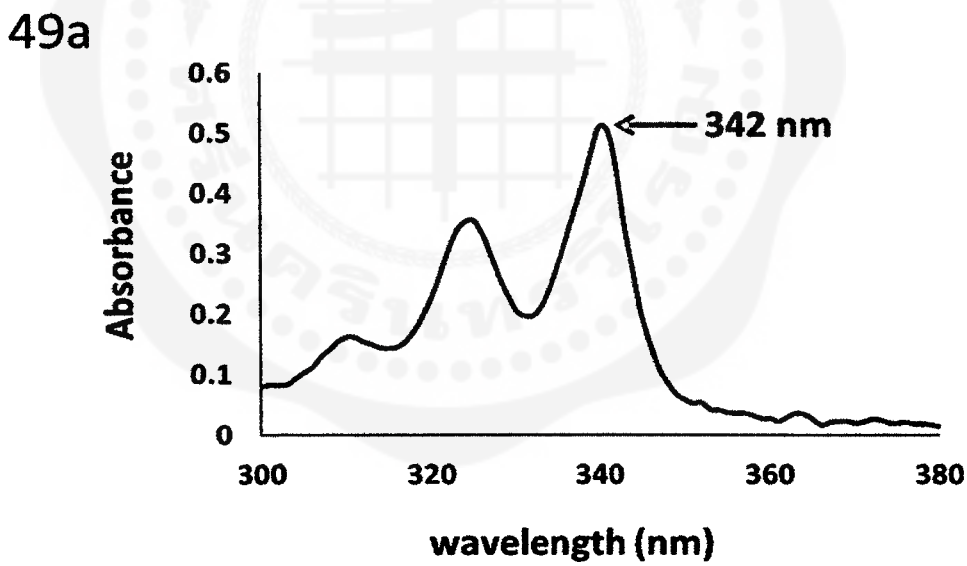


Figure 48 Characterization of PMA-1A by ^{1}H NMR.

The maximum absorption wavelength of PMA-1A was 342 nm (Figure 49a). Molar extinction coefficient (ε) of PMA-1A was 4.73×10^{4} M^{-1} cm^{-1} (Figure 49b). The fluorescence emission of PMA-1A was monitored at 375 nm with excitation wavelength of 342 nm (Figure 49c).



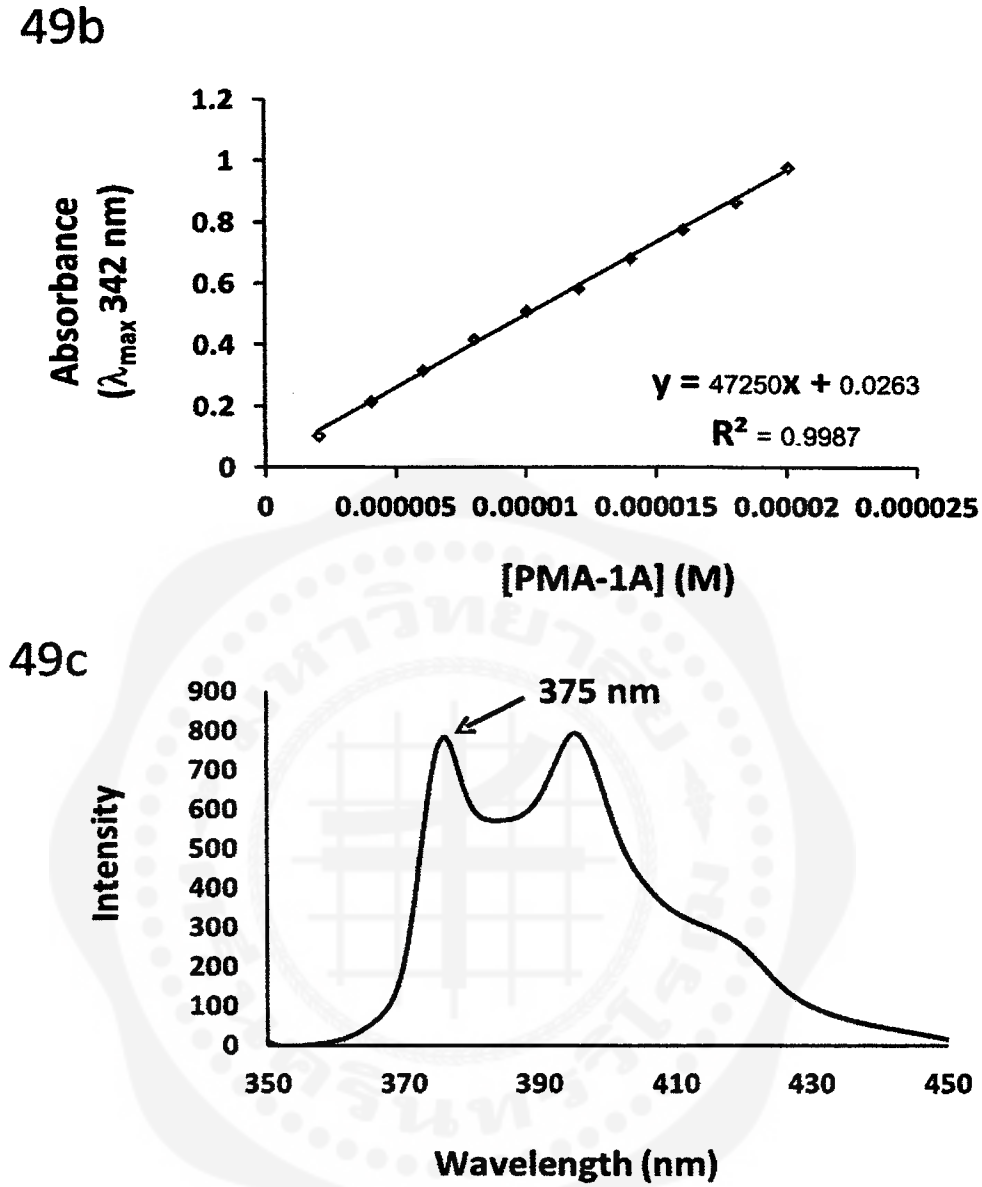


Figure 49 (a) Absorption spectrum of PMA-1A (10 μM) with the maximum wavelength of 342 nm. (b) The linear plot of PMA-1A absorbance at 342 nm versus [PMA-1A] (2-20 μM) with linear dependent coefficient (R^2) of 0.9987. (c) Fluorescence spectrum of PMA-1A (0.5 μM) with excitation wavelength at 342 nm. All data were from the average of three experiments.

Synthesis of PMA-2A

The product of PMA-2A was yellow powder (74 mg, 59.68%) with m.p. of 208–209 °C. PMA-2A was characterized by ^{1}H NMR, mass spectroscopy, UV–VIS and fluorescence. ^{1}H NMR (300 MHz; d_6-DMSO): 8.5 (1H, t, NH), 8.0–8.4 (9H, m, ArH), 5.0 (2H, d, $ArCH_2$), 2.4–2.6 (4H, m, 2×$COCH_2$) (Figure 50); MS (ES): m/z (%) 331.3 (100) $[M+H]^+$.

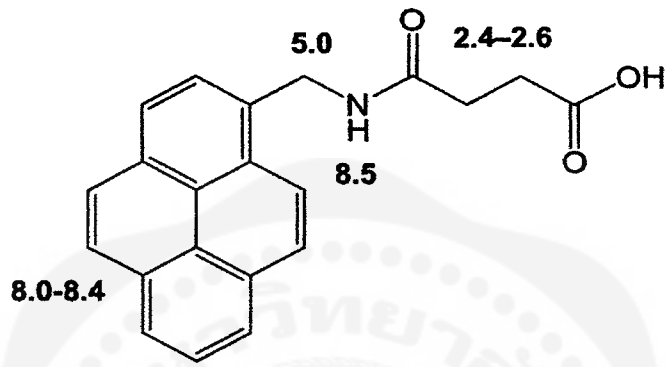
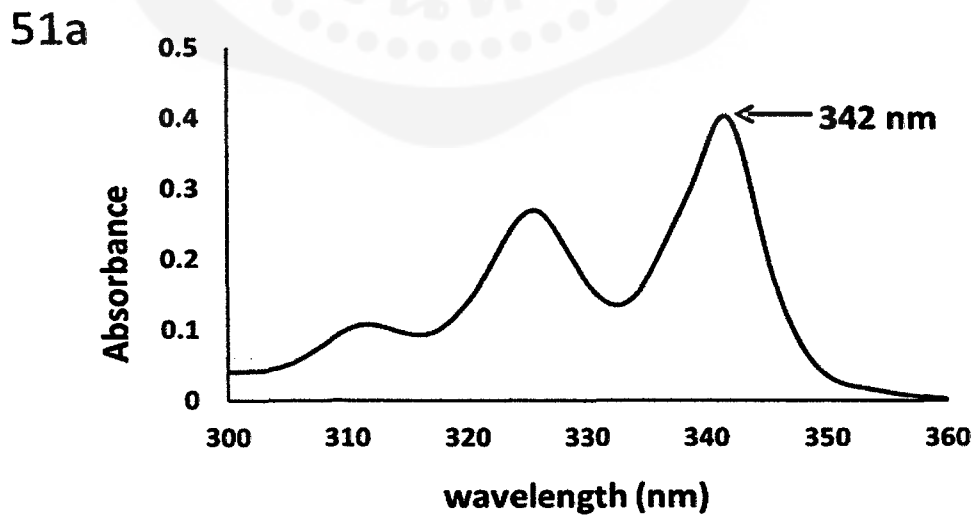


Figure 50 Characterization of PMA-2A by ^{1}H NMR.

The maximum absorption wavelength of PMA-2A was 342 nm (Figure 51a). Molar extinction coefficient (ε) of PMA-2A was 2.83 × 10^4 M^{-1} cm^{-1} (Figure 51b). The fluorescence emission of PMA-2A was monitored at 375 nm with excitation wavelength of 342 nm (Figure 51c).



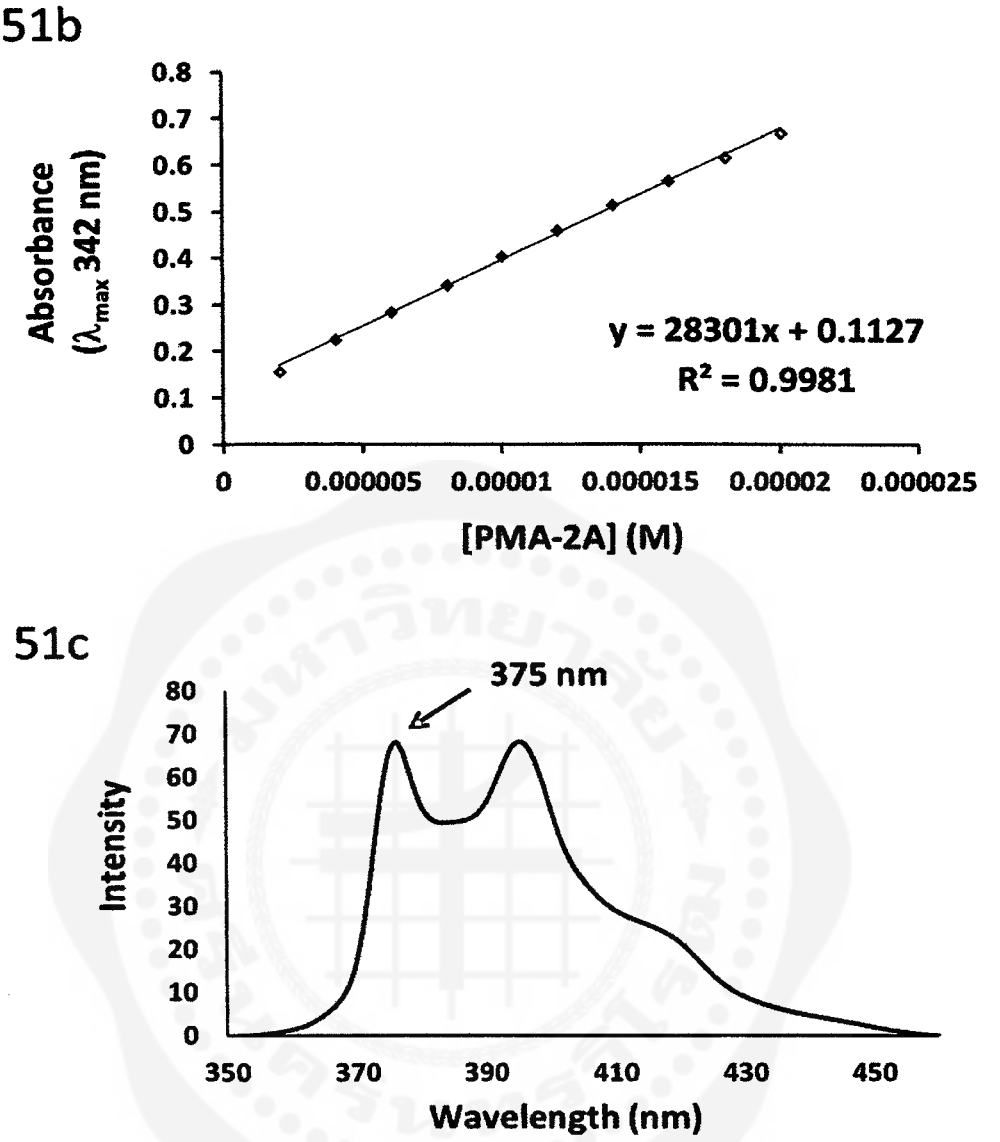


Figure 51 (a) Absorption spectrum of PMA-2A (10 μM) with the maximum wavelength of 342 nm. (b) The linear plot of PMA-2A absorbance at 342 nm versus [PMA-2A] (2-20 μM) with linear dependent coefficient (R^2) of 0.9981. (c) Fluorescence spectrum of PMA-2A (0.5 μM) with excitation wavelength at 342 nm. All data were from the average of three experiments.

Synthesis of PMA-3A

The product of PMA-3A was yellowish amorphous powder (26 mg, 66.67%) with m.p. of 160–161 °C. The product was characterized using UV-Vis, fluorescence, NMR and mass spectrometry. ^{1}H NMR (300 MHz; d_6-DMSO): 8.5 (1H, t, NH), 8.0-8.4 (9H, m, ArH), 5.0 (2H, d, $ArCH_2N$), 2.2-2.3 (4H, m, $2\times COCH_2$), 1.8-1.9 (2H, m, CH_2) (Figure 52); MS (ES): m/z (%) 346.1 $[M+H]^+$.

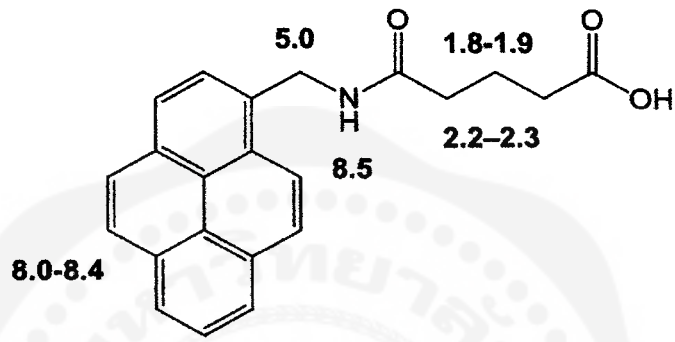
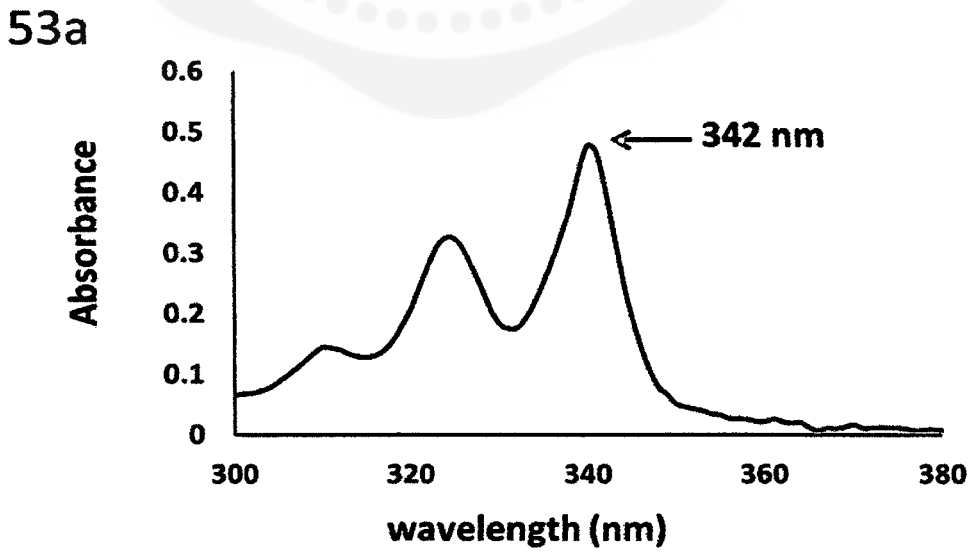


Figure 52 Characterization of PMA-3A by ^{1}H NMR.

The maximum absorption wavelength of PMA-3A was 342 nm (Figure 53a). Molar extinction coefficient (ε) of PMA-3A was 3.87 × 10^4 M^{-1} cm^{-1} (Figure 53b). The fluorescence emission of PMA-3A was monitored at 375 nm with excitation wavelength of 342 nm (Figure 53c).



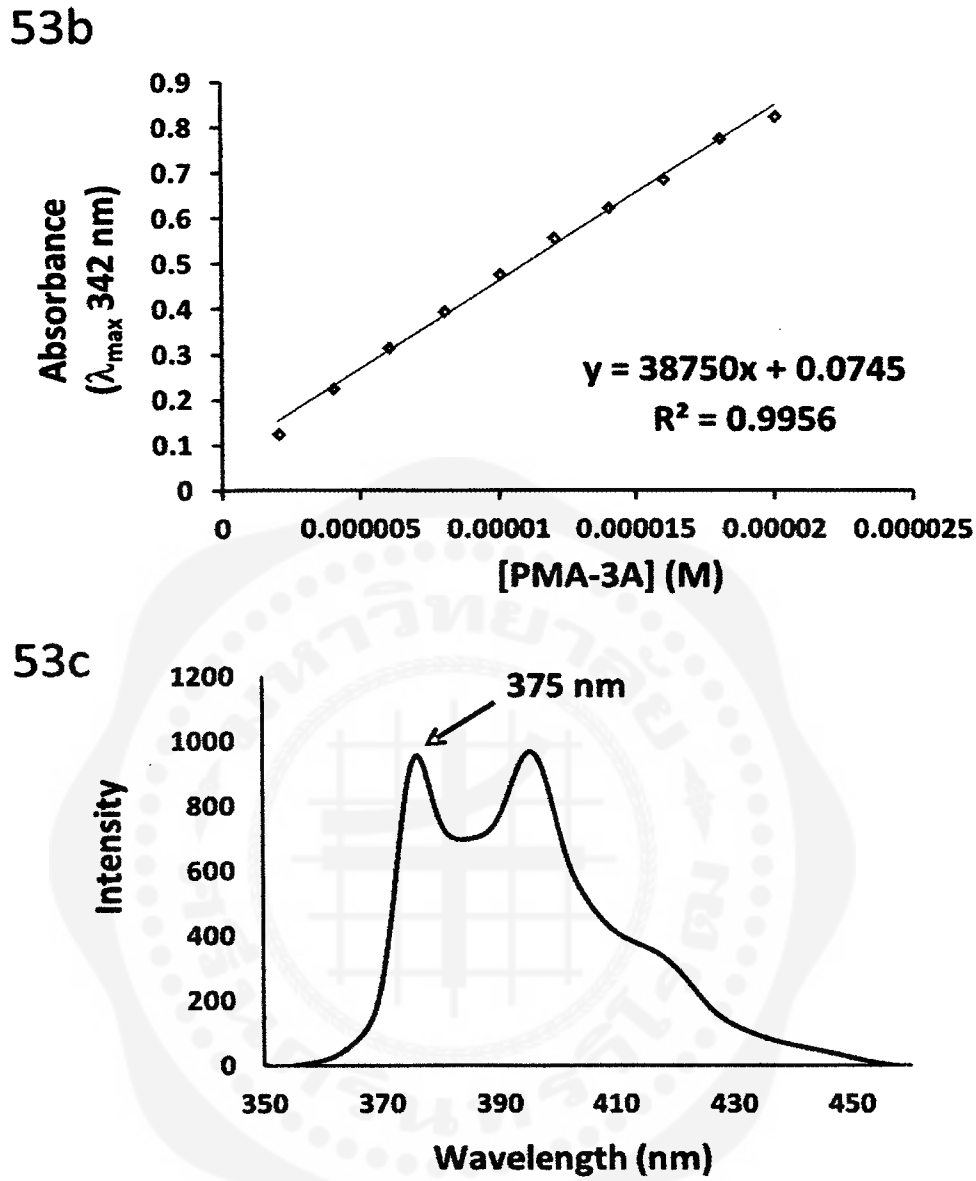


Figure 53 (a) Absorption spectrum of PMA-3A (10 μM) with the maximum wavelength of 342 nm. (b) The linear plot of PMA-3A absorbance at 342 nm versus [PMA-3A] (2-20 μM) with linear dependent coefficient (R^2) of 0.9956. (c) Fluorescence spectrum of PMA-3A (0.5 μM) with excitation wavelength at 342 nm. All data were from the average of three experiments.

1.2 Protein photocleavage by new chemical reagents

Protein photocleavage reactions were successfully completed by irradiation at 342 nm (from a 150 W xenon lamp) to the mixture solution containing protein (15 μM), new photochemical reagent (15 μM) and CoHA (1 mM), in 50 mM Tris-HCl buffer, pH 7.0 (total volume 200 μl) at room temperature for 20 min, as demonstrated in Table 8. The peptide fragments from protein cleavage were demonstrated in sodium dodecyl sulfate-polyacrylamide gel electrophoresis (SDS-PAGE) experiment. The gel was scanned with an Epson scanner (TX220), and the product yields were quantitated using ImageJ program. The model proteins used in this study are avidin, lysozyme, α-chymotrypsin, β-lactoglobulin B, myoglobin, bovine serum albumin (BSA), Human serum albumin (HSA), α-casein, pepsin, concanavalin A and β-glucosidase.

Table 8 The success of protein photocleavage reaction.

protein	PMA-1A	PMA-2A	PMA-3A
avidin	✓	✓	✓
lysozyme	✓	✓	✓
α-chymotrypsin	X	X	X
β- lactoglobulin B	X	X	X
myoglobin	X	X	X
HSA	X	X	X
BSA	X	X	X
α-casein	X	X	X
pepsin	X	X	X
concanavalin A	X	X	X
β-glucosidase	X	X	X

✓ = occurred photocleavage reaction

X = un-occurred photocleavage reaction

From the SDS-PAGE experiments, PMA-1A, PMA-2A, PMA-3A cleaved only avidin and lysozyme. At least two peptide fragments were observed from the cleavage of avidin (Figures 54-56). Protein photocleavage was not achieved in the absence of either photochemical reagent, CoHA or light. SDS-PAGE of other proteins that were not cleaved by PMA-1A, PMA-2A and PMA-3A are demonstrated in the appendix (Figures 100-126).

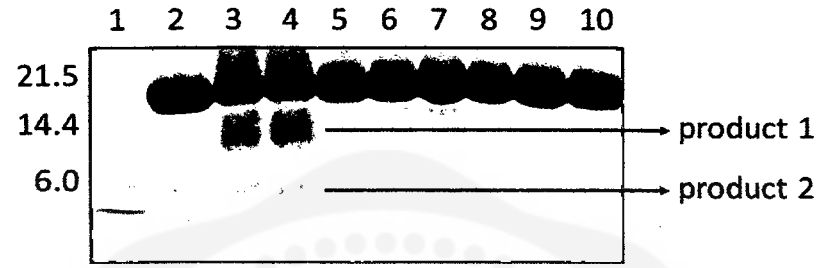


Figure 54 Photocleavage of avidin obtained from the reaction with PMA-1A.
Lane 1: molecular weight markers (kDa)
Lane 2: avidin (15 μM), PMA-1A (15 μM) and CoHA (1 mM), dark control
Lane 3: avidin (15 μM), PMA-1A (15 μM) and CoHA (1 mM), 342 nm, 10 min
Lane 4: avidin (15 μM), PMA-1A (15 μM) and CoHA (1 mM), 342 nm, 20 min
Lane 5: avidin (15 μM), dark control
Lane 6: avidin (15 μM), 342 nm, 20 min
Lane 7: avidin (15 μM) and CoHA (1 mM), dark control
Lane 8: avidin (15 μM) and CoHA (1 mM), 342 nm, 20 min
Lane 9: avidin (15 μM) and PMA-1A (15 μM), dark control
Lane 10: avidin (15 μM) and PMA-1A (15 μM), 342 nm, 20 min

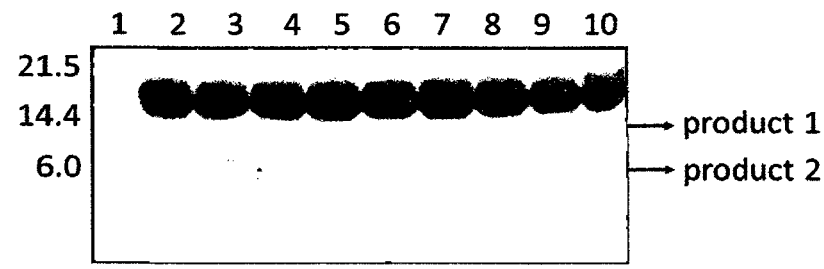


Figure 55 Photocleavage of avidin obtained from the reaction with PMA-2A.

Lane 1: molecular weight markers (kDa)

Lane 2: avidin (15 μM), dark control

Lane 3: avidin (15 μM), 342 nm, 20 min

Lane 4: avidin (15 μM) and CoHA (1 mM), dark control

Lane 5: avidin (15 μM) and CoHA (1 mM), 342 nm, 20 min

Lane 6: avidin (15 μM) and PMA-2A (15 μM), dark control

Lane 7: avidin (15 μM) and PMA-2A (15 μM), 342 nm, 20 min

Lane 8: avidin (15 μM), PMA-2A (15 μM) and CoHA (1 mM), dark control

Lane 9: avidin (15 μM), PMA-2A (15 μM) and CoHA (1 mM), 342 nm, 10 min

Lane 10: avidin (15 μM), PMA-2A (15 μM) and CoHA (1 mM), 342 nm, 20 min

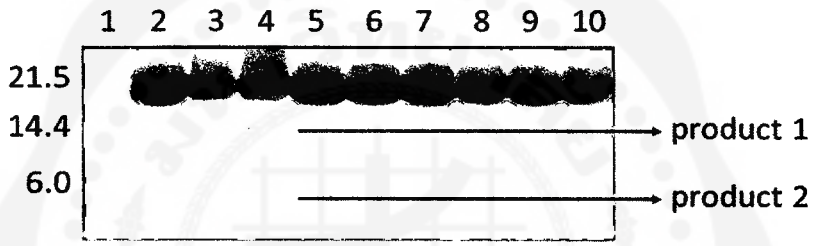


Figure 56 Photocleavage of avidin obtained from the reaction with PMA-3A.

Lane 1: molecular weight markers (kDa)

Lane 2: avidin (15 μM), PMA-3A (15 μM) and CoHA (1 mM), dark control

Lane 3: avidin (15 μM), PMA-3A (15 μM) and CoHA (1 mM), 342 nm, 10 min

Lane 4: avidin (15 μM), PMA-3A (15 μM) and CoHA (1 mM), 342 nm, 20 min

Lane 5: avidin (15 μM), dark control

Lane 6: avidin (15 μM), 342 nm, 20 min

Lane 7: avidin (15 μM) and CoHA (1 mM), dark control

Lane 8: avidin (15 μM) and CoHA (1 mM), 342 nm, 20 min

Lane 9: avidin (15 μM) and PMA-3A (15 μM), dark control

Lane 10: avidin (15 μM) and PMA-3A (15 μM), 342 nm, 20 min

In case of avidin, all three photochemical reagents (PMA-1A, PMA-2A, PMA-3A) cleaved avidin after only 1 min of irradiation (Figures 57a-57c). Increasing time of irradiation (1-20 min) increased the photoproduct yields (Figures 58a-58c). The product yields obtained from three photochemical reagents are slightly different. The maximum photoproduct yields can be summarized in Table 9.

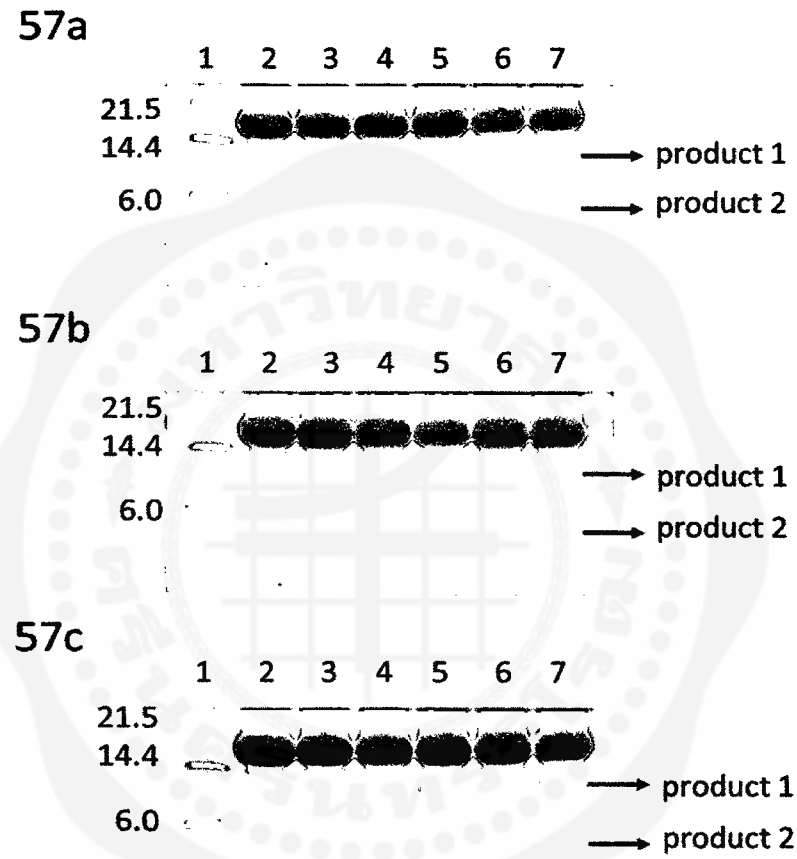


Figure 57 SDS-PAGE of photoproducts obtained from the reaction of avidin with the photochemical reagents, (a) PMA-1A, (b) PMA-2A and (c) PMA-3A. Lane 1: molecular weight markers (kDa). Lane 2: avidin (15 μM), photochemical reagents (15 μM) and CoHA (1 mM), dark control Lanes 3-7: avidin (15 μM), photochemical reagents (15 μM) and CoHA (1 mM), 342 nm (1, 5, 10, 15 and 20 min, respectively).

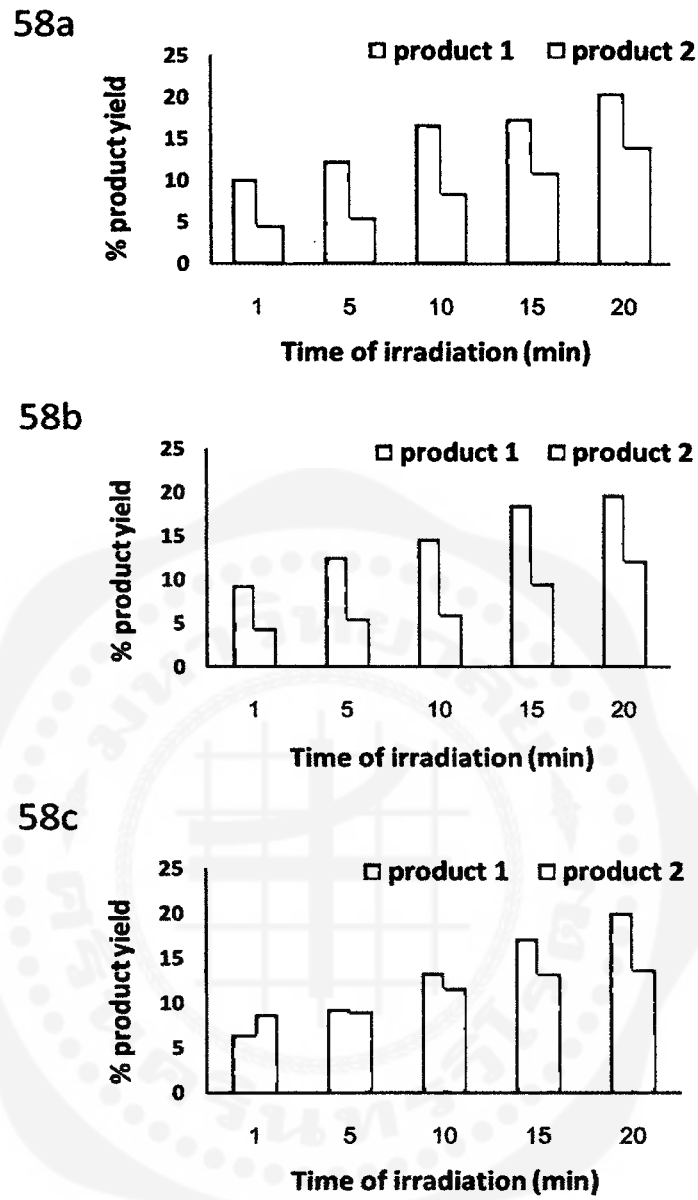


Figure 58 Photoproduct yields obtained from the reaction of photocleavage of avidin with photochemical reagents, (a) PMA-1A, (b) PMA2A and (c) PMA-3A.

Table 9 The maximum photoproduct yields obtained from SDS-PAGE.

Photocleavage of avidin/photochemical reagents	% maximum photoproduct yields of product 1	% maximum photoproduct yields of product 2
PMA-1A	20.44	14.07
PMA-2A	19.70	12.16
PMA-3A	20.07	13.71

The distances of standard proteins (R_f) are shown in Table 10. Molecular weights of two bands of the cleaved fragments from avidin cleavage are approximately 9.4 kDa and 4.8 kDa, as calculated from a linearity standard curve between logarithm of molecular weight of protein (log M) and distances of standard proteins (markers) (Figure 59).

Table 10 The distances of standard proteins obtained from SDS-PAGE.

Molecular weight of protein (kDa)	R_f (cm)	log MW
200	0.1	2.301029996
116.3	0.2	2.065579715
97.4	0.3	1.988558957
66.3	0.5	1.821513528
55.4	0.7	1.743509765
36.5	1.5	1.562292864
31	1.7	1.491361694
21.5	2.35	1.33243846
14.4	2.85	1.158362492
6	3.85	0.77815125
3.5	4.55	0.544068044

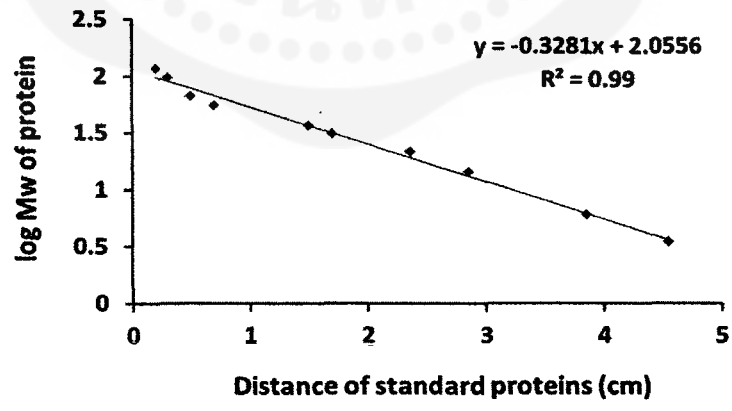


Figure 59 A standard curve of molecular weight markers for calculation of molecular weights of the cleaved fragments.

In case of lysozyme, the cleavage was achieved after irradiation of the mixture of lysozyme (15 μM), the photochemical reagents (PMA-1A, PMA-2A or PMA-3A) (15 μM) and CoHA (1 mM) at 345 nm (Figures 60-62) for 20 min. However, the cleavage of lysozyme was not achieved from the reaction with natural products (berberine and piperine).

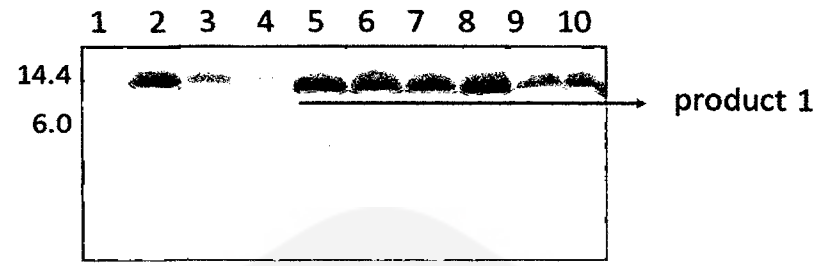


Figure 60 Photocleavage of lysozyme obtained from the reaction with PMA-1A.
Lane 1: molecular weight markers (kDa)
Lane 2: lysozyme (15 μM), PMA-1A (15 μM) and CoHA (1 mM), dark control
Lane 3: lysozyme (15 μM), PMA-1A (15 μM) and CoHA (1 mM), 342 nm, 10 min
Lane 4: lysozyme (15 μM), PMA-1A (15 μM) and CoHA (1 mM), 342 nm, 20 min
Lane 5: lysozyme (15 μM), dark control
Lane 6: lysozyme (15 μM), 342 nm, 20 min
Lane 7: lysozyme (15 μM) and CoHA (1 mM), dark control
Lane 8: lysozyme (15 μM) and CoHA (1 mM), 342 nm, 20 min
Lane 9: lysozyme (15 μM) and PMA-1A (15 μM), dark control
Lane 10: lysozyme (15 μM) and PMA-1A (15 μM), 342 nm, 20 min

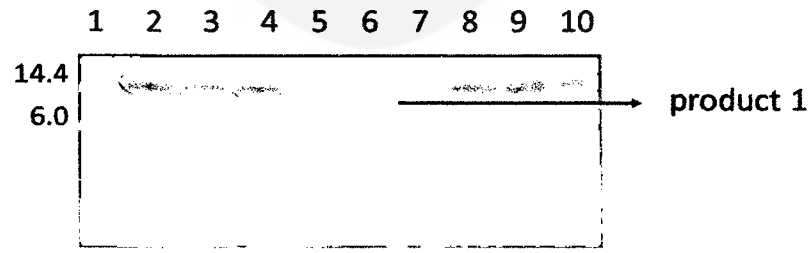


Figure 61 Photocleavage of lysozyme obtained from the reaction with PMA-2A.
Lane 1: molecular weight markers (kDa)
Lane 2: lysozyme (15 μM), dark control
Lane 3: lysozyme (15 μM), 342 nm, 20 min
Lane 4: lysozyme (15 μM), PMA-2A (15 μM) and CoHA (1 mM), dark control

Lane 5: lysozyme (15 μM), PMA-2A (15 μM) and CoHA (1 mM), 342 nm, 10 min

Lane 6: lysozyme (15 μM), PMA-2A (15 μM) and CoHA (1 mM), 342 nm, 20 min

Lane 7: lysozyme (15 μM) and PMA-2A (15 μM), dark control

Lane 8: lysozyme (15 μM) and PMA-2A (15 μM), 342 nm, 20 min

Lane 9: lysozyme (15 μM) and CoHA (1 mM), dark control

Lane 10: lysozyme (15 μM) and CoHA (1 mM), 342 nm, 20 min

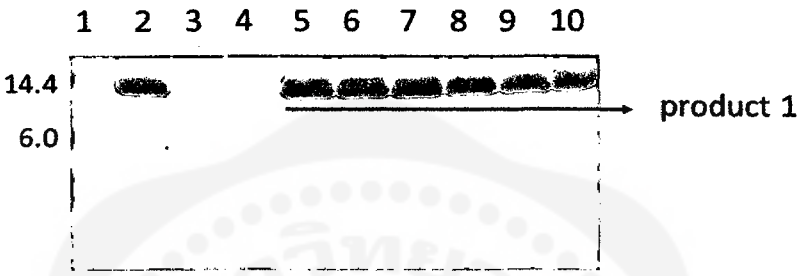


Figure 62 Photocleavage of lysozyme obtained from the reaction with PMA-3A.

Lane 1: molecular weight markers (kDa)

Lane 2: lysozyme (15 μM), PMA-3A (15 μM) and CoHA (1 mM), dark control

Lane 3: lysozyme (15 μM), PMA-3A (15 μM) and CoHA (1 mM), 342 nm, 10 min

Lane 4: lysozyme (15 μM), PMA-3A (15 μM) and CoHA (1 mM), 342 nm, 20 min

Lane 5: lysozyme (15 μM), dark control

Lane 6: lysozyme (15 μM), 342 nm, 20 min

Lane 7: lysozyme (15 μM) and CoHA (1 mM), dark control

Lane 8: lysozyme (15 μM) and CoHA (1 mM), 342 nm, 20 min

Lane 9: lysozyme (15 μM) and PMA-3A (15 μM), dark control

Lane 10: lysozyme (15 μM) and PMA-3A (15 μM), 342 nm, 20 min

The cleavage of lysozyme from the reaction with three synthesized photochemical reagents resulted in one cleavage position. The cleavage was observed after the reaction mixture was irradiated only for 1 min (Figures 63a-63c). The cleavage of lysozyme yielded two peptide fragments. However, only one peptide fragment can be observed on the gel due to very low molecular weight of the other cleaved fragment.

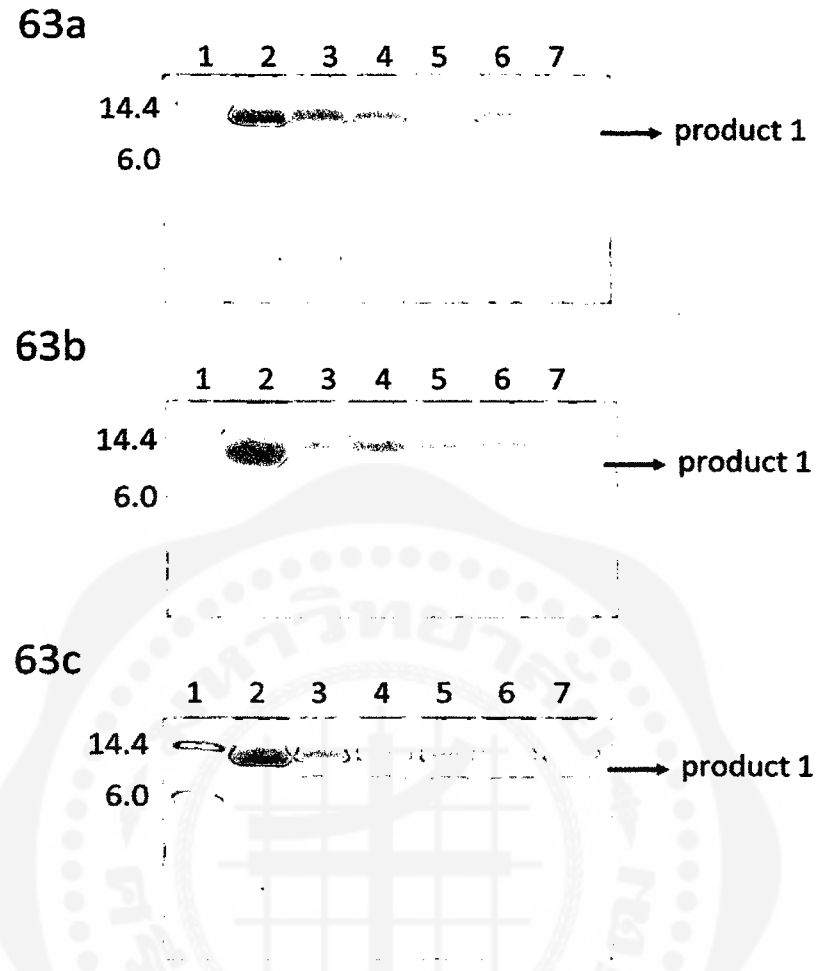


Figure 63 SDS-PAGE of photoproducts obtained from the reaction of lysozyme with the photochemical reagents, (a) PMA-1A, (b) PMA-2A and (c) PMA-3A. Lane 1: molecular weight markers (kDa). Lane 2: lysozyme (15 μM), photochemical reagents (15 μM) and CoHA (1 mM), dark control. Lanes 3-7: lysozyme (15 μM), photochemical reagents (15 μM) and CoHA (1 mM), 342 nm, (1, 5, 10, 15 and 20 min, respectively).

The product yields of peptide fragments obtained from the reaction of lysozyme with the three photochemical reagents are slightly different (Figures 64a-64c). The maximum photoproduct yields can be summarized in Table 11.

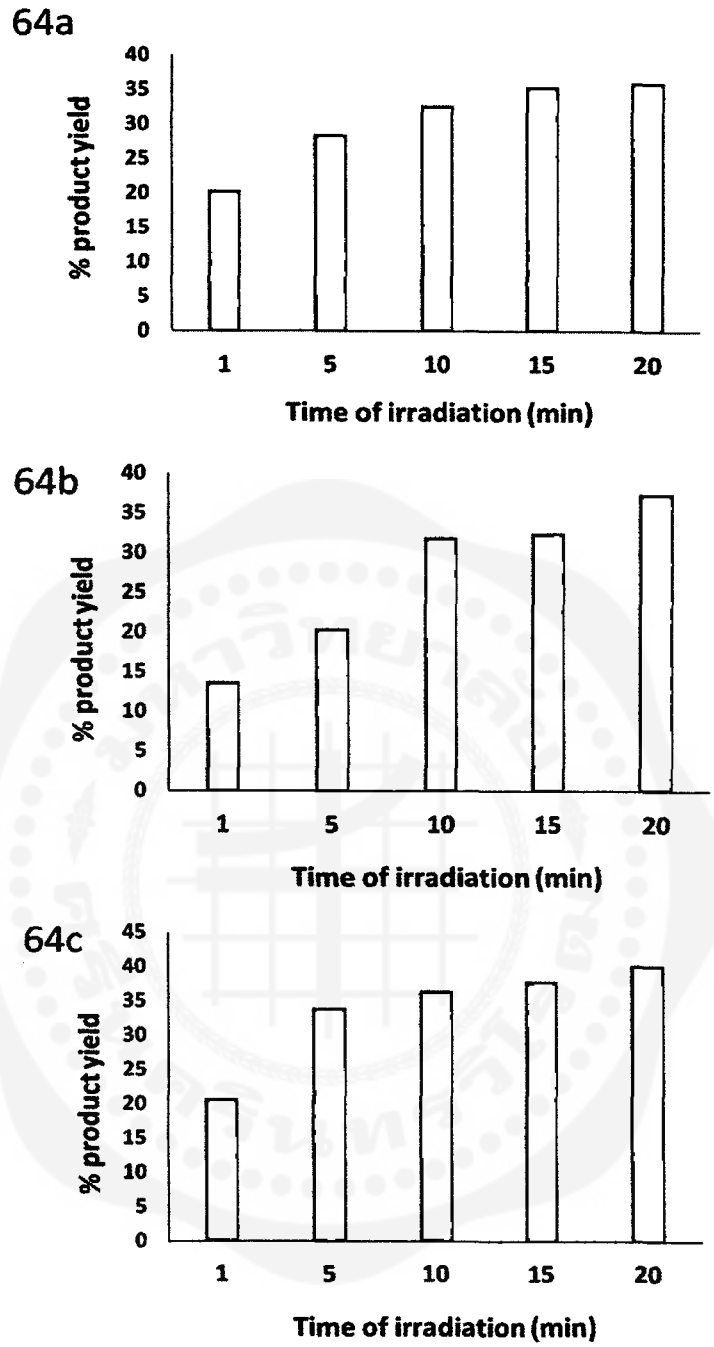


Figure 64 The product yields of photocleavage of lysozyme from the reaction with photochemical reagents, (a) PMA-1A, (b) PMA2A and (c) PMA-3A.

Table 11 The maximum photoproduct yields obtained from SDS-PAGE.

Photocleavage of lysozyme/photochemical reagents	% maximum photoproduct yields
PMA-1A	36.11
PMA-2A	37.52
PMA-3A	40.27

Molecular weight of the peptide fragment of lysozyme is ~9.7 kDa, as calculated from the standard curve (Figure 65). The distances of standard proteins (R_f) are shown in Table 12.

Table 12 The distances of standard proteins for calculation molecular weight of photoproducts obtained from lysozyme cleavage by photochemical reagents.

Molecular weight of protein (kDa)	R_f (cm)	log MW
200	0.1	2.301029996
116.3	0.2	2.065579715
97.4	0.25	1.988558957
66.3	0.4	1.821513528
55.4	0.5	1.743509765
36.5	1.05	1.562292864
31	1.2	1.491361694
21.5	1.6	1.33243846
14.4	2.1	1.158362492
6	3	0.77815125
3.5	3.6	0.544068044

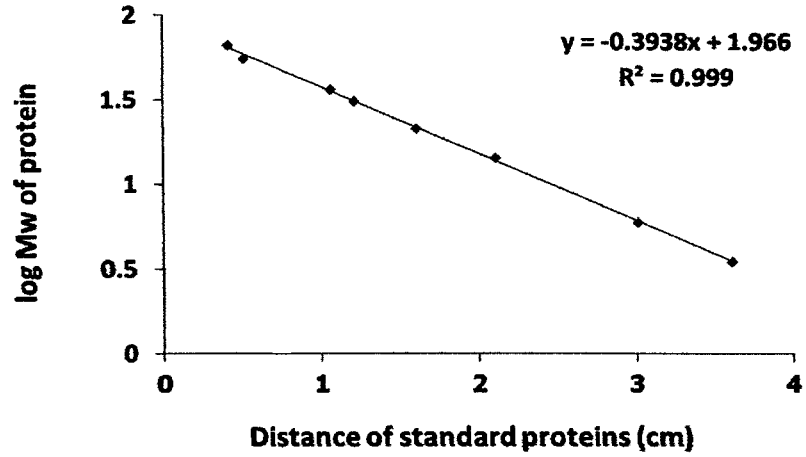


Figure 65 A standard curve of molecular weight markers for calculation of molecular weights of the cleaved fragments.

1.3 Protein transfer by western blot for amino acid sequencing analysis.

For amino acid sequencing studies, the peptide fragments from the gel were transferred to PVDF membrane by applying the electricity at 60 mA for 1.5 h using the Wet/Tank Blotting Systems (BIORAD) with CAPS buffer, pH 10.5. Peptide fragments on PVDF membrane were stained with Coomassie brilliant blue (0.1% Coomassie brilliant blue R-250 in 40% methanol and 1% acetic acid). The desired protein fragments were analyzed at Midwest Analytical, Inc., MO, USA for amino acid sequence.

N-terminal amino acid sequencing of the first peptide fragment (product 1) of avidin from the reaction with PMA-1A, PMA-2A and PMA-3A indicated the residues ARKCS (~8.4 kDa), which is known as *N*-terminal sequence of avidin (DeLange; & Huang. 1971: 698-709), while *N*-terminal amino acid sequencing of peptide fragments (product 2) indicated the major residues VFTGQ (~5.9 kDa). Thus, the sequencing data of all the three photochemical reagents indicated that the major cleavage site of avidin occurred between Thr77 and Val78. However, from the reaction of PMA-1A, a minor cleavage site of avidin indicated residues KFSES. This minor cleavage site of avidin occurred between Trp70-Lys71. Moreover, another cleavage sequence (AVTAT) was observed from the reaction of PMA-3A, suggesting a minor cleavage site of avidin between Thr35-Ala36 which was not observed with the other two photoreagents. The cleavage patterns of avidin from the reaction of all the three photochemical reagents are shown in Figures 66a-66c.

In addition, in case of lysozyme, *N*-terminal amino acid sequencing of peptide fragment (product 1) of lysozyme obtained from the reaction with PMA-1A, PMA-2A and PMA-3A indicated the residues LVFGR, which is the *N*-terminal sequence of lysozyme. However, the other peptide fragment of lysozyme was too faint and unable to be isolated from the gel. Molecular weight of fragment 1 is approximately 9.7 kDa. From the estimation of molecular weight of fragment 1, the cleavage sites of avidin may occur between Ile88-Thr89 (Figure 67).



Figure 66 The major and minor cleavage sites of avidin from the reaction of PMA-1A (a), PMA-2A (b) and PMA-3A (c).

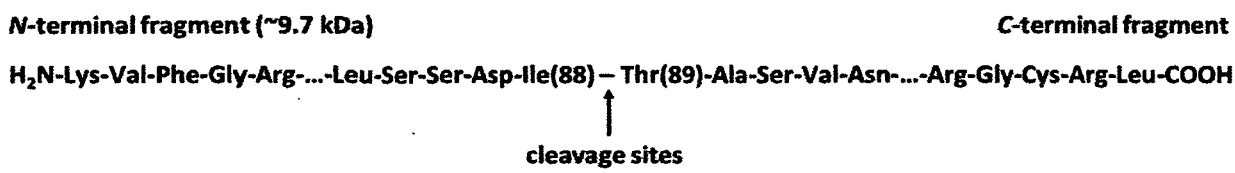


Figure 67 The cleavage sites of lysozyme from the reaction with three photochemical reagents.

The protein photocleavage reaction is initiated when CoHA quenches of the excited pyrene to produce pyrene cation radical ($Py^{+\bullet}$), followed by hydrogen atom abstraction at α-carbon from the amino acid by pyrene cation radical ($Py^{+\bullet}$) to produce α-carbon radical. The addition of oxygen to α-carbon radical results in hydroperoxyl radical, subsequently that could eventually lead to hydrolysis of the peptide backbone. This mechanism was proposed in the previous studies in which the intermediates were obtained from laser flash photolysis experiments. (Kumar; et al. 1998: 10361-10366) (Figure 68).

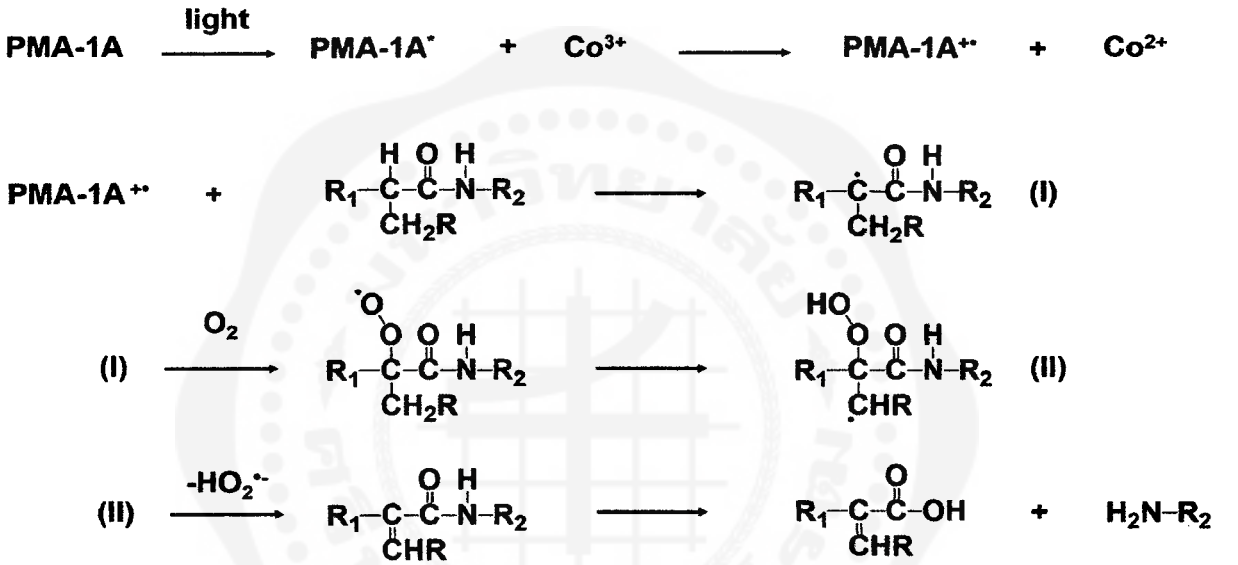


Figure 68 Proposed mechanism of protein photocleavage by photochemical reagent.

1.4 The interactions of new photochemical reagents with proteins.

Binding interaction

All of absorption spectra of PMA-1A, PMA2A, PMA3A (10 μM) with increasing concentrations of proteins (0-20 μM, avidin or lysozyme) were recorded in the range of 300-400 nm on a Shimadzu UV-2401 PC UV-VIS spectrophotometer.

The new photochemical reagents (PMA-1A, PMA-2A and PMA-3A) influence to conformational changes of avidin. The absorption spectra of PMA-1A/avidin, PMA-2A/avidin and PMA-3A/avidin resulted in hypochromism (decreased by 30%, 17% and 36%, respectively) (Figures 69-71). Moreover, bathochromic shift (2 nm) was observed in PMA-3A/avidin absorption band with isosbestic points at 328, 333, and 344 nm. The

binding constant can be calculated by Scatchard equation (discussed in chapter 2), and the results are demonstrated in Table 13.

Table 13 Binding constants and other binding properties of probe/avidin.

Binding interaction	PMA-1A/avidin	PMA-2A/avidin	PMA-3A/avidin
K_b (M^{-1})	6.2×10^5	6.7×10^5	4.6×10^5
Absorbance shifts	Hypochromic (-30%)	Hypochromic (-17%)	Hypochromic (-36%)

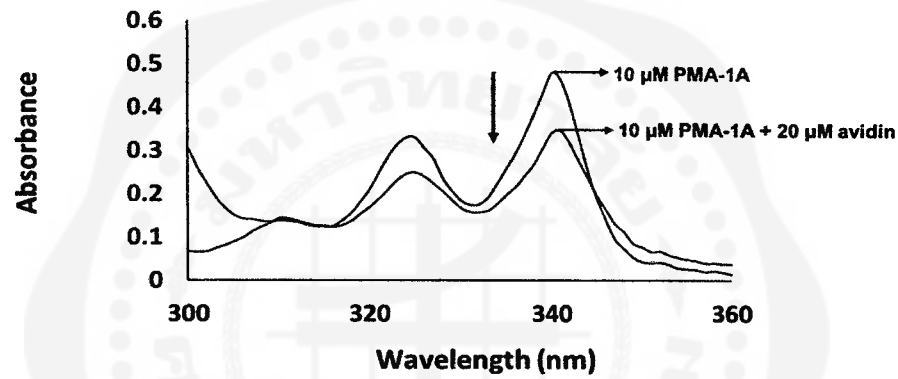


Figure 69 Absorption spectra of PMA-1A (10 μM) in the absence (blue) and presence (red) of avidin (0-20 μM).

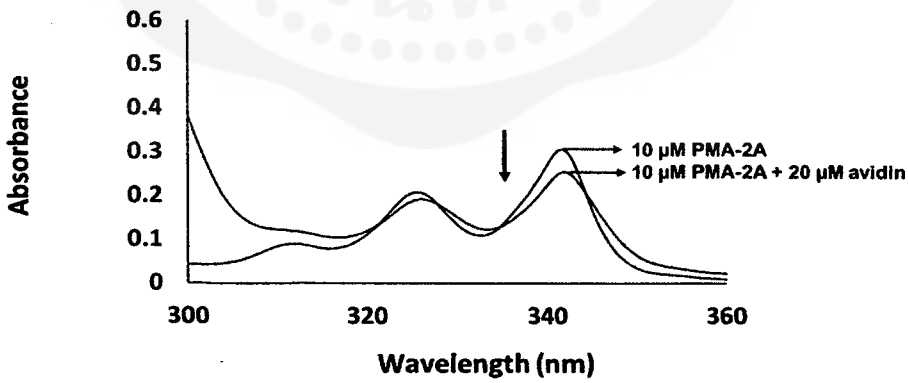


Figure 70 Absorption spectra of PMA-2A (10 μM) in the absence (blue) and presence (red) of avidin (0-20 μM).

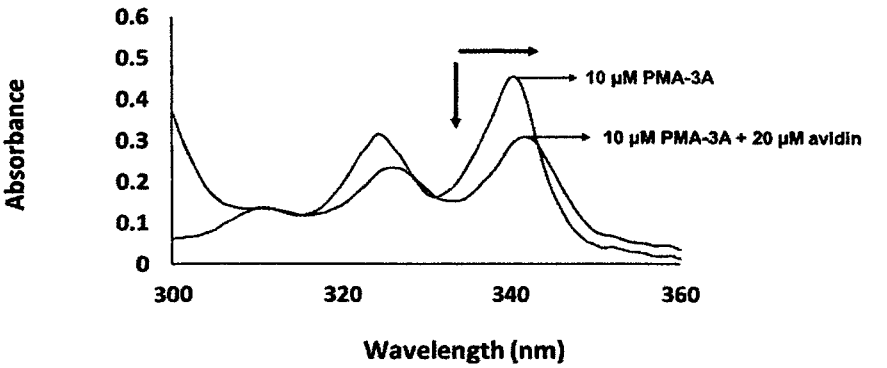


Figure 71 Absorption spectra of PMA-3A (10 μM) in the absence (blue) and presence (red) of avidin (0-20 μM).

In case of lysozyme, hypochromic shifts were observed in the absorption spectra of PMA-1A/lysozyme, PMA-2A/lysozyme and PMA-3A/lysozyme (decreased by 23%, 22% and 20%, respectively) (Figures 72-74). Binding constants and other binding properties obtained from the interaction between new photochemical reagents with lysozyme are shown in Table 14.

Table 14 Binding constant and other binding properties of probe/lysozyme.

Binding interaction	PMA-1A/lysozyme	PMA-2A/lysozyme	PMA-3A/lysozyme
K_b (M^{-1})	1.7×10^5	2.4×10^5	1.9×10^5
Absorbance shifts	Hypochromic (-23%)	Hypochromic (-22%)	Hypochromic (-20%)

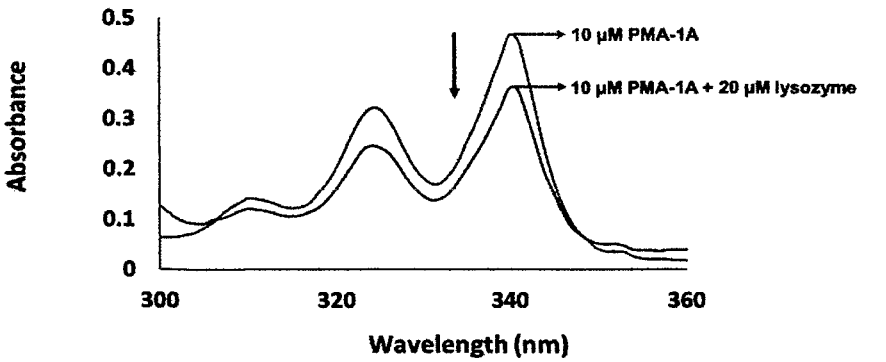


Figure 72 Absorption spectra of PMA-1A (10 μM) in the absence (blue) and presence (red) of lysozyme (0-20 μM).

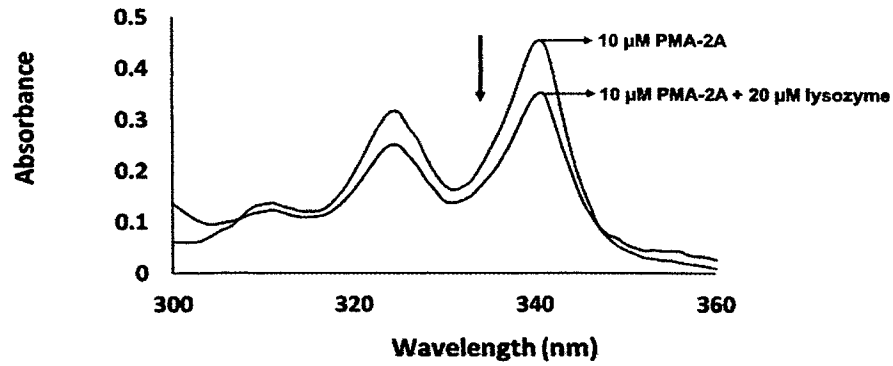


Figure 73 Absorption spectra of PMA-2A (10 μM) in the absence (blue) and presence (red) of lysozyme (0-20 μM).

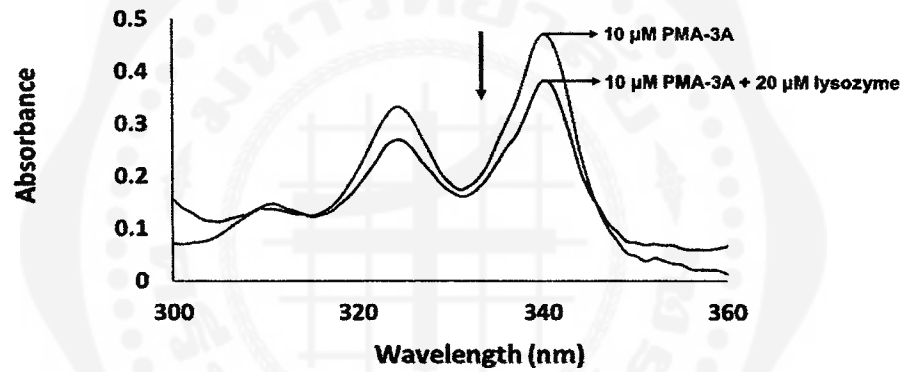


Figure 74 Absorption spectra of PMA-3A (10 μM) in the absence (blue) and presence (red) of lysozyme (0-20 μM).

Binding interaction results indicated that binding constants of PMA-1A, PMA-2A and PMA-3A bound to avidin were higher than those bound to lysozyme. These hypochromisms of the absorption spectra indicated that the pyrenyl chromophore could be located at the hydrophobic sites on the protein. Therefore, the side chain and functional group of the probe play an important role in the binding interaction which can effect protein conformational changes, as demonstrated from above spectral changes.

Fluorescence quenching studies

The fluorescence spectra of the mixtures of PMA-1A, PMA-2A or PMA-3A (0.5 μM) in the absence and presence of protein (10 μM, avidin or lysozyme), by titration with CoHA (0-1 mM), were recorded in the range of 350-550 nm with excitation at 342 nm. The fluorescence intensities of three probes decreased when increasing concentration of CoHA. Stern-Volmer quenching constant (K_{sv}) can be calculated from the slope of the plot between the ratio of fluorescence intensity in the absence and presence of the quencher (I_0/I) as a function of quencher concentration [CoHA] (Figures 75a-75c).

In the absence of protein, analysis of the fluorescence quenching data of PMA-1A, PMA-2A and PMA-3A by CoHA indicated the K_{sv} values of 1.93 $\times 10^3$ M^{-1}, 2.64 $\times 10^3$ M^{-1}, 1.76 $\times 10^3$ M^{-1}, respectively.

In the presence of avidin, analysis of the fluorescence quenching data of PMA-1A, PMA-2A and PMA-3A by CoHA indicated the K_{sv} values of 1.94 $\times 10^3$ M^{-1}, 2.36 $\times 10^3$ M^{-1}, 1.49 $\times 10^3$ M^{-1}, respectively.

In addition, in the presence of lysozyme, analysis of the fluorescence quenching data of PMA-1A, PMA-2A and PMA-3A by CoHA indicated the K_{sv} values of 2.00 $\times 10^3$ M^{-1}, 2.61 $\times 10^3$ M^{-1}, 1.60 $\times 10^3$ M^{-1}, respectively.

Quenching constant, obtained from the slope of the linear regression curve of Stern-Volmer equation (discussed in chapter 2), can be demonstrated in Table 15.

Table 15 Stern-Volmer quenching constants (K_{sv}) of PMA-1A, PMA-2A and PMA-3A.

Photochemical reagents	PMA-1A	PMA-2A	PMA-3A
K_{sv} (free form),	1.93 $\times 10^3$	2.64 $\times 10^3$	1.76 $\times 10^3$
K_{sv} (bound with avidin),	1.94 $\times 10^3$	2.36 $\times 10^3$	1.49 $\times 10^3$
K_{sv} (bound with lysozyme),	2.00 $\times 10^3$	2.61 $\times 10^3$	1.60 $\times 10^3$

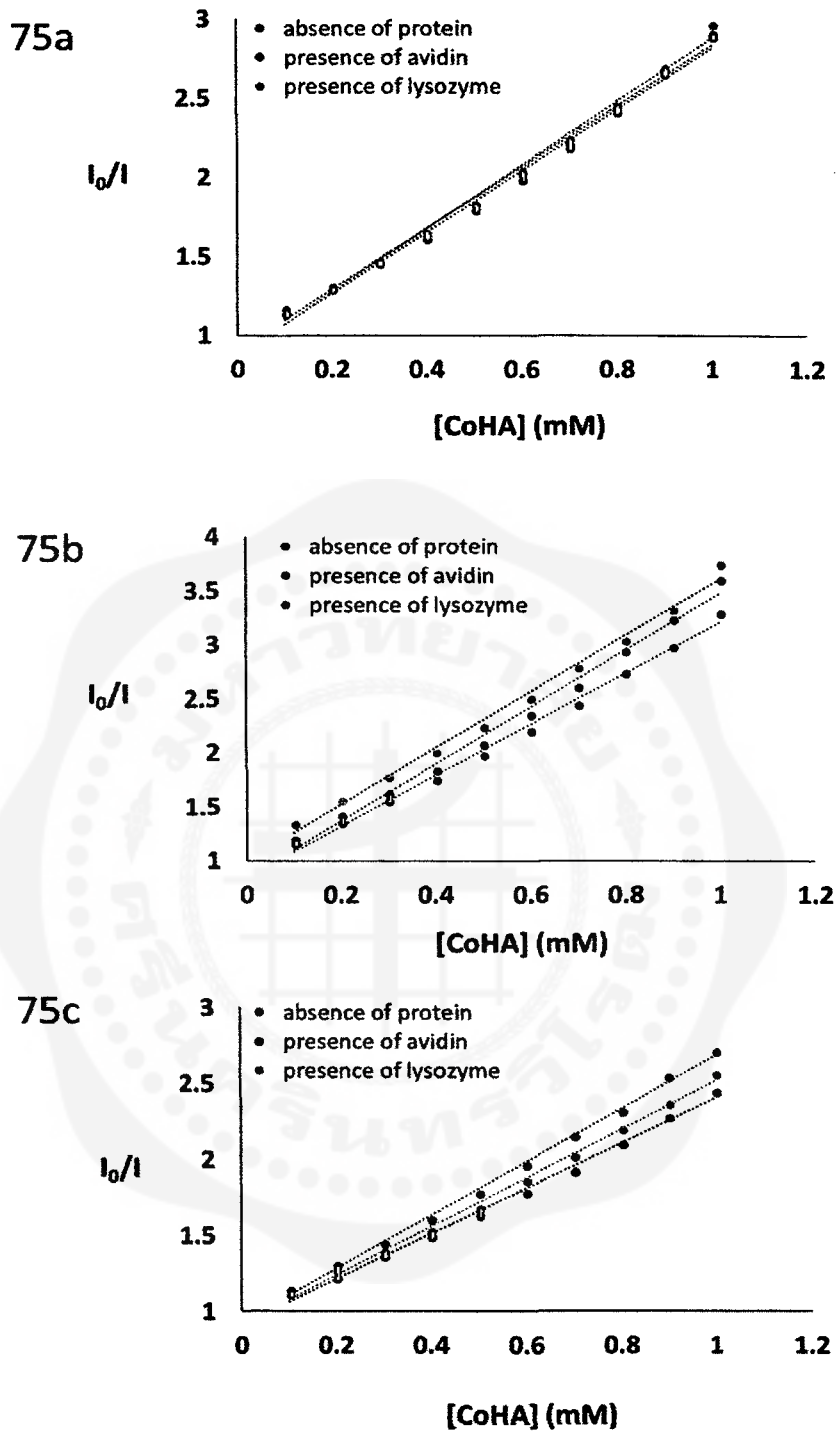


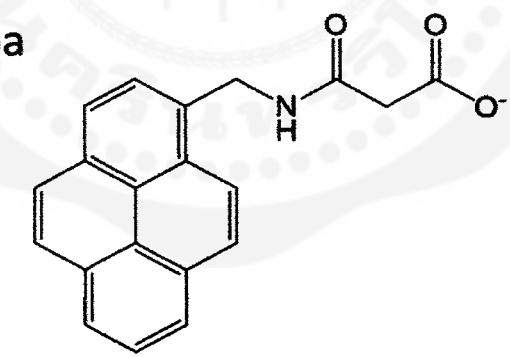
Figure 75 The Stern–Volmer plots of new photochemical reagents (0.5 μM) by titration with CoHA (0–1.0 mM), in the absence of protein (○), in the presence of avidin (10 μM) (○) and in the presence of lysozyme (10 μM) (○), the fluorescence quenching data of PMA-1A (a), PMA-2A (b) and PMA-3A (c).

The K_{sv} values of PMA-1A in the absence and presence of the protein (avidin or lysozyme) showed no differences, indicating that the probe bound at the surface of avidin. K_{sv} values of PMA-2A, with CoHA quenching, reduced by 11% and only 1% in the presence of avidin and lysozyme, respectively. K_{sv} values of PMA-3A, with CoHA quenching, reduced by 15% and 9% in the presence of avidin and lysozyme, respectively. These K_{sv} values suggested the accessibility of CoHA to quench the photochemical reagents upon binding to the protein. These K_{sv} values are consistent with the photoproduct yields from above experiments, indicating that the probe bind near the surface of the protein with sufficient exposure to the solvent. Therefore, deeply buried probe in the protein matrix could lead to less reactive intermediates generated on light excitation, resulting to less product yields.

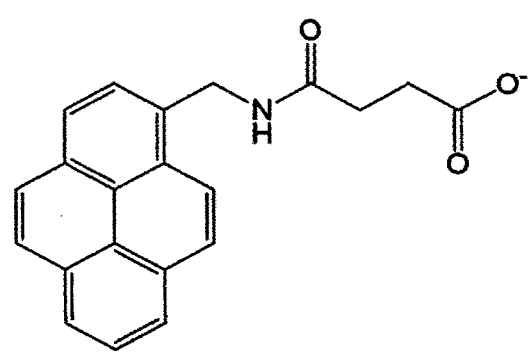
1.5 Binding mechanism of new photochemical reagents with the proteins.

The crystal structures of avidin (1AVD) and lysozyme (4HPI) were downloaded from the Protein Data Bank. Since the pH of mixture solution reaction (pH = 7.0) was higher than the pKa of malonic acid (pH ~5.69), succinic acid (~5.6) and glutaric acid (pH 5.22), anionic forms of these probes were expected (Figures 76a-76c). Binding positions of new photochemical reagents on the proteins were studied in computational modelling.

76a



76b



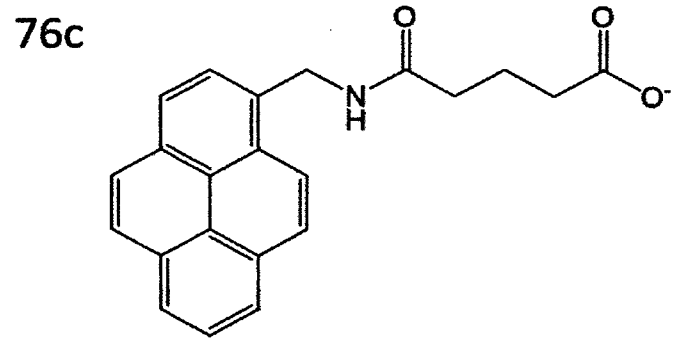


Figure 76 The structures of (a) anionic PMA-1A, (b) anionic PMA-2A and (c) anionic PMA-3A.

In case of avidin, docking studies demonstrated that anionic PMA-1A, anionic PMA-2A and anionic PMA-3A bound to avidin at similar sites. The results are related to the same major cleavage site (Thr77- Val78) obtained from photocleavage experiments. Moreover, docking results indicated that anionic PMA-1A, anionic PMA-2A and anionic PMA-3A bound on the part of hydrophilic site and hydrophobic site of avidin. These photochemical reagents bound to avidin by hydrogen bonding with the minimum of binding free energies of -8.88, -9.32 and -8.67 kcal/mol, respectively. The data are consistent with the binding constants (K_b) obtained from the absorption titration experiments. The lower binding free energy from the docking studies indicated higher stability for binding interaction. The binding free energy of PMA-2A was lower than that of PMA-1A and PMA-3A, which was correlated to the binding constants obtained from the absorption titration experiments (Table 16).

Table 16 Binding constant of probe/avidin from absorption titration studies and binding free energy from docking studies.

Binding interaction	Binding constant (M^{-1})	binding free energy (kcal/mol)
PMA-1A (10 μM) + avidin (0-20 μM)	6.2×10^5	-8.88
PMA-2A (10 μM) + avidin (0-20 μM)	6.7×10^5	-9.32
PMA-3A (10 μM) + avidin (0-20 μM)	4.6×10^5	-8.67

In case of avidin/anionic PMA-1A, the amino acid residues, lining along the binding site with donor-acceptor within the distance of less than 5 Å, were comprised of Asn12, Leu14, Ser16, Tyr33, Thr35, Val37, Thr38, Ala39, Thr40, Trp70, Phe72, Ser73, Ser75, Thr77, Phe79, Trp97, leu99, Ile117 and Asn118 with three hydrogen bonding interactions of anionic PMA-1A with Ala39, Thr40 and Ser73 of avidin (Figures 77a-77c).

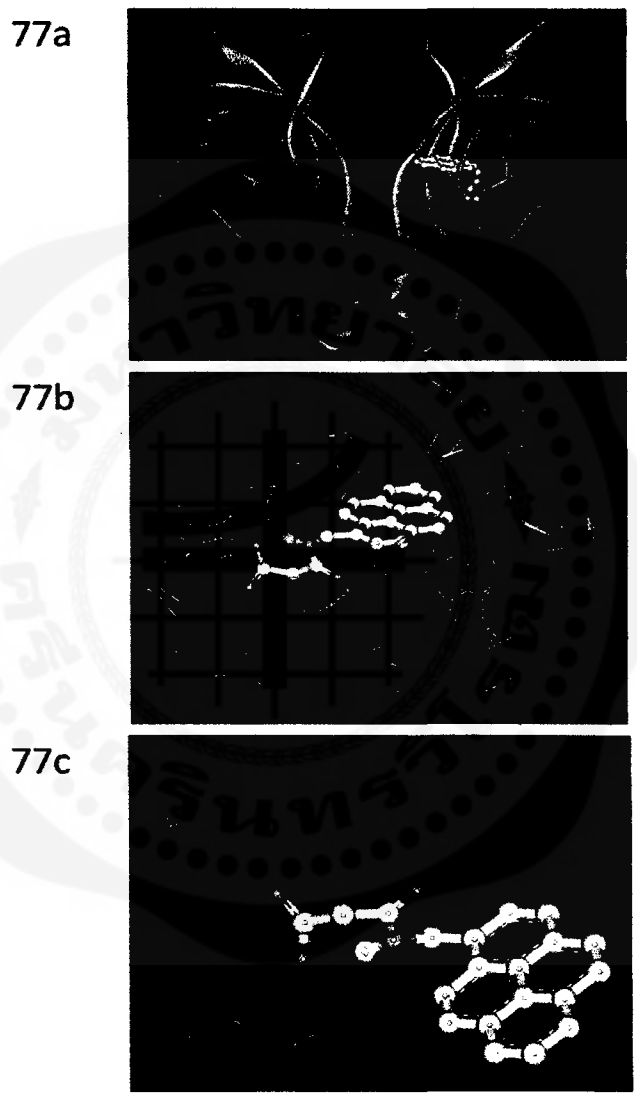


Figure 77 (a) The binding location of PMA-1A on the part of hydrophilic site and hydrophobic site of avidin. (b) The amino acid residues of avidin surrounding PMA-1A within the distance of less than 5 Å. (c) Three hydrogen bonding interactions of anionic PMA-1A with three amino acid residues of avidin (dotted green lines).

In case of avidin/anionic PMA-2A, the amino acid residues, lining along the binding site with donor-acceptor within the distance of less than 5 Å, were comprised of Leu14, Thr35, Val37, Thr38, Ala39, Thr40, Trp70, Phe72, Ser73, Ser75, Thr77, Phe79, Trp97, Leu99, Ile117 and Asn118 with five hydrogen bonding interactions of anionic PMA-2A with Thr35, Ala39, Thr40, Ser73 and Ser75 of avidin (Figures 78a-78c).

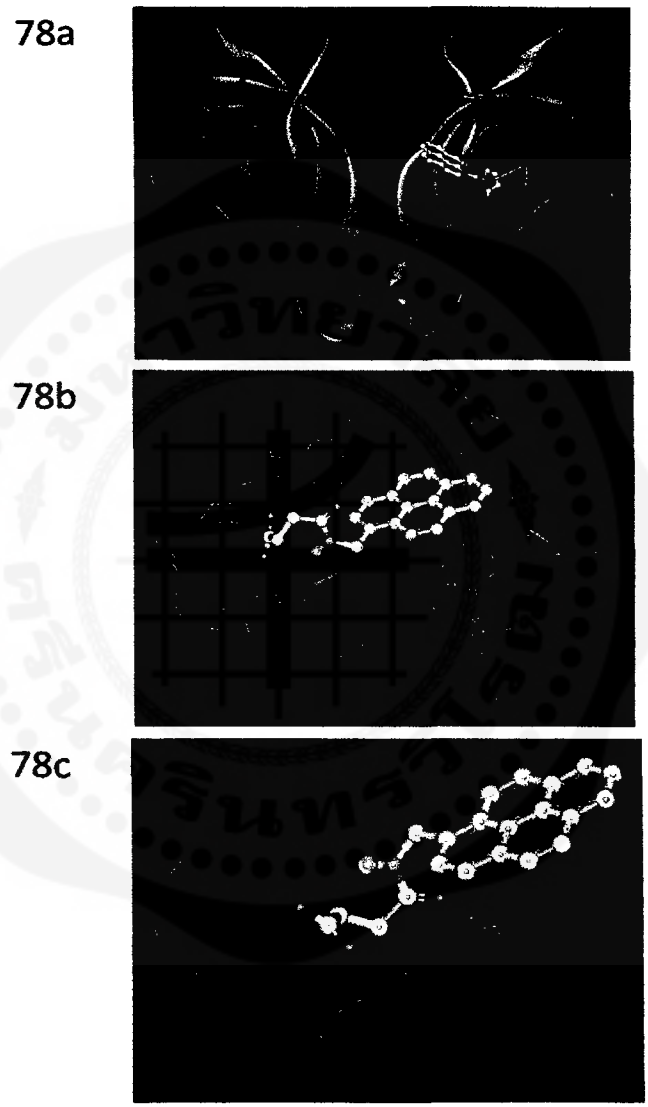


Figure 78 (a) The binding location of PMA-2A on the part of hydrophilic site and hydrophobic site of avidin. (b) The amino acid residues of avidin surrounding PMA-2A within the distance of less than 5 Å. (c) Five hydrogen bonding interactions of anionic PMA-2A with five amino acid residues of avidin (dotted green lines).

In case of avidin/anionic PMA-3A, the amino acid residues, lining along the binding site with donor-acceptor within the distance of less than 5 Å, were comprised of Leu14, Thr35, Val37, Thr38, Ala39, Thr40, Trp70, Phe72, Ser73, Ser75, Thr77, Phe79, Trp97, Leu99, Ser101, Ile117 and Asn118 with three hydrogen bonding interactions of anionic PMA-3A with Thr35, Ser73 and Ser75 of avidin (Figures 79a-79c).

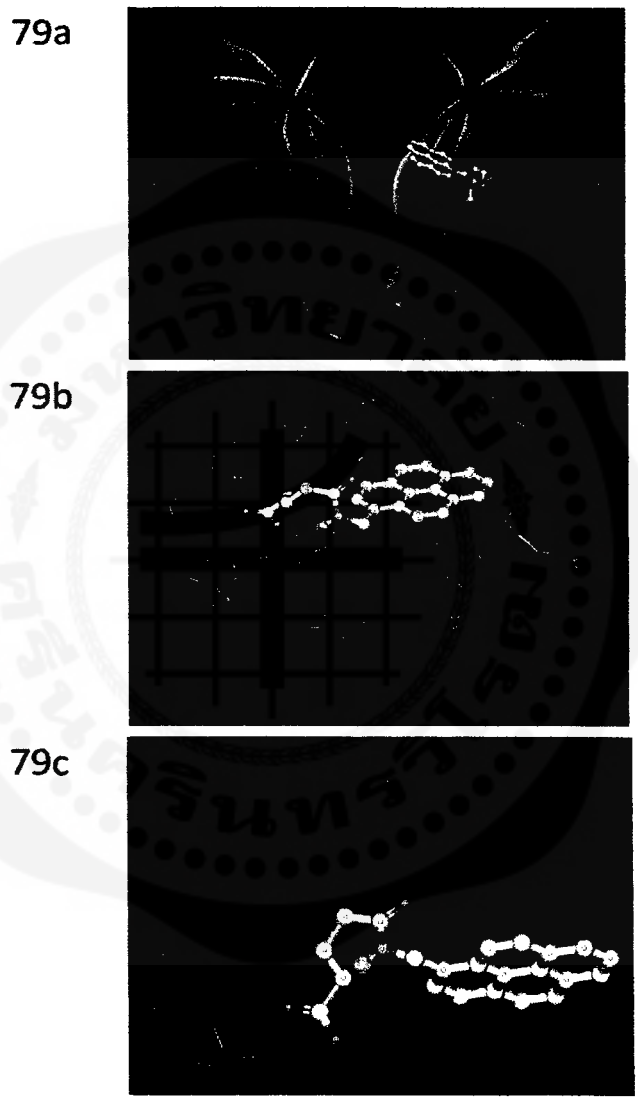


Figure 79 (a) The binding location of PMA-3A on the part of hydrophilic site and hydrophobic site of avidin. (b) The amino acid residues of avidin surrounding PMA-3A within the distance of less than 5 Å. (c) Three hydrogen bonding interactions of anionic PMA-3A with three amino acid residues of avidin (dotted green lines).

From above experimental data, the docking results were related to the major cleavage site of avidin (between Thr77-Val78) from the reaction with three photochemical reagents. The distances between Val78 and three photochemical reagents were insignificantly different. Moreover, the minor cleavage site of avidin, occurred between Trp70-Lys71 from the reaction with PMA-1A, also can be explained by the docking studies. The distance of Lys71 of avidinwas closer to PMA-1A than PMA-2A and PMA-3A. Whereas, the distance of Ala36 of avidin (minor cleavage site of avidin by PMA-3A) was closer to PMA-3A than PMA-1A and PMA-2A. The distances between the new photochemical reagents and amino acid residues of avidin at cleavage site were demonstrated in Table 17.

Table 17 The distances between the new photochemical reagents and amino acid residues at cleavage site of avidin.

Photochemical reagents	Amino acid residues of avidin		
	Ala36	Lys71	Val78
PMA-1A	6.065 Å	6.428 Å	7.567 Å
PMA-2A	5.518 Å	6.886 Å	7.518 Å
PMA-3A	5.369 Å	7.682 Å	7.449 Å

In case of lysozyme, docking studies results demonstrated that anionic PMA-1A, anionic PMA-2A and anionic PMA-3A bound to lysozyme at similar sites. Moreover, docking studies indicated the location of anionic PMA-1A, anionic PMA-2A and anionic PMA-3A on the part of hydrophilic site and hydrophobic site of lysozyme by hydrogen bonding with the minimum of binding free energies of -7.95, -8.50 and -8.36 kcal/mol, respectively. These data were consistent with the binding constants (K_b) obtained from the absorption titration experiments.

In case of lysozyme/anionic PMA-1A, the amino acid residues, lining along the binding site with donor-acceptor within the distance of less than 5 Å, were comprised of Glu35, Asp52, Leu56, Gln57, Ile58, Asn59, Trp62, Trp63, Ile98, Asn106, Ala107, Trp108, Val109 and Arg112 with a hydrogen bonding interaction of anionic PMA-1A with Arg112 of lysozyme (Figures 80a-80c).

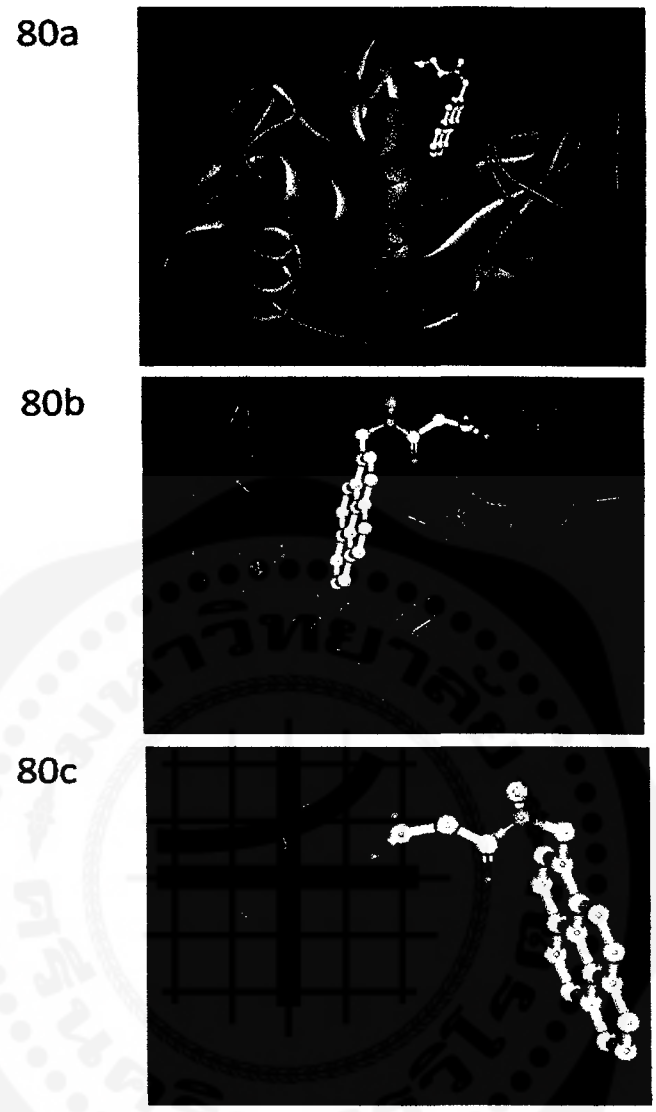


Figure 80 (a) The binding location of PMA-1A on the part of hydrophilic site and hydrophobic site of lysozyme. (b) The amino acid residues of lysozyme surrounding PMA-1A within the distance of less than 5 Å. (c) A hydrogen bonding interaction of anionic PMA-1A with an amino acid residue of lysozyme (dotted green lines).

In case of lysozyme/anionic PMA-2A, the amino acid residues, lining along the binding site with donor-acceptor within the distance of less than 5 Å, were comprised of Phe34, Glu35, Asn46, Asp52, Leu56, Gln57, Ile58, Asn59, Trp62, Trp63, Ile98, Ala107, Trp108, Val109, Ala110, Asn113 and Arg114 with two hydrogen bonding interactions of anionic PMA-2A with Glu35 and Asn113 of lysozyme (Figures 81a-81c).

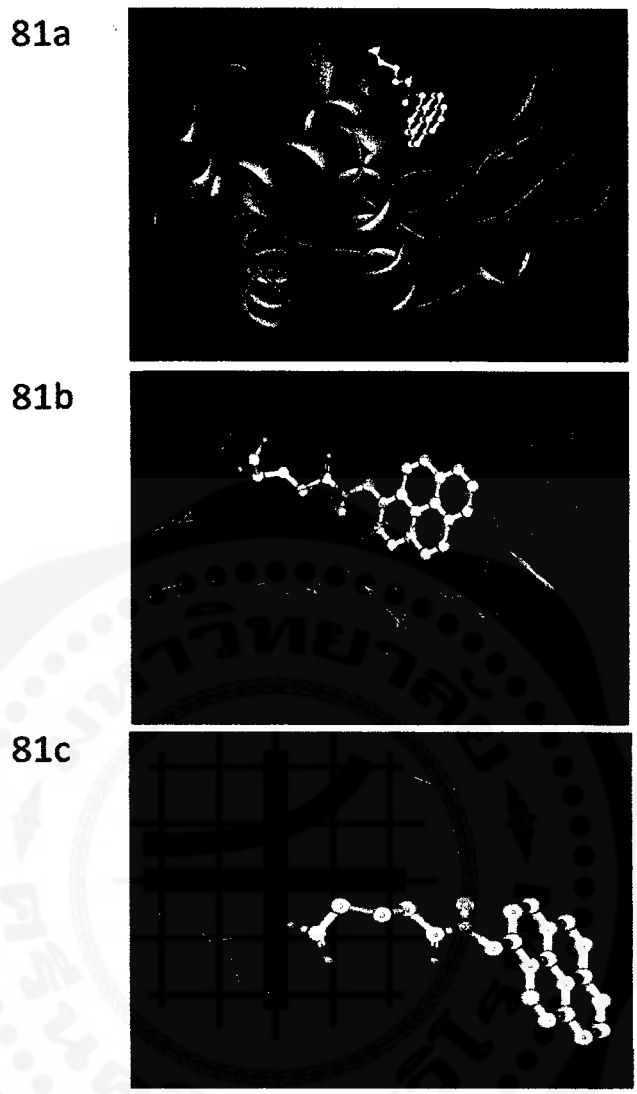


Figure 81 (a) The binding location of PMA-2A on the part of hydrophilic site and hydrophobic site of lysozyme. (b) The amino acid residues of lysozyme surrounding PMA-2A within the distance of less than 5 Å. (c) Two hydrogen bonding interactions of anionic PMA-2A with two amino acid residues of lysozyme (dotted green lines).

In case of lysozyme/anionic PMA-3A, the amino acid residues, lining along the binding site with donor-acceptor within the distance of less than 5 Å, were comprised of Phe34, Glu35, Asp52, Leu56, Gln57, Ile58, Asn59, Trp62, Trp63, Ile98, Ala107, Trp108, Val109, Ala110, Asn113 and Arg114 with two hydrogen bonding interactions of anionic PMA-3A with Glu35 and Asn113 of lysozyme (Figures 82a-82c).

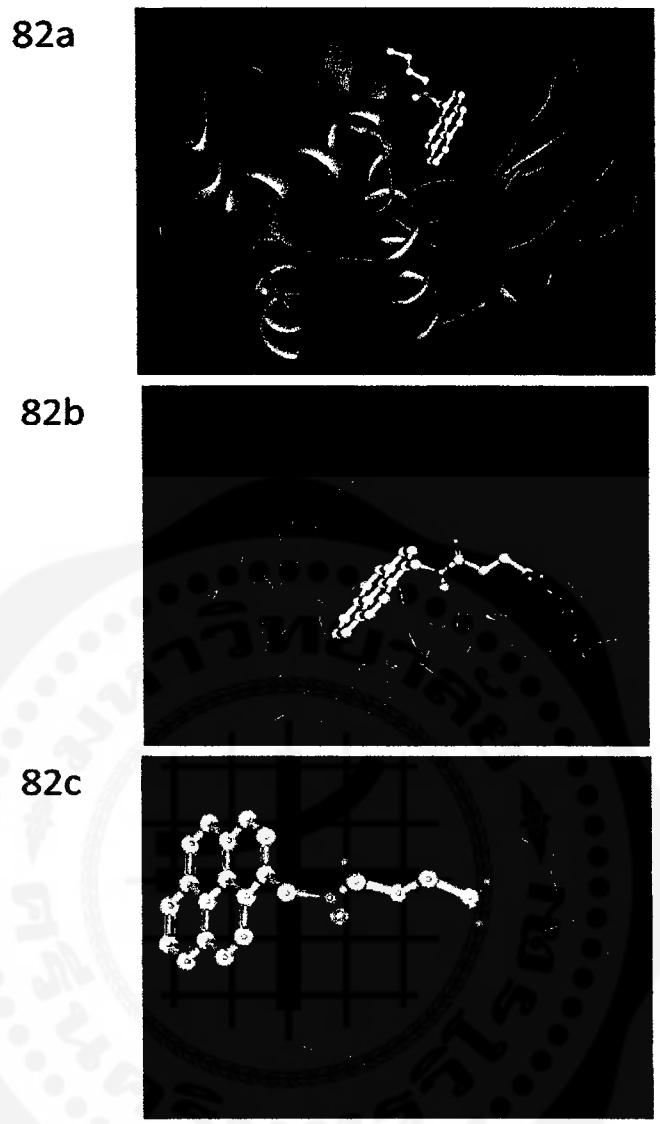


Figure 82 (a) The binding location of PMA-3A on the part of hydrophilic site and hydrophobic site of lysozyme. (b) The amino acid residues of lysozyme surrounding PMA-3A within the distance of less than 5 Å. (c) Two hydrogen bonding interactions of anionic PMA-3A with two amino acid residues of lysozyme (dotted green lines).

The observed binding free energies of all probes bound to avidin were less than those bound to lysozyme. The results corresponded to the binding constants of these probes bound to avidin and lysozyme. Therefore, the docking results confirmed the experimental data and supported the results from the photoreaction experiments.

2. Natural products

2.1 Protein photocleavage by natural products.

Protein photocleavage reactions were successfully achieved by irradiation at 345 nm (from a 150 W xenon lamp) to the mixture solution containing protein (15 μM), natural product (15 μM) and CoHA (1 mM), in 50 mM Tris-HCl buffer, pH 7.0 (total volume 200 μl) at room temperature for 20 min, as demonstrated in Table 18. The model proteins used in this study were avidin, lysozyme, α-chymotrypsin, β-lactoglobulin B, myoglobin, bovine serum albumin (BSA), Human serum albumin (HSA), α-casein, pepsin, concanacalin A and β-glucosidase. From the SDS-PAGE experiments, avidin was cleaved by berberine after 20 min of irradiation at 345 nm. SDS-PAGE of other proteins that were not cleaved by berberine, berberine derivatives (SST-29 and SST-31) and piperine are demonstrated in the appendix (Figures 127-169). Structures of berberine derivatives (SST-29 and SST-31) are demonstrated in Figure 83. Three peptide fragments of berberine were obtained from the photoreaction as shown in Figure 84.

Table 18 The successful of protein photocleavage reaction.

protein	Berberine	SST-29	SST-31	Piperine
avidin	✓	X	X	X
lysozyme	X	X	X	X
α-chymotrypsin	X	X	X	X
β- lactoglobulin B	X	X	X	X
myoglobin	X	X	X	X
HSA	X	X	X	X
BSA	X	X	X	X
α-casein	X	X	X	X
pepsin	X	X	X	X
concanavalin A	X	X	X	X
β-glucosidase	X	X	X	X

✓ = occurred photocleavage reaction

X = un-occurred photocleavage reaction

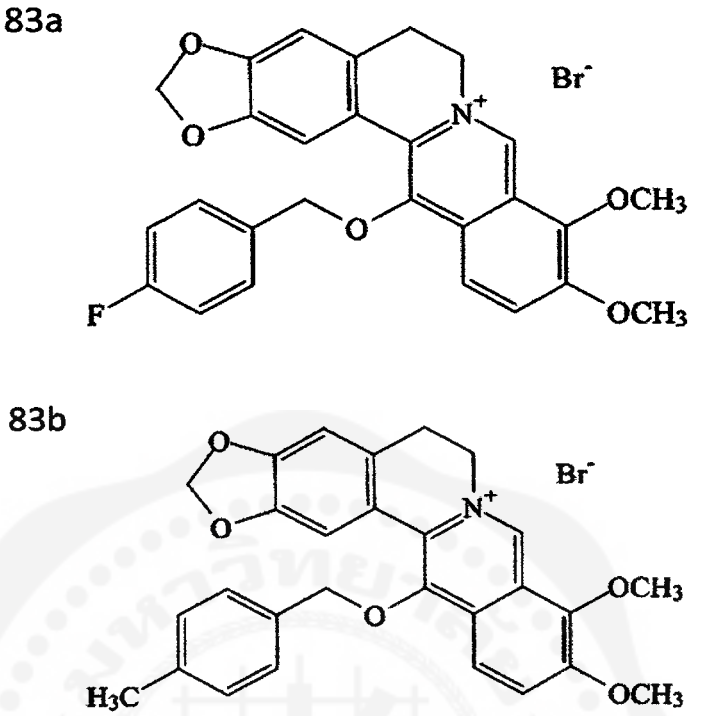


Figure 83 The structures of berberine derivatives (a) SST-29 and (b) SST-31.



Figure 84 Photocleavage of avidin obtained from the reaction with berberine.

Lane 1: molecular weight markers (kDa)

Lane 2: avidin (15 μM), berberine (15 μM) and CoHA (1 mM), dark control

Lane 3: avidin (15 μM), berberine (15 μM) and CoHA (1 mM), 345 nm, 10 min

Lane 4: avidin (15 μM), berberine (15 μM) and CoHA (1 mM), 345 nm, 20 min

Lane 5: avidin (15 μM), dark control

Lane 6: avidin (15 μM), 345 nm, 20 min

Lane 7: avidin (15 μM) and CoHA (1 mM), dark control

Lane 8: avidin (15 μM) and CoHA (1 mM), 345 nm, 20 min

Lane 9: avidin (15 μM) and berberine (15 μM), dark control

Lane 10: avidin (15 μM) and berberine (15 μM), 345 nm, 20 min

Photoproduct yields of three peptide fragments obtained from the reaction of photocleavage of avidin with berberine were shown in Figure 85. The distances of standard proteins (R_f) are shown in Table 19. Molecular weights of each peptide bands from the cleavage were estimated for 8.7 kDa, 5.6 kDa and 3.7 kDa (Figure 86).

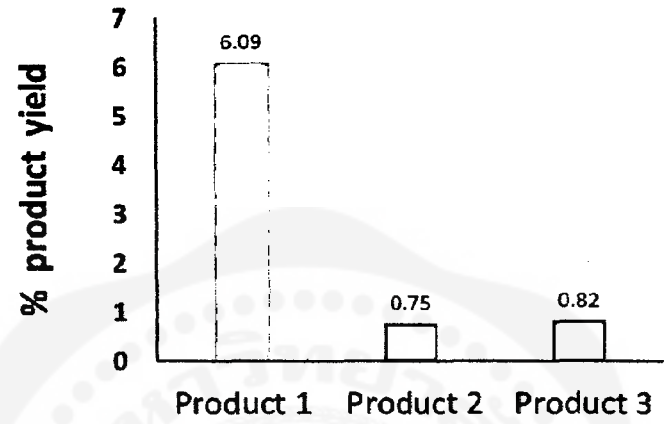


Figure 85 Photoproduct yields obtained from the reaction of photocleavage of avidin with berberine.

Table 19 The distances of standard proteins for calculation of molecular weight of photoproducts obtained from avidin cleavage by berberine.

Molecular weight of protein (kDa)	R_f (cm)	log MW
200	0.1	2.301029996
116.3	0.2	2.065579715
97.4	0.3	1.988558957
66.3	0.5	1.821513528
55.4	1.15	1.743509765
36.5	1.3	1.562292864
31	1.4	1.491361694
21.5	1.9	1.33243846
14.4	2.4	1.158362492
6	3	0.77815125
3.5	3.5	0.544068044

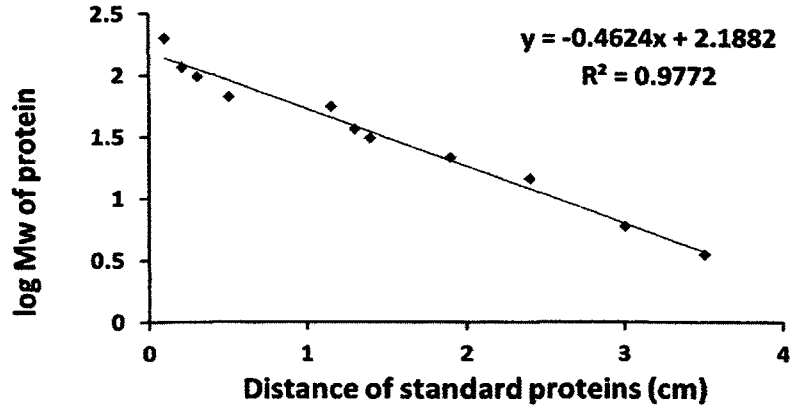


Figure 86 A standard curve of molecular weight markers for calculation of molecular weights of the cleaved fragments.

2.2 Protein transfer by Western blot for amino acid sequencing analysis.

For amino acid sequencing studies, the peptide fragments from the gel were transferred to PVDF membrane by applying the electricity at 60 mA for 1.5 h using the Wet/Tank Blotting Systems (BIORAD) with CAPS buffer, pH 10.5. Peptide fragments on PVDF membrane were stained with Coomassie brilliant blue (0.1% Coomassie brilliant blue R-250 in 40% methanol and 1% acetic acid). The desired protein fragments were analyzed at Midwest Analytical, Inc., MO, USA for amino acid sequence.

N-terminal amino acid sequencing of the first peptide fragment (product 1) of avidin obtained from the reaction with berberine indicated the residues ARKCS, which is the *N*-terminal sequence of avidin. The other peptide bands (product 2 and product 3) of avidin on the gel from the reaction with berberine were too faint, resulting in the difficulty for protein transfer from gel to membrane. However, molecular weights of product 1, product 2 and product 3, calculated from the standard curve, were ~8.7 kDa, ~5.6 kDa and ~3.7 kDa, respectively, which can be used to predict the position of the cleavage site. From the estimation of molecular weights of product 2 and product 3, the cleavage site of avidin may occur between Thr80-Gly81 and Met96-Trp97, respectively (Figure 87).

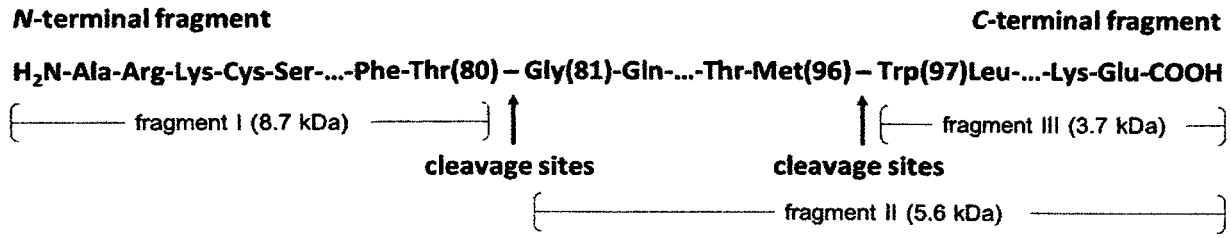


Figure 87 The cleavage sites of avidin from the reaction of berberine.

2.3 Binding interactions of natural products with proteins

The absorption spectra of berberine (10 μM) and its derivatives (10 μM, SST-29 or SST-31) with increasing concentration of protein (0-10 μM, avidin or lysozyme) were recorded in the range of 300-400 nm on a Shimadzu UV-2401 PC UV-VIS spectrophotometer.

Berberine and its derivatives (SST-29 and SST-31) influence to conformational changes of avidin. The absorption spectra of berberine/avidin resulted in hyperchromism (increased by 19%), whereas SST-29/avidin and SST-31/avidin resulted in hypochromism (decreased by 31% and 35%, respectively) (Figures 88-90).

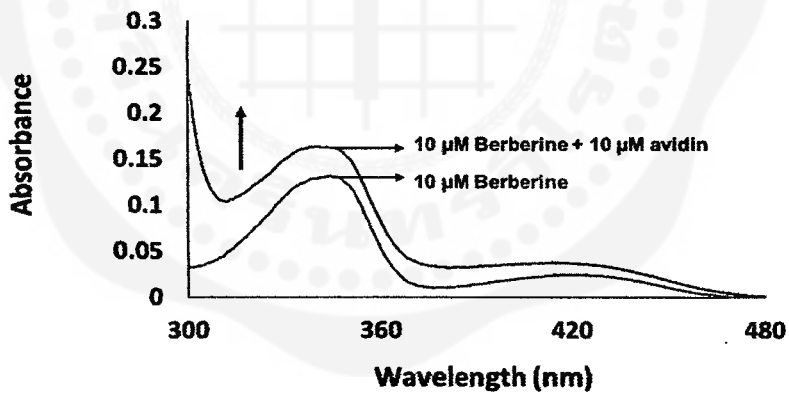


Figure 88 Absorption spectra of berberine (10 μM) in the absence (blue) and presence (red) of avidin (0-10 μM).

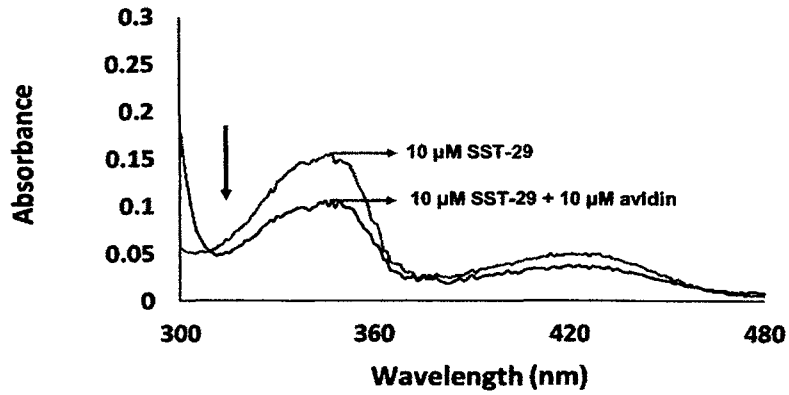


Figure 89 Absorption spectra of SST-29 (10 μM) in the absence (blue) and presence (red) of avidin (0-10 μM).

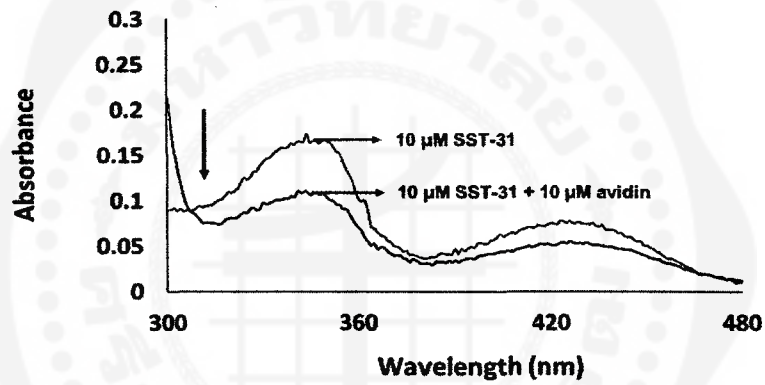


Figure 90 Absorption spectra of SST-31 (10 μM) in the absence (blue) and presence (red) of avidin (0-10 μM).

In case of lysozyme, hyperchromic shifts were observed in the absorption spectra of berberine/lysozyme, SST-29/lysozyme and SST-31/lysozyme (increased by 20%, 23% and 13%, respectively) (Figures 91-93).

The binding constant can be calculated by Scatchard equation (discussed in chapter 2), and berberine, SST-29, SST-31 bound to both proteins with high constant that results are demonstrated in Table 20. These results indicated that the binding mechanism and environment surrounding berberine, SST-29, SST-31 could be different with three photochemical reagents.

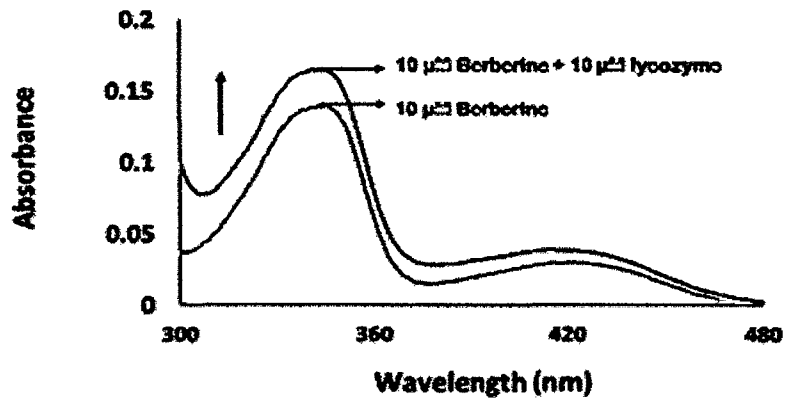


Figure 91 Absorption spectra of berberine (10 μM) in the absence (blue) and presence (red) of lysozyme (0-10 μM).

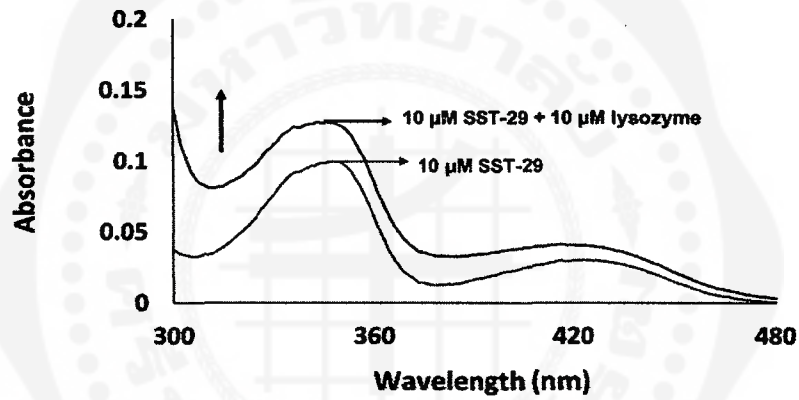


Figure 92 Absorption spectra of SST-29 (10 μM) in the absence (blue) and presence (red) of lysozyme (0-10 μM).

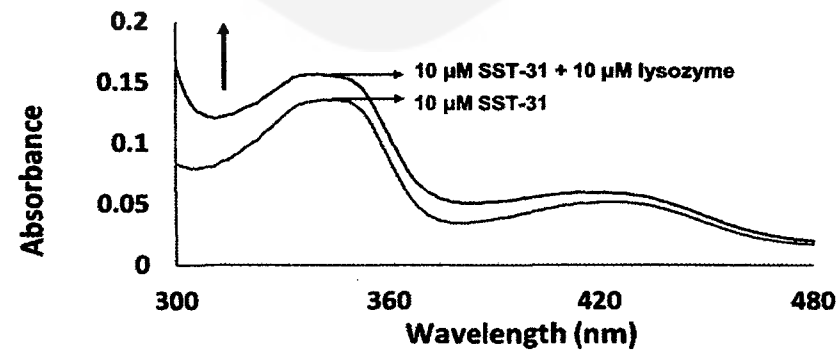


Figure 93 Absorption spectra of SST-31 (10 μM) in the absence (blue) and presence (red) of avidin (0-10 μM).

Table 20 Binding constants and other binding properties of berberine/protein and berberine derivative/protein.

Binding interaction	K_b (M^{-1})	Absorbance shifts
berberine/avidin	4.0×10^5	Hyperchromic (+19%)
SST-29/avidin	6.1×10^5	Hypochromic (-31%)
SST-31/avidin	6.6×10^5	Hypochromic (-35%)
berberine/lysozyme	3.1×10^5	Hyperchromic (+20%)
SST-29/lysozyme	4.6×10^5	Hyperchromic (+23%)
SST-31/lysozyme	4.3×10^5	Hyperchromic (+13%)

2.4 Binding mechanism of natural products with the proteins.

Docking studies results indicated that the location of berberine and its derivatives (SST-29 and SST-31) bound on the part of hydrophilic site and hydrophobic site of avidin and lysozyme. Berberine and its derivatives (SST-29 and SST-31) bound to avidin by hydrogen bonding with the minimum of binding free energies of -7.90, -8.36 and -8.67 kcal/mol, respectively. The data were consistent with the binding constants (K_b) from above experiment. The lower binding free energy from the docking studies indicated higher stability for binding interaction. The binding free energy of SST-31 was lower than that of SST-29 and berberine, which was correlated to the binding constant obtained from the absorption titration experiments (Table 21).

Table 21 Binding constant of berberine/avidin and its derivatives/avidin from absorption titration studies and binding free energy from docking studies.

Binding interaction	Binding constant (M^{-1})	binding free energy (kcal/mol)
berberine (10 μM) + avidin (0-10 μM)	4.0×10^5	-7.90
SST-29 (10 μM) + avidin (0-10 μM)	6.1×10^5	-8.36
SST-31 (10 μM) + avidin (0-10 μM)	6.6×10^5	-8.67

In case of avidin/berberine, the amino acid residues, lining along the binding site with donor-acceptor within the distance of less than 5 Å, were comprised of Leu14, Tyr33, Thr35, Val37, Thr38, Ala39, Thr40, Trp70, Phe72, Ser73, Ser75, Thr77, Phe79, Trp97, Leu99, Ile117 and Asn118 with hydrogen bonding interactions between berberine and Ala39 of avidin (Figures 94a-94c). Berberine aligned close to the cleavage sites of avidin at Thr80-Gly81 and Met96-Trp97 with distances of 11.39 Å and 3.66 Å, respectively. The data were related to the photocleavage experiments.

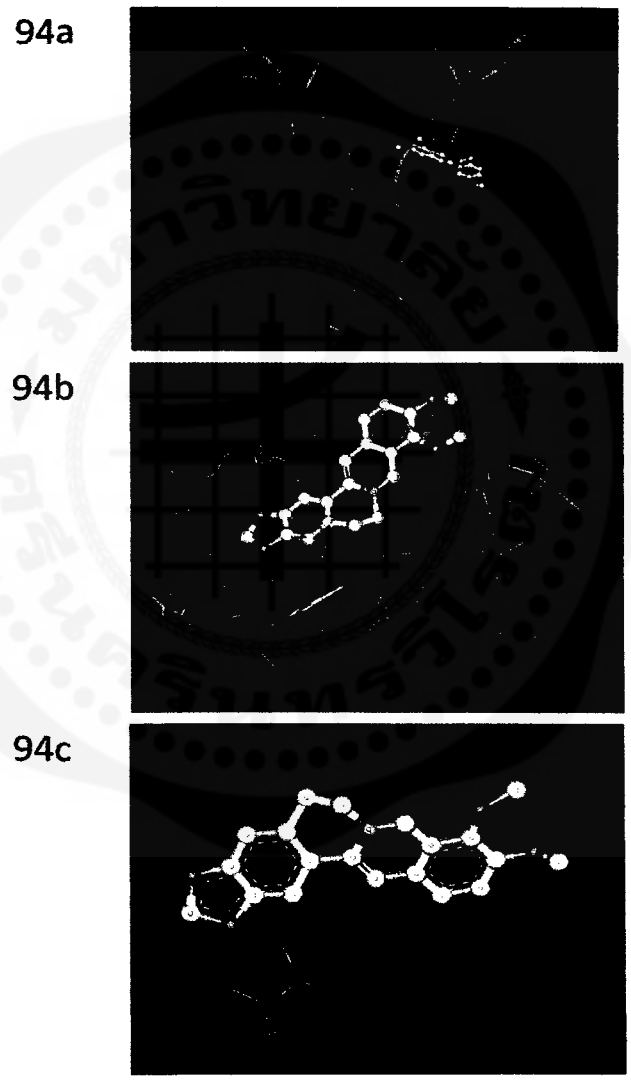


Figure 94 (a) The binding location of berberine on the part of hydrophilic site and hydrophobic site of avidin. (b) The amino acid residues of avidin surrounding berberine within the distance of less than 5 Å. (c) A hydrogen bonding interaction of berberine with an amino acid residue of avidin (dotted green lines).

In case of avidin/SST-29, the amino acid residues, lining along the binding site with donor-acceptor within the distance of less than 5 Å, were comprised of Asp13, Leu14, Ser16, Tyr33, Thr35, Val37, Thr38, Ala39, Thr40, Trp70, Phe72, Ser73, Ser75, Phe79, Trp97, Leu99, Arg114, Val115, Gly116, Ile117 and Asn118 with a hydrogen bonding interactions of SST-29 with Ala39 of avidin (Figures 95a-95c).

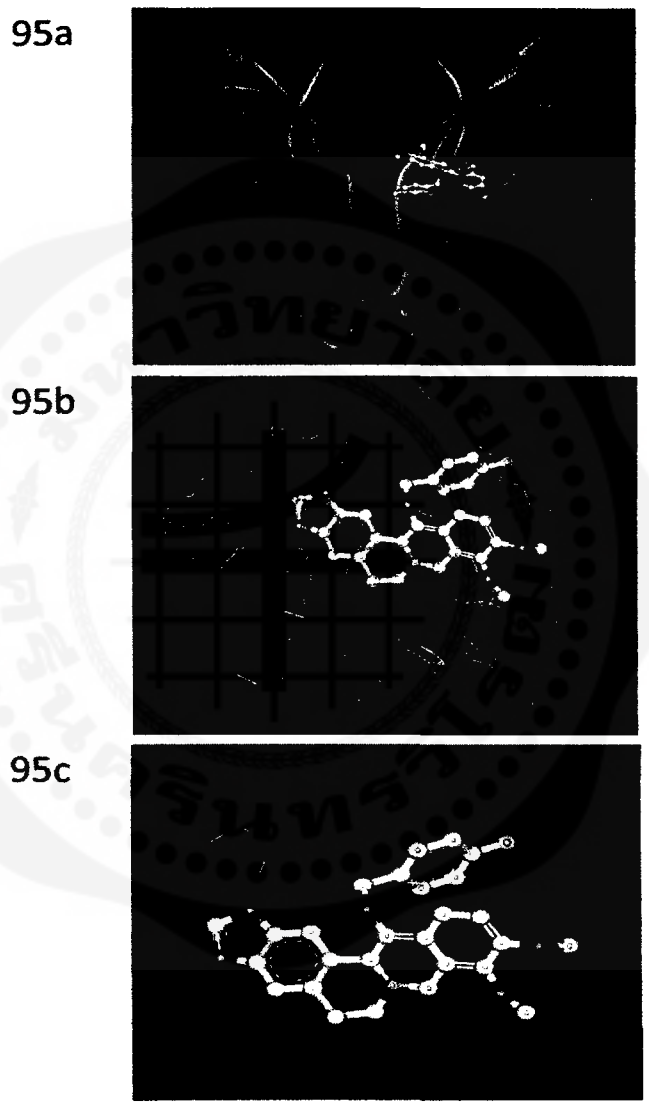


Figure 95 (a) The binding location of SST-29 on the part of hydrophilic site and hydrophobic site of avidin. (b) The amino acid residues of avidin surrounding SST-29 within the distance of less than 5 Å. (c) A hydrogen bonding interaction of SST-29 with an amino acid residue of avidin (dotted green lines).

In case of avidin/SST-31, the amino acid residues, lining along the binding site with donor-acceptor within the distance of less than 5 Å, were comprised of Asp13, Leu14, Ser16, Tyr33, Thr35, Val37, Thr38, Ala39, Thr40, Trp70, Phe72, Ser73, Ser75, Phe79, Trp97, Leu99, Arg114, Val115, Gly116, Ile117 and Asn118 with a hydrogen bonding interactions of SST-31 with Ala39 of avidin (Figures 96a-96c).

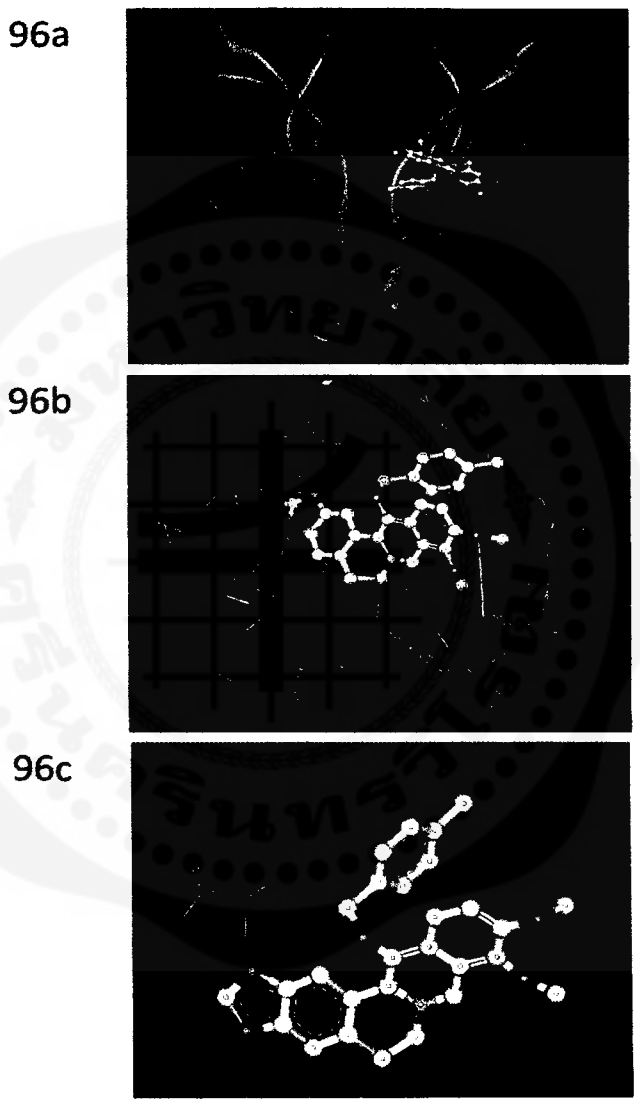


Figure 96 (a) The binding location of SST-31 on the part of hydrophilic site and hydrophobic site of avidin. (b) The amino acid residues of avidin surrounding SST-31 within the distance of less than 5 Å. (c) A hydrogen bonding interaction of SST-31 with an amino acid residue of avidin (dotted green lines).

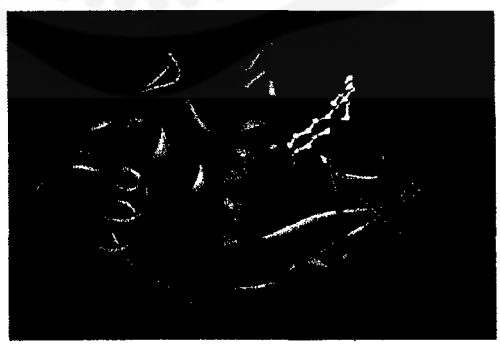
In case of lysozyme, docking studies results demonstrated that berberine, SST-29 and SST-31 bound to lysozyme at similar sites. Moreover, docking studies indicated the location of berberine, SST-29 and SST-31, binding on the part of hydrophilic site and hydrophobic site of lysozyme with hydrogen bonding with the minimum of binding free energies of -7.26, -8.26 and -8.21 kcal/mol, respectively. The binding free energy of SST-29 is lower than that of SST-31 and berberine, which was correlated to the binding constants obtained from the absorption titration experiments (Table 22).

Table 22 Binding constant of berberine/lysozyme and its derivatives/lysozyme from absorption titration studies and binding free energy from docking studies.

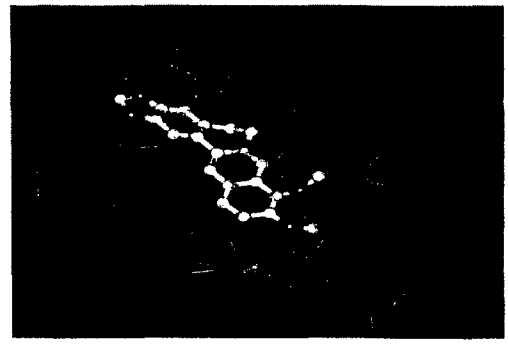
Binding interaction	Binding constant (M^{-1})	binding free energy (kcal/mol)
berberine (10 μM) + lysozyme (0-10 μM)	3.1×10^5	-7.26
SST-29 (10 μM) + lysozyme (0-10 μM)	4.6×10^5	-8.26
SST-31 (10 μM) + lysozyme (0-10 μM)	4.3×10^5	-8.21

In case of lysozyme/berberine, the amino acid residues, lining along the binding site with donor-acceptor within the distance of less than 5 Å, were comprised of Glu35, Asn46, Asp52, Leu56, Gln57, Ile58, Asn59, Trp62, Trp63, Leu75, Ile98, Asp101, Ala107, Trp108 and Val109 with Pi(π) interaction of berberine with Trp62 of lysozyme (Figures 97a-97c).

97a



97b



97c

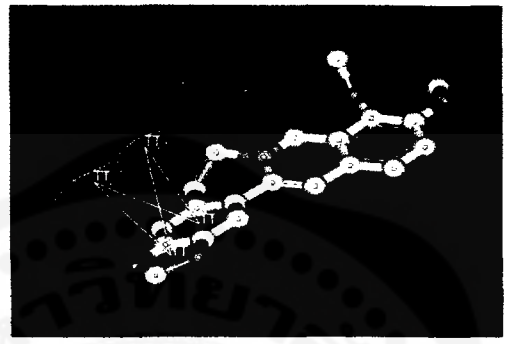
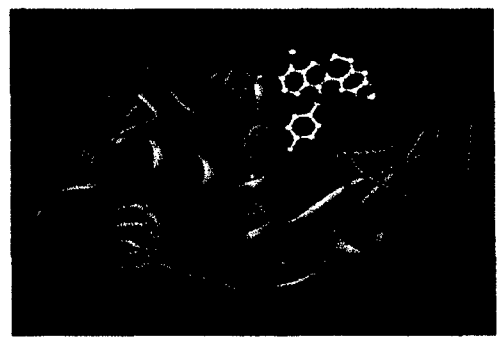


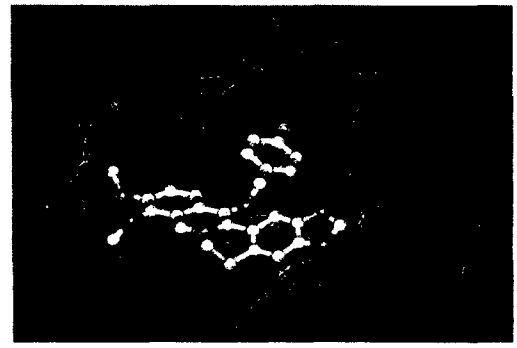
Figure 97 (a) The binding location of berberine on the part of hydrophilic site and hydrophobic site of lysozyme. (b) The amino acid residues of avidin surrounding berberine within the distance of less than 5 Å. (c) Pi(π) interaction of berberine with an amino acid residue of lysozyme (orange lines).

In case of lysozyme/SST-29, the amino acid residues, lining along the binding site with donor-acceptor within the distance of less than 5 Å, were comprised of Asp48, Ser50, Asp52, Leu56, Gln57, Ile58, Asn59, Trp62, Trp63, Ile98, Val99, Ser100, Asp101, Gly102, Asn103, Gly104, Ala107 and Trp108 with three hydrogen bonding interactions of berberine with Gly102, Asn103 and Trp108 of lysozyme (Figures 98a-98c).

98a



98b



98c

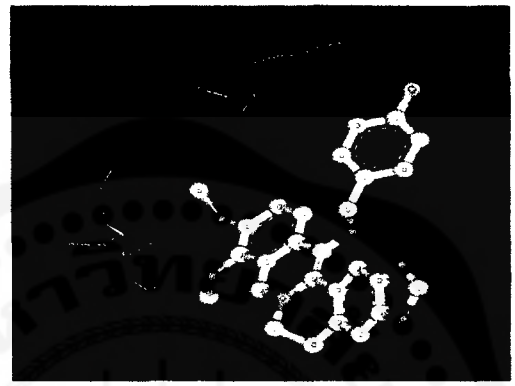


Figure 98 (a) The binding location of SST-29 on the part of hydrophilic site and hydrophobic site of lysozyme. (b) The amino acid residues of lysozyme surrounding SST-29 within the distance of less than 5 Å. (c) Three hydrogen bonding interactions of SST-29 with three amino acid residues of lysozyme (dotted green lines).

In case of lysozyme/SST-31, the amino acid residues, lining along the binding site with donor-acceptor within the distance of less than 5 Å, were comprised of Asp48, Leu56, Gln57, Ile58, Asn59, Trp62, Trp63, Ile98, Val99, Ser100, Asp101, Gly102, Asn103, Gly104, Ala107 and Trp108 with a hydrogen bonding interaction of berberine with Asn103 of lysozyme (Figures 99a-99c).

99a



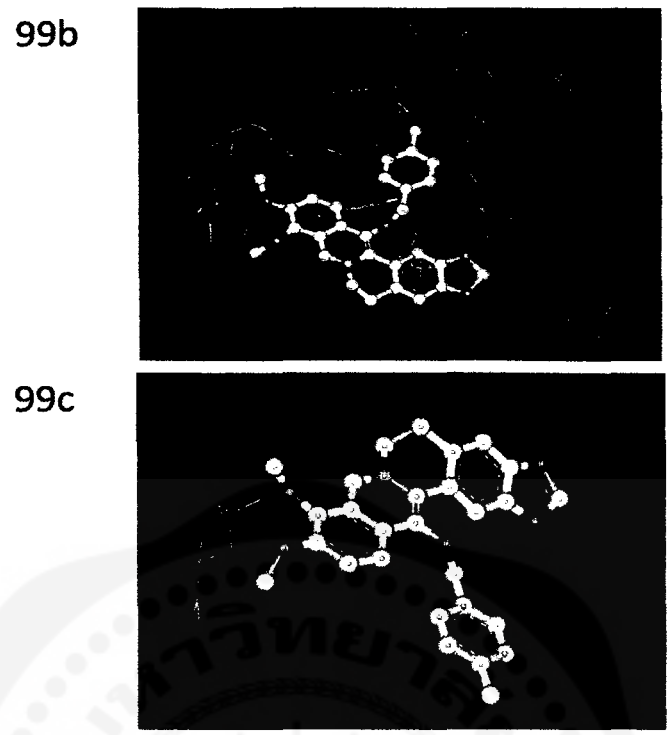


Figure 99 (a) The binding location of SST-31 on the part of hydrophilic site and hydrophobic site of lysozyme. (b) The amino acid residues of lysozyme surrounding SST-31 within the distance of less than 5 Å. (c) A hydrogen bonding interaction of SST-31 with an amino acid residue of lysozyme (dotted green lines).

Spectral changes of berberine, SST-29 and SST-31 in the presence of the protein indicated strong binding interaction with high binding constant. Berberine, SST-29 and SST-31 showed stronger binding interaction with avidin than binding interaction with lysozyme. SST-31 bound to avidin better than SST-29 and berberine bound to avidin, whereas SST-29 bound to lysozyme better than SST-31 and berberine bound to lysozyme. However, the product yields of photocleaved fragments obtained with the reaction with berberine were lower than that obtained with the reaction with the synthesized photochemical reagents. Therefore, the structure of berberine could be suitable (in size, shape, functional group, polarity and charged groups) for high specific and efficient cleavage of protein backbone.

CHAPTER 5

Conclusions and Recommendation

The main objective of this desertation was to use new synthesized photochemical reagents and natural products to specifically bind to protein and cleave protein backbone. The binding properties of the synthesized photochemical reagents (PMA-1A, PMA-2A, PMA-3A) and natural products (berberine and piperine), including their derivatives (SST-29 and SST-31) with proteins (avidin, lysozyme, α-chymotrypsin, β-lactoglobulin B, myoglobin, BSA, HSA, α-casein, pepsin, concanacalin A and β-glucosidase) have been investigated.

Photochemical reagents

The results for photocleavage of proteins clearly showed that avidin can be specifically cleaved at one position, providing 2 fragments with molecular weights of ~8.4 kDa and ~5.9 kDa, by PMA-1A, PMA-2A, PMA-3A, in the presence of an electron acceptor (CoHA). Avidin photocleavage studies demonstrated high specificity, efficiency and high photoproduct yields. The residues of fragment 1 of avidin/photochemical reagents was *N*-terminal sequence of avidin (ARKCS). The major residues of fragment 2 of avidin/photochemical reagents was VFTGQ, indicating that the major cleavage site of avidin occurred between Thr77 and Val78. From the known primary sequence of avidin, fragment 1 (~8.4 kDa) was the *N*-terminal sequence, while fragment 2 (~5.9 kDa) was the *C*-terminal sequence of avidin. Moreover, the minor cleavage sites of avidin were also observed and demonstrated in Table 23. Photocleavage of lysozyme was also succeeded by these three synthesized photochemical reagents, resulting to two cleaved fragments with molecular weights of ~9.7 kDa and ~4.6 kDa. However, the 4.6 kDa fragment was too faint for subjecting to amino acid sequencing.

Table 23 Photocleavage sites of avidin.

Photoreagents	PMA-1A	PMA-2A	PMA-3A
major cleavage site	Thr77-Val78	Thr77-Val78	Thr77-Val78
minor cleavage site	Trp70-Lys71		Thr35-Ala36

The maximum absorption wavelength of all photochemical reagents was observed at 342 nm. Spectral changes of the photochemical reagents (PMA-1A, PMA-2A and PMA-3A) in the presence of the proteins indicated strong binding interactions with high binding constants, as demonstrated in Table 24. The hypochromic shifts in the absorption bands of the PMA-1A/avidin, PMA-2A/avidin, PMA-3A/avidin, PMA-1A/lysozyme, PMA-2A/lysozyme and PMA-3A/lysozyme were obtained from the titration of the photochemical reagent with the protein (decreased by 30%, 17%, 36%, 23%, 22% and 20%, respectively). Spectral changes indicated that the binding mechanism could be different, which depended on the linker length, providing a strong evidence that the side chain of the probe plays an important role in the binding interaction with protein.

Fluorescence quenching studies demonstrated that the binding sites were exposed to the quencher as the quenching constants of the bound probes were not significantly decreased. Therefore, the quencher (CoHA) can easily access to the photochemical reagents, giving high cleavage yields. The observed K_{sv} values paralleled with the cleavage yield, in which the cleavage yield decreased with the increase in the linker length. PMA-1A/avidin showed no changing in the K_{sv} values, suggesting that PMA-1A could bind to avidin at more accessible site for the quencher than the other two reagants. The data supported the higher product yields obtained from the reaction of PMA-1A/avidin than that of the other two reagents. Since the other two reagents have some nominal protection from the quencher by the protein matrix, the accessibility to CoHA could be less. Access to the excited state by CoHA is essential to produce reactive intermediates at the binding site, upon the photoexcitation in the photocleavage studies. Therefore, deeply buried probe in the protein matrix could lead to less reactive intermediates generated on light excitation, resulting to less product yields.

Mechanisms were demonstrated by molecular docking studies, indicating that the position of proteins photocleavage can occur in the proximity to the binding site of the probe on the protein. In addition, all probes bound to proteins by hydrogen bonding with minimum of binding free energy which indicated stability upon binding. The change in Gibbs free energy (ΔG) can be calculated by equation 25. This energy change indicated that binding interaction is spontaneous. Gibbs free energy from calculation related with binding free energy from docking studies. Binding free energies were consistent with the binding constants (K_b) and Gibbs free energy from spectroscopic experiments, as demonstrated in Table 24.

$$\Delta G = -RT \ln K \quad \text{---- [25]}$$

Where, ΔG is Gibbs free energy (kcal)

R is gas constant (1.9872×10^3 kcal/K•mol)

T is temperature (K)

K is binding constant from experiments (1/mol)

Table 24 Binding constant (M^{-1}) from absorption titration studies, Gibbs free energy from calculation and binding free energy (kcal/mol) from docking studies of probe/protein.

Binding interaction	Binding constant from experiments	Gibbs free energy from calculation	binding free energy from docking studies
PMA-1A + avidin	6.2×10^5	-7.90	-8.88
PMA-2A + avidin	6.7×10^5	-7.95	-9.32
PMA-3A + avidin	4.6×10^5	-7.73	-8.67
PMA-1A + lysozyme	1.7×10^5	-7.14	-7.95
PMA-2A + lysozyme	2.4×10^5	-7.34	-8.50
PMA-3A + lysozyme	1.9×10^5	-7.20	-8.36

The molecular docking results supported above all photocleavage and spectroscopic results. In case of avidin, molecular docking studies indicated that the location of anionic PMA-1A, anionic PMA-2A, anionic PMA-3A bound to polar amino acid residues and nonpolar amino acid residues which are near the hydrophilic sites of avidin. In case of lysozyme, molecular docking studies indicated that anionic PMA-1A, anionic PMA-2A, anionic PMA-3A bound to polar uncharged amino acid residues, nonpolar amino acid residues and electrically charged amino acid residues of lysozyme. These binding sites were found to align near the surface of lysozyme. Therefore, a series of new synthesized fluorescent probes with variation of chain lengths has the potential to position the photochemical reagent at particular locations and influence the photocleavage site on the protein.

In this study, we have designed and synthesized new fluorescent probes that can specifically and efficiently cleave protein backbone. Moreover, these photochemical reagents can bind to proteins with high binding affinity. The structure of the probe should be suitable in size, shape, functional group, polarity and charged groups. From the results, side chain length the photochemical reagent can be systematically tuned to provide an excellent control over the cleavage site location.

Natural products

Using natural products is another alternative way to investigate probe/protein binding interaction. Avidin was successfully cleaved by berberine, in the presence of CoHA, while the reaction was not observed with piperine. The cleavage of avidin by berberine resulted in 3 fragments (~8.7 kDa, ~5.6 kDa and ~3.7 kDa). The residues of fragment 1 (8.7 kDa) was *N*-terminal sequence of avidin (ARKCS). However, the 5.6 kDa and 3.7 kDa fragments were too faint for subjecting to amino acid sequencing, making inadequate data to predict the position of the cleavage site. However, from the estimation of molecular weights of fragment 2 and fragment 3, the cleavage sites of avidin may occur between Thr80-Gly81 and Met96-Trp97, respectively.

The maximum absorption wavelength of berberine, SST-29 and SST-31 were 345 nm. Spectral changes of berberine, SST-29 and SST-31 in the presence of the protein indicated strong binding interaction with high binding constant. In case of avidin, binding constants of berberine/avidin, SST-29/avidin and SST-31/avidin were 4.0×10^5 M^{-1}, 6.1×10^5 M^{-1} and 6.6×10^5 M^{-1}, respectively. The hyperchromic shifts in the absorption bands were observed upon binding of berberine/avidin (increased by 19%) while hypochromic shifts in the absorption bands were observed upon binding of SST-29/avidin and SST-31/avidin (decreased by 31% and 35%, respectively). In case of lysozyme, binding constants of berberine/lysozyme, SST-29/lysozyme and SST-31/lysozyme were 3.1×10^5 M^{-1}, 4.6×10^5 M^{-1} and 4.3×10^5 M^{-1}, respectively. The hyperchromic shifts in the absorption bands were observed upon binding of berberine/lysozyme, SST-29/lysozyme and SST-31/lysozyme (increased by 20%, 23% and 13%, respectively). Berberine and berberine derivatives (SST-29 and SST-31) showed stronger binding interaction with avidin than binding to lysozyme.

The mechanisms of berberine/protein, SST-29/protein and SST-31/protein interactions were investigated in molecular docking studies. The cleavage site of protein from the photoreaction occurred in the proximity to the binding site of protein. In addition, all probes bound to proteins by hydrogen bonding with minimum of binding free energy which

indicated stability upon binding. In case of avidin, molecular docking studies indicated that all probes bound to polar amino acid residues and nonpolar amino acid residues of avidin which are near the hydrophilic sites of avidin. In case of lysozyme, molecular docking studies indicated that all probes bound to polar uncharged amino acid residues, nonpolar amino acid residues and electrically charged amino acid residues of lysozyme which aligned near the surface of lysozyme. Binding free energies were consistent with the binding constants (K_b) and Gibbs free energy from spectroscopic experiments, as demonstrated in Table 25. Gibbs free energy change indicated that binding interaction is spontaneous.

Table 25 Binding constant (M^{-1}) from absorption titration studies, Gibbs free energy from calculation and binding free energy (kcal/mol) from docking studies of probe/protein.

Binding interaction	Binding constant from experiments	Gibbs free energy from calculation	binding free energy from docking studies
berberine + avidin	4.0×10^5	-7.64	-7.90
SST-29 + avidin	6.1×10^5	-7.89	-8.36
SST-31 + avidin	6.6×10^5	-7.94	-8.67
berberine + lysozyme	3.1×10^5	-7.49	-7.26
SST-29 + lysozyme	4.6×10^5	-7.73	-8.26
SST-31 + lysozyme	4.3×10^5	-7.69	-8.21

Moreover, binding constant of berberine, SST-29 and SST-31 in the presence of both proteins indicated strong binding interaction with high binding constant. Berberine, SST-29 and SST-31 showed stronger binding interaction with avidin than binding interaction with lysozyme. SST-31 bound to avidin better than SST-29 and berberine bound to avidin, whereas SST-29 bound to lysozyme better than SST-31 and berberine bound to lysozyme, indicating that the environment surrounding these probes could be different. Binding constant of berberine/protein was higher than binding constant obtained from the synthesized photochemical reagent/protein.

However, the product yields of photocleaved fragments obtained from the reaction with berberine were lower than that obtained from the reaction with the synthesized photochemical reagents. Therefore, the structure of berberine could be suitable (in size, shape, functional group, polarity and charged groups) for high specific and efficient cleavage of protein backbone. Development of berberine structure may be of interest for the improvement of photochemical reagents to provide important insights into the interactions of small ligand with protein in the future studies.

Improvement of these fluorescent probes could be useful for converting larger proteins into smaller fragments, understanding protein-ligand interactions. The interaction of probe and protein will give more important insights in life sciences, chemistry, biology and pharmacology for the development of therapeutic drug design in the future.

APPENDIX

APPENDIX

Proteins were not cleaved by PMA-1A, PMA-2A, PMA-3A, berberine and piperine, as demonstrated in Figure 100-169.

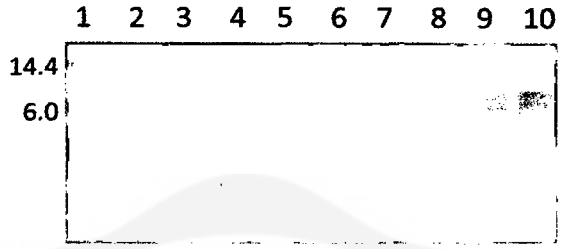


Figure 100 Photocleavage of α-chymotrypsin obtained from the reaction with PMA-1A.
Lane 1: molecular weight markers (kDa)
Lane 2: α-chymotrypsin (15 μM), PMA-1A (15 μM) and CoHA (1 mM), dark control
Lane 3: α-chymotrypsin (15 μM), PMA-1A (15 μM) and CoHA (1 mM), 342 nm, 10 min
Lane 4: α-chymotrypsin (15 μM), PMA-1A (15 μM) and CoHA (1 mM), 342 nm, 20 min
Lane 5: α-chymotrypsin (15 μM), dark control
Lane 6: α-chymotrypsin (15 μM), 342 nm, 20 min
Lane 7: α-chymotrypsin (15 μM) and CoHA (1 mM), dark control
Lane 8: α-chymotrypsin (15 μM) and CoHA (1 mM), 342 nm, 20 min
Lane 9: α-chymotrypsin (15 μM) and PMA-1A (15 μM), dark control
Lane 10: α-chymotrypsin (15 μM) and PMA-1A (15 μM), 342 nm, 20 min

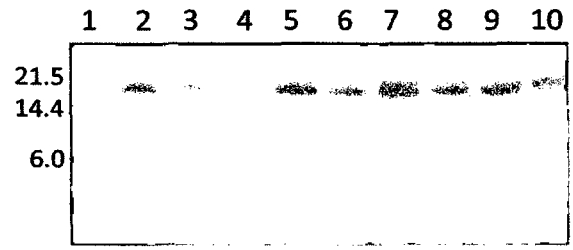


Figure 101 Photocleavage of β-lactoglobulin B obtained from the reaction with PMA-1A.
Lane 1: molecular weight markers (kDa)
Lane 2: β-lactoglobulin B (15 μM), PMA-1A (15 μM) and CoHA (1 mM), dark control

Lane 3: β-lactoglobulin B (15 μM), PMA-1A (15 μM) and CoHA (1 mM), 342 nm, 10 min

Lane 4: β-lactoglobulin B (15 μM), PMA-1A (15 μM) and CoHA (1 mM), 342 nm, 20 min

Lane 5: β-lactoglobulin B (15 μM), dark control

Lane 6: β-lactoglobulin B (15 μM), 342 nm, 20 min

Lane 7: β-lactoglobulin B (15 μM) and CoHA (1 mM), dark control

Lane 8: β-lactoglobulin B (15 μM) and CoHA (1 mM), 342 nm, 20 min

Lane 9: β-lactoglobulin B (15 μM) and PMA-1A (15 μM), dark control

Lane 10: β-lactoglobulin B (15 μM) and PMA-1A (15 μM), 342 nm, 20 min

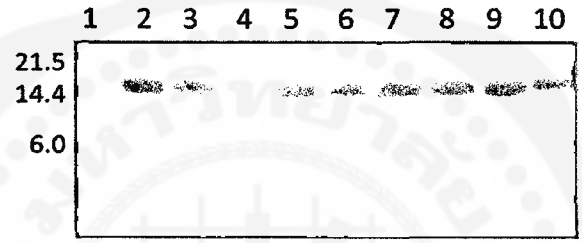


Figure 102 Photocleavage of myoglobin obtained from the reaction with PMA-1A.

Lane 1: molecular weight markers (kDa)

Lane 2: myoglobin (15 μM), PMA-1A (15 μM) and CoHA (1 mM), dark control

Lane 3: myoglobin (15 μM), PMA-1A (15 μM) and CoHA (1 mM), 342 nm, 10 min

Lane 4: myoglobin (15 μM), PMA-1A (15 μM) and CoHA (1 mM), 342 nm, 20 min

Lane 5: myoglobin (15 μM), dark control

Lane 6: myoglobin (15 μM), 342 nm, 20 min

Lane 7: myoglobin (15 μM) and CoHA (1 mM), dark control

Lane 8: myoglobin (15 μM) and CoHA (1 mM), 342 nm, 20 min

Lane 9: myoglobin (15 μM) and PMA-1A (15 μM), dark control

Lane 10: myoglobin (15 μM) and PMA-1A (15 μM), 342 nm, 20 min

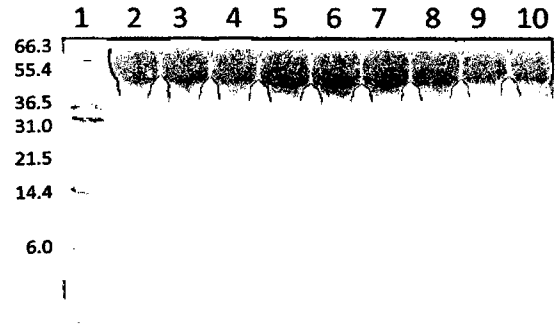


Figure 103 Photocleavage of HSA obtained from the reaction with PMA-1A.

Lane 1: molecular weight markers (kDa)

Lane 2: HSA (15 μM), PMA-1A (15 μM) and CoHA (1 mM), dark control

Lane 3: HSA (15 μM), PMA-1A (15 μM) and CoHA (1 mM), 342 nm, 10 min

Lane 4: HSA (15 μM), PMA-1A (15 μM) and CoHA (1 mM), 342 nm, 20 min

Lane 5: HSA (15 μM), dark control

Lane 6: HSA (15 μM), 342 nm, 20 min

Lane 7: HSA (15 μM) and CoHA (1 mM), dark control

Lane 8: HSA (15 μM) and CoHA (1 mM), 342 nm, 20 min

Lane 9: HSA (15 μM) and PMA-1A (15 μM), dark control

Lane 10: HSA (15 μM) and PMA-1A (15 μM), 342 nm, 20 min

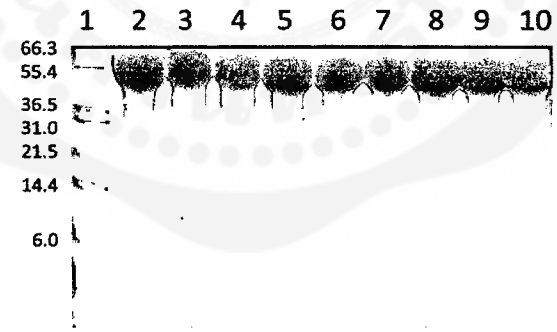


Figure 104 Photocleavage of BSA obtained from the reaction with PMA-1A.

Lane 1: molecular weight markers (kDa)

Lane 2: BSA (15 μM), PMA-1A (15 μM) and CoHA (1 mM), dark control

Lane 3: BSA (15 μM), PMA-1A (15 μM) and CoHA (1 mM), 342 nm, 10 min

Lane 4: BSA (15 μM), PMA-1A (15 μM) and CoHA (1 mM), 342 nm, 20 min

Lane 5: BSA (15 μM), dark control

Lane 6: BSA (15 μM), 342 nm, 20 min

Lane 7: BSA (15 μM) and CoHA (1 mM), dark control

Lane 8: BSA (15 μM) and CoHA (1 mM), 342 nm, 20 min

Lane 9: BSA (15 μM) and PMA-1A (15 μM), dark control

Lane 10: BSA (15 μM) and PMA-1A (15 μM), 342 nm, 20 min

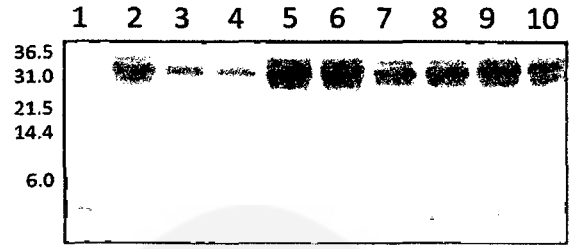


Figure 105 Photocleavage of α-casein obtained from the reaction with PMA-1A.

Lane 1: molecular weight markers (kDa)

Lane 2: α-casein (15 μM), PMA-1A (15 μM) and CoHA (1 mM), dark control

Lane 3: α-casein (15 μM), PMA-1A (15 μM) and CoHA (1 mM), 342 nm, 10 min

Lane 4: α-casein (15 μM), PMA-1A (15 μM) and CoHA (1 mM), 342 nm, 20 min

Lane 5: α-casein (15 μM), dark control

Lane 6: α-casein (15 μM), 342 nm, 20 min

Lane 7: α-casein (15 μM) and CoHA (1 mM), dark control

Lane 8: α-casein (15 μM) and CoHA (1 mM), 342 nm, 20 min

Lane 9: α-casein (15 μM) and PMA-1A (15 μM), dark control

Lane 10: α-casein (15 μM) and PMA-1A (15 μM), 342 nm, 20 min

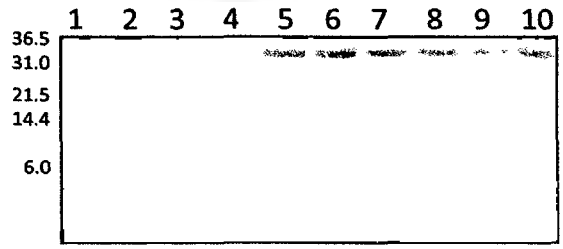


Figure 106 Photocleavage of pepsin obtained from the reaction with PMA-1A.

Lane 1: molecular weight markers (kDa)

Lane 2: pepsin (15 μM), PMA-1A (15 μM) and CoHA (1 mM), dark control

Lane 3: pepsin (15 μM), PMA-1A (15 μM) and CoHA (1 mM), 342 nm, 10 min

Lane 4: pepsin (15 μM), PMA-1A (15 μM) and CoHA (1 mM), 342 nm, 20 min

Lane 5: pepsin (15 μM), dark control

Lane 6: pepsin (15 μM), 342 nm, 20 min

Lane 7: pepsin (15 μM) and CoHA (1 mM), dark control

Lane 8: pepsin (15 μM) and CoHA (1 mM), 342 nm, 20 min

Lane 9: pepsin (15 μM) and PMA-1A (15 μM), dark control

Lane 10: pepsin (15 μM) and PMA-1A (15 μM), 342 nm, 20 min

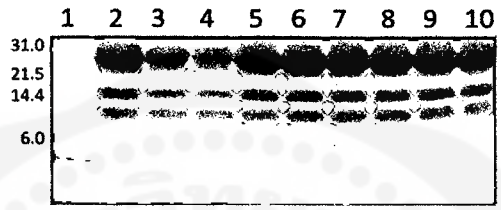


Figure 107 Photocleavage of concanavalin A obtained from the reaction with PMA-1A.

Lane 1: molecular weight markers (kDa)

Lane 2: concanavalin A (15 μM), PMA-1A (15 μM) and CoHA (1 mM), dark control

Lane 3: concanavalin A (15 μM), PMA-1A (15 μM) and CoHA (1 mM), 342 nm, 10 min

Lane 4: concanavalin A (15 μM), PMA-1A (15 μM) and CoHA (1 mM), 342 nm, 20 min

Lane 5: concanavalin A (15 μM), dark control

Lane 6: concanavalin A (15 μM), 342 nm, 20 min

Lane 7: concanavalin A (15 μM) and CoHA (1 mM), dark control

Lane 8: concanavalin A (15 μM) and CoHA (1 mM), 342 nm, 20 min

Lane 9: concanavalin A (15 μM) and PMA-1A (15 μM), dark control

Lane 10: concanavalin A (15 μM) and PMA-1A (15 μM), 342 nm, 20 min

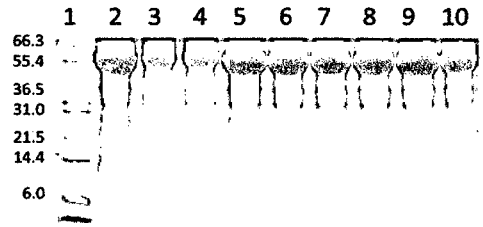


Figure 108 Photocleavage of β-glucosidase obtained from the reaction with PMA-1A.

Lane 1: molecular weight markers (kDa)

Lane 2: β-glucosidase (15 μM), PMA-1A (15 μM) and CoHA (1 mM), dark control

Lane 3: β-glucosidase (15 μM), PMA-1A (15 μM) and CoHA (1 mM), 342 nm, 10 min

Lane 4: β-glucosidase (15 μM), PMA-1A (15 μM) and CoHA (1 mM), 342 nm, 20 min

Lane 5: β-glucosidase (15 μM), dark control

Lane 6: β-glucosidase (15 μM), 342 nm, 20 min

Lane 7: β-glucosidase (15 μM) and CoHA (1 mM), dark control

Lane 8: β-glucosidase (15 μM) and CoHA (1 mM), 342 nm, 20 min

Lane 9: β-glucosidase (15 μM) and PMA-1A (15 μM), dark control

Lane 10: β-glucosidase (15 μM) and PMA-1A (15 μM), 342 nm, 20 min

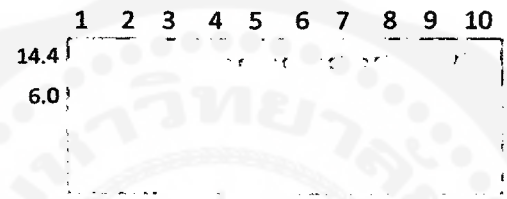


Figure 109 Photocleavage of α-chymotrypsin obtained from the reaction with PMA-2A.

Lane 1: molecular weight markers (kDa)

Lane 2: α-chymotrypsin (15 μM), dark control

Lane 3: α-chymotrypsin (15 μM), 342 nm, 20 min

Lane 4: α-chymotrypsin (15 μM) and CoHA (1 mM), dark control

Lane 5: α-chymotrypsin (15 μM) and CoHA (1 mM), 342 nm, 20 min

Lane 6: α-chymotrypsin (15 μM) and PMA-2A (15 μM), dark control

Lane 7: α-chymotrypsin (15 μM) and PMA-2A (15 μM), 342 nm, 20 min

Lane 8: α-chymotrypsin (15 μM), PMA-2A (15 μM) and CoHA (1 mM), dark control

Lane 9: α-chymotrypsin (15 μM), PMA-2A (15 μM) and CoHA (1 mM), 342 nm, 10 min

Lane 10: α-chymotrypsin (15 μM), PMA-2A (15 μM) and CoHA (1 mM), 342 nm, 20 min

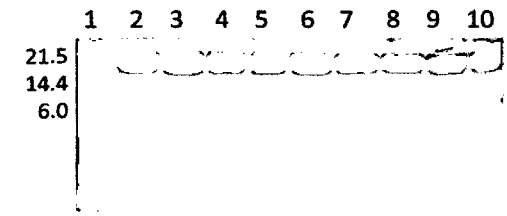


Figure 110 Photocleavage of β-lactoglobulin B obtained from the reaction with PMA-2A.

Lane 1: molecular weight markers (kDa)

Lane 2: β-lactoglobulin B (15 μM), dark control

Lane 3: β-lactoglobulin B (15 μM), 342 nm, 20 min

Lane 4: β-lactoglobulin B (15 μM) and CoHA (1 mM), dark control

Lane 5: β-lactoglobulin B (15 μM) and CoHA (1 mM), 342 nm, 20 min

Lane 6: β-lactoglobulin B (15 μM) and PMA-2A (15 μM), dark control

Lane 7: β-lactoglobulin B (15 μM) and PMA-2A (15 μM), 342 nm, 20 min

Lane 8: β-lactoglobulin B (15 μM), PMA-2A (15 μM) and CoHA (1 mM), dark control

Lane 9: β-lactoglobulin B (15 μM), PMA-2A (15 μM) and CoHA (1 mM), 342 nm, 10 min

Lane 10: β-lactoglobulin B (15 μM), PMA-2A (15 μM) and CoHA (1 mM), 342 nm, 20 min

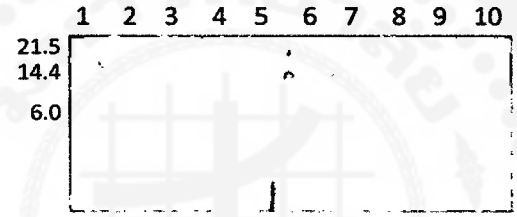


Figure 111 Photocleavage of myoglobin obtained from the reaction with PMA-2A.

Lane 1: molecular weight markers (kDa)

Lane 2: myoglobin (15 μM), dark control

Lane 3: myoglobin (15 μM), 342 nm, 20 min

Lane 4: myoglobin (15 μM) and CoHA (1 mM), dark control

Lane 5: myoglobin (15 μM) and CoHA (1 mM), 342 nm, 20 min

Lane 6: myoglobin (15 μM) and PMA-2A (15 μM), dark control

Lane 7: myoglobin (15 μM) and PMA-2A (15 μM), 342 nm, 20 min

Lane 8: myoglobin (15 μM), PMA-2A (15 μM) and CoHA (1 mM), dark control

Lane 9: myoglobin (15 μM), PMA-2A (15 μM) and CoHA (1 mM), 342 nm, 10 min

Lane 10: myoglobin (15 μM), PMA-2A (15 μM) and CoHA (1 mM), 342 nm, 20 min

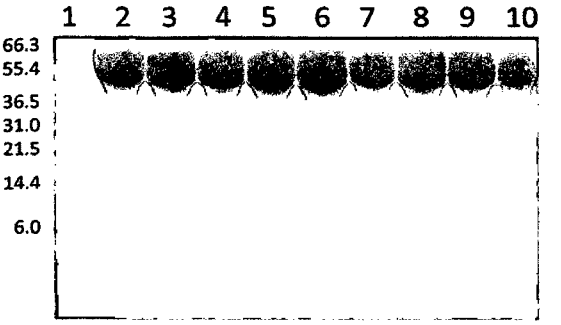


Figure 112 Photocleavage of HSA obtained from the reaction with PMA-2A.

Lane 1: molecular weight markers (kDa)

Lane 2: HSA (15 μM), dark control

Lane 3: HSA (15 μM), 342 nm, 20 min

Lane 4: HSA (15 μM) and CoHA (1 mM), dark control

Lane 5: HSA (15 μM) and CoHA (1 mM), 342 nm, 20 min

Lane 6: HSA (15 μM) and PMA-2A (15 μM), dark control

Lane 7: HSA (15 μM) and PMA-2A (15 μM), 342 nm, 20 min

Lane 8: HSA (15 μM), PMA-2A (15 μM) and CoHA (1 mM), dark control

Lane 9: HSA (15 μM), PMA-2A (15 μM) and CoHA (1 mM), 342 nm, 10 min

Lane 10: HSA (15 μM), PMA-2A (15 μM) and CoHA (1 mM), 342 nm, 20 min

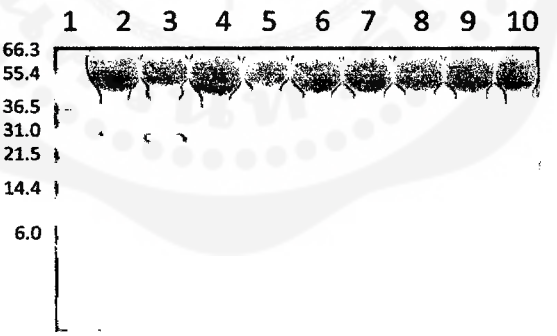


Figure 113 Photocleavage of BSA obtained from the reaction with PMA-2A.

Lane 1: molecular weight markers (kDa)

Lane 2: BSA (15 μM), dark control

Lane 3: BSA (15 μM), 342 nm, 20 min

Lane 4: BSA (15 μM) and CoHA (1 mM), dark control

Lane 5: BSA (15 μM) and CoHA (1 mM), 342 nm, 20 min

Lane 6: BSA (15 μM) and PMA-2A (15 μM), dark control

Lane 7: BSA (15 μM) and PMA-2A (15 μM), 342 nm, 20 min

Lane 8: BSA (15 μM), PMA-2A (15 μM) and CoHA (1 mM), dark control

Lane 9: BSA (15 μM), PMA-2A (15 μM) and CoHA (1 mM), 342 nm, 10 min

Lane 10: BSA (15 μM), PMA-2A (15 μM) and CoHA (1 mM), 342 nm, 20 min

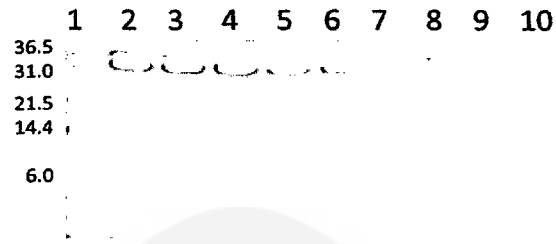


Figure 114 Photocleavage of α-casein obtained from the reaction with PMA-2A.

Lane 1: molecular weight markers (kDa)

Lane 2: α-casein (15 μM), dark control

Lane 3: α-casein (15 μM), 342 nm, 20 min

Lane 4: α-casein (15 μM) and CoHA (1 mM), dark control

Lane 5: α-casein (15 μM) and CoHA (1 mM), 342 nm, 20 min

Lane 6: α-casein (15 μM) and PMA-2A (15 μM), dark control

Lane 7: α-casein (15 μM) and PMA-2A (15 μM), 342 nm, 20 min

Lane 8: α-casein (15 μM), PMA-2A (15 μM) and CoHA (1 mM), dark control

Lane 9: α-casein (15 μM), PMA-2A (15 μM) and CoHA (1 mM), 342 nm, 10 min

Lane 10: α-casein (15 μM), PMA-2A (15 μM) and CoHA (1 mM), 342 nm, 20 min

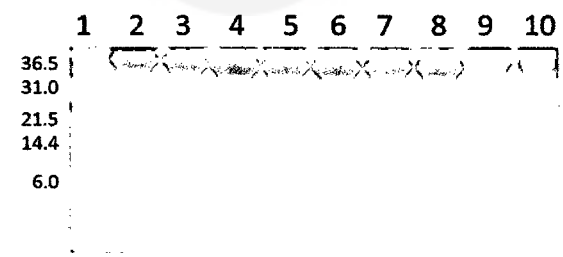


Figure 115 Photocleavage of pepsin obtained from the reaction with PMA-2A.

Lane 1: molecular weight markers (kDa)

Lane 2: pepsin (15 μM), dark control

Lane 3: pepsin (15 μM), 342 nm, 20 min

Lane 4: pepsin (15 μM) and CoHA (1 mM), dark control

Lane 5: pepsin (15 μM) and CoHA (1 mM), 342 nm, 20 min

Lane 6: pepsin (15 μM) and PMA-2A (15 μM), dark control

Lane 7: pepsin (15 μM) and PMA-2A (15 μM), 342 nm, 20 min

Lane 8: pepsin (15 μM), PMA-2A (15 μM) and CoHA (1 mM), dark control

Lane 9: pepsin (15 μM), PMA-2A (15 μM) and CoHA (1 mM), 342 nm, 10 min

Lane 10: pepsin (15 μM), PMA-2A (15 μM) and CoHA (1 mM), 342 nm, 20 min

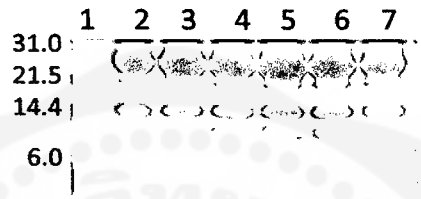


Figure 116 Photocleavage of concanavalin A obtained from the reaction with PMA-2A.

Lane 1: molecular weight markers (kDa)

Lane 2: concanavalin A (15 μM) and CoHA (1 mM), dark control

Lane 3: concanavalin A (15 μM) and CoHA (1 mM), 342 nm, 20 min

Lane 4: concanavalin A (15 μM) and PMA-2A (15 μM), dark control

Lane 5: concanavalin A (15 μM) and PMA-2A (15 μM), 342 nm, 20 min

Lane 6: concanavalin A (15 μM), PMA-2A (15 μM) and CoHA (1 mM), dark control

Lane 7: concanavalin A (15 μM), PMA-2A (15 μM) and CoHA (1 mM), 342 nm, 20 min

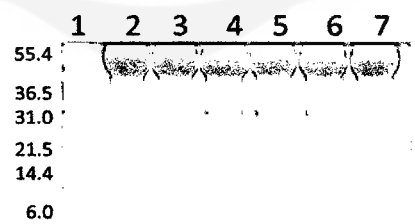


Figure 117 Photocleavage of β-glucosidase obtained from the reaction with PMA-2A.

Lane 1: molecular weight markers (kDa)

Lane 2: β-glucosidase (15 μM) and CoHA (1 mM), dark control

Lane 3: β-glucosidase (15 μM) and CoHA (1 mM), 342 nm, 20 min

Lane 4: β-glucosidase (15 μM) and PMA-2A (15 μM), dark control

Lane 5: β-glucosidase (15 μM) and PMA-2A (15 μM), 342 nm, 20 min

Lane 6: β-glucosidase (15 μM), PMA-2A (15 μM) and CoHA (1 mM), dark control

Lane 7: β-glucosidase (15 μM), PMA-2A (15 μM) and CoHA (1 mM), 342 nm, 20 min

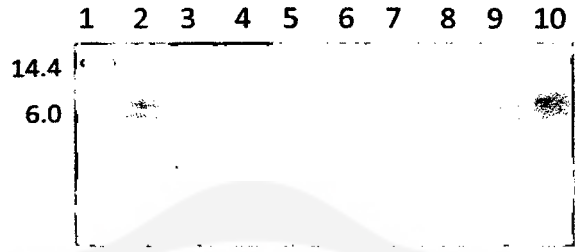


Figure 118 Photocleavage of α-chymotrypsin obtained from the reaction with PMA-3A.

Lane 1: molecular weight markers (kDa)

Lane 2: α-chymotrypsin (15 μM), PMA-3A (15 μM) and CoHA (1 mM), dark control

Lane 3: α-chymotrypsin (15 μM), PMA-3A (15 μM) and CoHA (1 mM), 342 nm, 10 min

Lane 4: α-chymotrypsin (15 μM), PMA-3A (15 μM) and CoHA (1 mM), 342 nm, 20 min

Lane 5: α-chymotrypsin (15 μM), dark control

Lane 6: α-chymotrypsin (15 μM), 342 nm, 20 min

Lane 7: α-chymotrypsin (15 μM) and CoHA (1 mM), dark control

Lane 8: α-chymotrypsin (15 μM) and CoHA (1 mM), 342 nm, 20 min

Lane 9: α-chymotrypsin (15 μM) and PMA-3A (15 μM), dark control

Lane 10: α-chymotrypsin (15 μM) and PMA-3A (15 μM), 342 nm, 20 min

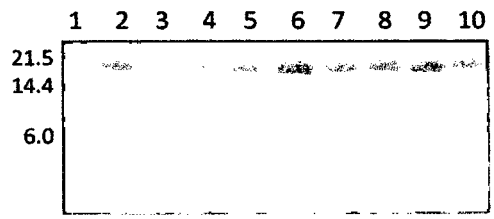


Figure 119 Photocleavage of β-lactoglobulin B obtained from the reaction with PMA-3A.

Lane 1: molecular weight markers (kDa)

Lane 2: β-lactoglobulin B (15 μM), PMA-3A (15 μM) and CoHA (1 mM), dark control

Lane 3: β-lactoglobulin B (15 μM), PMA-3A (15 μM) and CoHA (1 mM), 342 nm, 10 min

Lane 4: β-lactoglobulin B (15 μM), PMA-3A (15 μM) and CoHA (1 mM), 342 nm, 20 min

Lane 5: β-lactoglobulin B (15 μM), dark control

Lane 6: β-lactoglobulin B (15 μM), 342 nm, 20 min

Lane 7: β-lactoglobulin B (15 μM) and CoHA (1 mM), dark control

Lane 8: β-lactoglobulin B (15 μM) and CoHA (1 mM), 342 nm, 20 min

Lane 9: β-lactoglobulin B (15 μM) and PMA-3A (15 μM), dark control

Lane 10: β-lactoglobulin B (15 μM) and PMA-3A (15 μM), 342 nm, 20 min

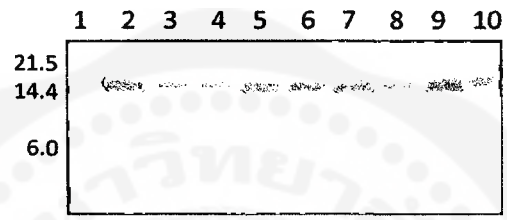


Figure 120 Photocleavage of myoglobin obtained from the reaction with PMA-3A.

Lane 1: molecular weight markers (kDa)

Lane 2: myoglobin (15 μM), PMA-3A (15 μM) and CoHA (1 mM), dark control

Lane 3: myoglobin (15 μM), PMA-3A (15 μM) and CoHA (1 mM), 342 nm, 10 min

Lane 4: myoglobin (15 μM), PMA-3A (15 μM) and CoHA (1 mM), 342 nm, 20 min

Lane 5: myoglobin (15 μM), dark control

Lane 6: myoglobin (15 μM), 342 nm, 20 min

Lane 7: myoglobin (15 μM) and CoHA (1 mM), dark control

Lane 8: myoglobin (15 μM) and CoHA (1 mM), 342 nm, 20 min

Lane 9: myoglobin (15 μM) and PMA-3A (15 μM), dark control

Lane 10: myoglobin (15 μM) and PMA-3A (15 μM), 342 nm, 20 min

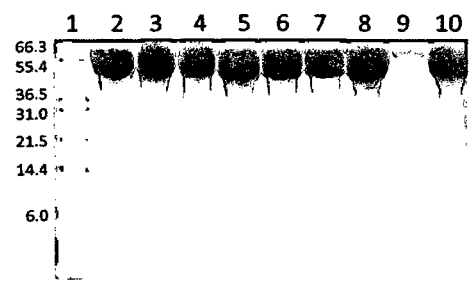


Figure 121 Photocleavage of HSA obtained from the reaction with PMA-3A.

Lane 1: molecular weight markers (kDa)

Lane 2: HSA (15 μM), PMA-3A (15 μM) and CoHA (1 mM), dark control

Lane 3: HSA (15 μM), PMA-3A (15 μM) and CoHA (1 mM), 342 nm, 10 min

Lane 4: HSA (15 μM), PMA-3A (15 μM) and CoHA (1 mM), 342 nm, 20 min

Lane 5: HSA (15 μM), dark control

Lane 6: HSA (15 μM), 342 nm, 20 min

Lane 7: HSA (15 μM) and CoHA (1 mM), dark control

Lane 8: HSA (15 μM) and CoHA (1 mM), 342 nm, 20 min

Lane 9: HSA (15 μM) and PMA-3A (15 μM), dark control

Lane 10: HSA (15 μM) and PMA-3A (15 μM), 342 nm, 20 min

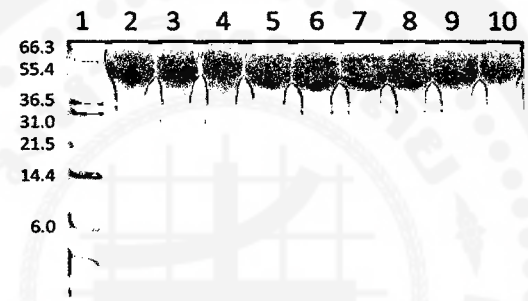


Figure 122 Photocleavage of BSA obtained from the reaction with PMA-3A.

Lane 1: molecular weight markers (kDa)

Lane 2: BSA (15 μM), PMA-3A (15 μM) and CoHA (1 mM), dark control

Lane 3: BSA (15 μM), PMA-3A (15 μM) and CoHA (1 mM), 342 nm, 10 min

Lane 4: BSA (15 μM), PMA-3A (15 μM) and CoHA (1 mM), 342 nm, 20 min

Lane 5: BSA (15 μM), dark control

Lane 6: BSA (15 μM), 342 nm, 20 min

Lane 7: BSA (15 μM) and CoHA (1 mM), dark control

Lane 8: BSA (15 μM) and CoHA (1 mM), 342 nm, 20 min

Lane 9: BSA (15 μM) and PMA-3A (15 μM), dark control

Lane 10: BSA (15 μM) and PMA-3A (15 μM), 342 nm, 20 min

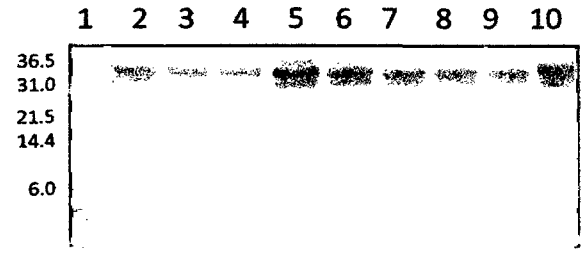


Figure 123 Photocleavage of α-casein obtained from the reaction with PMA-3A.

Lane 1: molecular weight markers (kDa)

Lane 2: α-casein (15 μM), PMA-3A (15 μM) and CoHA (1 mM), dark control

Lane 3: α-casein (15 μM), PMA-3A (15 μM) and CoHA (1 mM), 342 nm, 10 min

Lane 4: α-casein (15 μM), PMA-3A (15 μM) and CoHA (1 mM), 342 nm, 20 min

Lane 5: α-casein (15 μM), dark control

Lane 6: α-casein (15 μM), 342 nm, 20 min

Lane 7: α-casein (15 μM) and CoHA (1 mM), dark control

Lane 8: α-casein (15 μM) and CoHA (1 mM), 342 nm, 20 min

Lane 9: α-casein (15 μM) and PMA-3A (15 μM), dark control

Lane 10: α-casein (15 μM) and PMA-3A (15 μM), 342 nm, 20 min

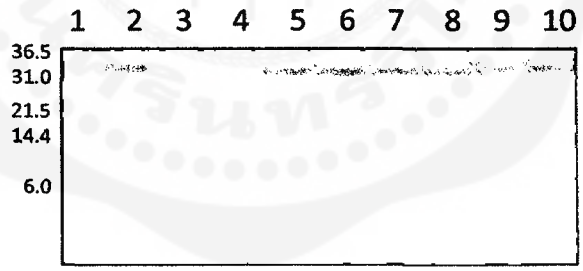


Figure 124 Photocleavage of pepsin obtained from the reaction with PMA-3A.

Lane 1: molecular weight markers (kDa)

Lane 2: pepsin (15 μM), PMA-3A (15 μM) and CoHA (1 mM), dark control

Lane 3: pepsin (15 μM), PMA-3A (15 μM) and CoHA (1 mM), 342 nm, 10 min

Lane 4: pepsin (15 μM), PMA-3A (15 μM) and CoHA (1 mM), 342 nm, 20 min

Lane 5: pepsin (15 μM), dark control

Lane 6: pepsin (15 μM), 342 nm, 20 min

Lane 7: pepsin (15 μM) and CoHA (1 mM), dark control

Lane 8: pepsin (15 μM) and CoHA (1 mM), 342 nm, 20 min

Lane 9: pepsin (15 μM) and PMA-3A (15 μM), dark control

Lane 10: pepsin (15 μM) and PMA-3A (15 μM), 342 nm, 20 min

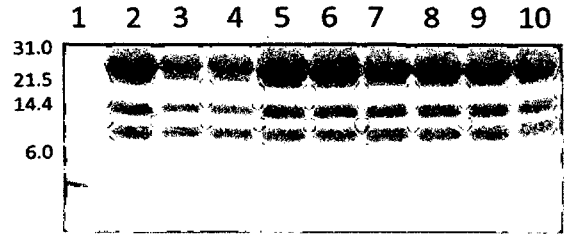


Figure 125 Photocleavage of concanavalin A obtained from the reaction with PMA-3A.

Lane 1: molecular weight markers (kDa)

Lane 2: concanavalin A (15 μM), PMA-3A (15 μM) and CoHA (1 mM), dark control

Lane 3: concanavalin A (15 μM), PMA-3A (15 μM) and CoHA (1 mM), 342 nm, 10 min

Lane 4: concanavalin A (15 μM), PMA-3A (15 μM) and CoHA (1 mM), 342 nm, 20 min

Lane 5: concanavalin A (15 μM), dark control

Lane 6: concanavalin A (15 μM), 342 nm, 20 min

Lane 7: concanavalin A (15 μM) and CoHA (1 mM), dark control

Lane 8: concanavalin A (15 μM) and CoHA (1 mM), 342 nm, 20 min

Lane 9: concanavalin A (15 μM) and PMA-3A (15 μM), dark control

Lane 10: concanavalin A (15 μM) and PMA-3A (15 μM), 342 nm, 20 min

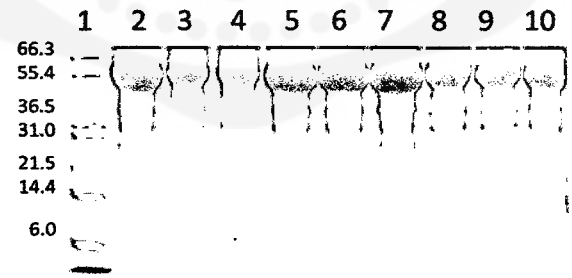


Figure 126 Photocleavage of β-glucosidase obtained from the reaction with PMA-3A.

Lane 1: molecular weight markers (kDa)

Lane 2: β-glucosidase (15 μM), PMA-3A (15 μM) and CoHA (1 mM), dark control

Lane 3: β-glucosidase (15 μM), PMA-3A (15 μM) and CoHA (1 mM), 342 nm, 10 min

Lane 4: β-glucosidase (15 μM), PMA-3A (15 μM) and CoHA (1 mM), 342 nm, 20 min

Lane 5: β-glucosidase (15 μM), dark control

Lane 6: β-glucosidase (15 μM), 342 nm, 20 min

Lane 7: β-glucosidase (15 μM) and CoHA (1 mM), dark control

Lane 8: β-glucosidase (15 μM) and CoHA (1 mM), 342 nm, 20 min

Lane 9: β-glucosidase (15 μM) and PMA-3A (15 μM), dark control

Lane 10: β-glucosidase (15 μM) and PMA-3A (15 μM), 342 nm, 20 min

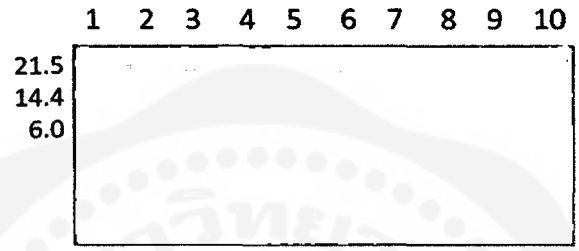


Figure 127 Photocleavage of lysozyme obtained from the reaction with berberine.

Lane 1: molecular weight markers (kDa)

Lane 2: lysozyme (15 μM), berberine (15 μM) and CoHA (1 mM), dark control

Lane 3: lysozyme (15 μM), berberine (15 μM) and CoHA (1 mM), 345 nm, 10 min

Lane 4: lysozyme (15 μM), berberine (15 μM) and CoHA (1 mM), 345 nm, 20 min

Lane 5: lysozyme (15 μM), dark control

Lane 6: lysozyme (15 μM), 345 nm, 20 min

Lane 7: lysozyme (15 μM) and CoHA (1 mM), dark control

Lane 8: lysozyme (15 μM) and CoHA (1 mM), 345 nm, 20 min

Lane 9: lysozyme (15 μM) and berberine (15 μM), dark control

Lane 10: lysozyme (15 μM) and berberine (15 μM), 345 nm, 20 min

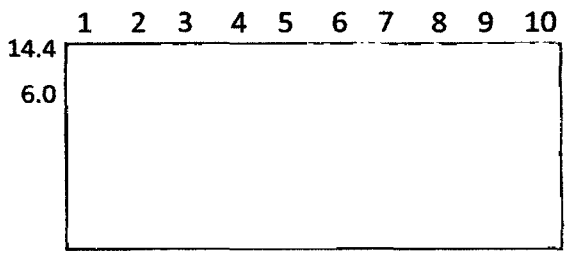


Figure 128 Photocleavage of α-chymotrypsin obtained from the reaction with berberine.

Lane 1: molecular weight markers (kDa)

Lane 2: α-chymotrypsin (15 μM), berberine (15 μM) and CoHA (1 mM), dark control

Lane 3: α-chymotrypsin (15 μM), berberine (15 μM) and CoHA (1 mM), 345 nm, 10 min

Lane 4: α-chymotrypsin (15 μM), berberine (15 μM) and CoHA (1 mM), 345 nm, 20 min

Lane 5: α-chymotrypsin (15 μM), dark control

Lane 6: α-chymotrypsin (15 μM), 345 nm, 20 min

Lane 7: α-chymotrypsin (15 μM) and CoHA (1 mM), dark control

Lane 8: α-chymotrypsin (15 μM) and CoHA (1 mM), 345 nm, 20 min

Lane 9: α-chymotrypsin (15 μM) and berberine (15 μM), dark control

Lane 10: α-chymotrypsin (15 μM) and berberine (15 μM), 345 nm, 20 min

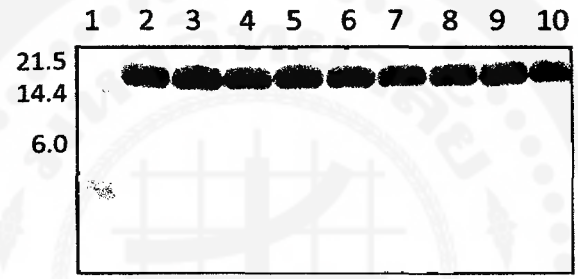


Figure 129 Photocleavage of β-lactoglobulin B obtained from the reaction with berberine.

Lane 1: molecular weight markers (kDa)

Lane 2: β-lactoglobulin B (15 μM), berberine (15 μM) and CoHA (1 mM), dark control

Lane 3: β-lactoglobulin B (15 μM), berberine (15 μM) and CoHA (1 mM), 345 nm, 10 min

Lane 4: β-lactoglobulin B (15 μM), berberine (15 μM) and CoHA (1 mM), 345 nm, 20 min

Lane 5: β-lactoglobulin B (15 μM), dark control

Lane 6: β-lactoglobulin B (15 μM), 345 nm, 20 min

Lane 7: β-lactoglobulin B (15 μM) and CoHA (1 mM), dark control

Lane 8: β-lactoglobulin B (15 μM) and CoHA (1 mM), 345 nm, 20 min

Lane 9: β-lactoglobulin B (15 μM) and berberine (15 μM), dark control

Lane 10: β-lactoglobulin B (15 μM) and berberine (15 μM), 345 nm, 20 min

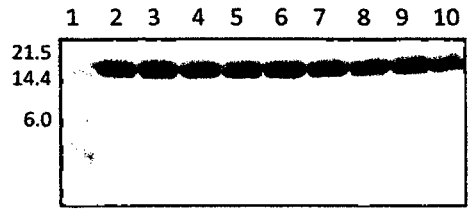


Figure 130 Photocleavage of myoglobin obtained from the reaction with berberine.

Lane 1: molecular weight markers (kDa)

Lane 2: myoglobin (15 μM), berberine (15 μM) and CoHA (1 mM), dark control

Lane 3: myoglobin (15 μM), berberine (15 μM) and CoHA (1 mM), 345 nm, 10 min

Lane 4: myoglobin (15 μM), berberine (15 μM) and CoHA (1 mM), 345 nm, 20 min

Lane 5: myoglobin (15 μM), dark control

Lane 6: myoglobin (15 μM), 345 nm, 20 min

Lane 7: myoglobin (15 μM) and CoHA (1 mM), dark control

Lane 8: myoglobin (15 μM) and CoHA (1 mM), 345 nm, 20 min

Lane 9: myoglobin (15 μM) and berberine (15 μM), dark control

Lane 10: myoglobin (15 μM) and berberine (15 μM), 345 nm, 20 min

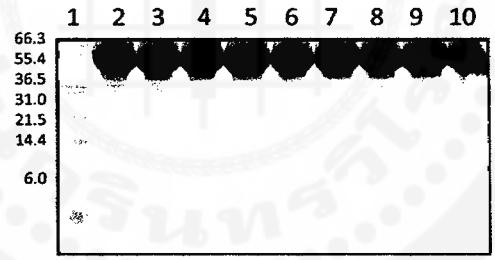


Figure 131 Photocleavage of HSA obtained from the reaction with berberine.

Lane 1: molecular weight markers (kDa)

Lane 2: HSA (15 μM), berberine (15 μM) and CoHA (1 mM), dark control

Lane 3: HSA (15 μM), berberine (15 μM) and CoHA (1 mM), 345 nm, 10 min

Lane 4: HSA (15 μM), berberine (15 μM) and CoHA (1 mM), 345 nm, 20 min

Lane 5: HSA (15 μM), dark control

Lane 6: HSA (15 μM), 345 nm, 20 min

Lane 7: HSA (15 μM) and CoHA (1 mM), dark control

Lane 8: HSA (15 μM) and CoHA (1 mM), 345 nm, 20 min

Lane 9: HSA (15 μM) and berberine (15 μM), dark control

Lane 10: HSA (15 μM) and berberine (15 μM), 345 nm, 20 min

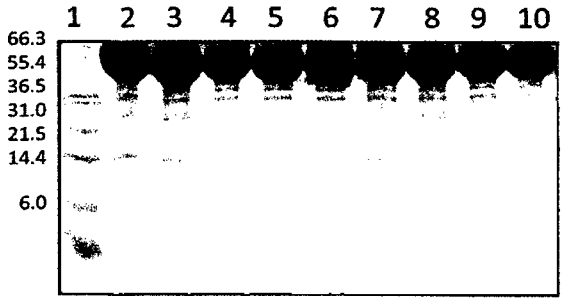


Figure 132 Photocleavage of BSA obtained from the reaction with berberine.

Lane 1: molecular weight markers (kDa)

Lane 2: BSA (15 μM), berberine (15 μM) and CoHA (1 mM), dark control

Lane 3: BSA (15 μM), berberine (15 μM) and CoHA (1 mM), 345 nm, 10 min

Lane 4: BSA (15 μM), berberine (15 μM) and CoHA (1 mM), 345 nm, 20 min

Lane 5: BSA (15 μM), dark control

Lane 6: BSA (15 μM), 345 nm, 20 min

Lane 7: BSA (15 μM) and CoHA (1 mM), dark control

Lane 8: BSA (15 μM) and CoHA (1 mM), 345 nm, 20 min

Lane 9: BSA (15 μM) and berberine (15 μM), dark control

Lane 10: BSA (15 μM) and berberine (15 μM), 345 nm, 20 min

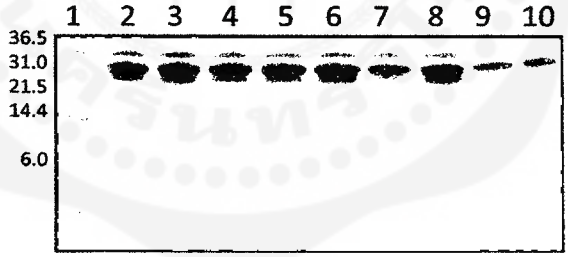


Figure 133 Photocleavage of α-casein obtained from the reaction with berberine.

Lane 1: molecular weight markers (kDa)

Lane 2: α-casein (15 μM), berberine (15 μM) and CoHA (1 mM), dark control

Lane 3: α-casein (15 μM), berberine (15 μM) and CoHA (1 mM), 345 nm, 10 min

Lane 4: α-casein (15 μM), berberine (15 μM) and CoHA (1 mM), 345 nm, 20 min

Lane 5: α-casein (15 μM), dark control

Lane 6: α-casein (15 μM), 345 nm, 20 min

Lane 7: α-casein (15 μM) and CoHA (1 mM), dark control

Lane 8: α-casein (15 μM) and CoHA (1 mM), 345 nm, 20 min

Lane 9: α-casein (15 μM) and berberine (15 μM), dark control

Lane 10: α-casein (15 μM) and berberine (15 μM), 345 nm, 20 min

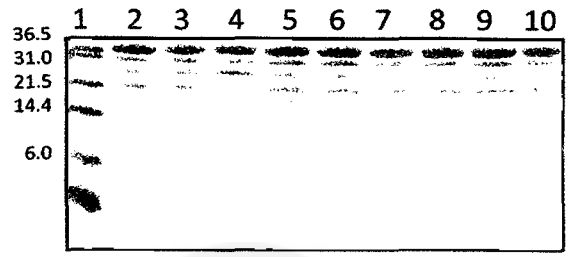


Figure 134 Photocleavage of pepsin obtained from the reaction with berberine.

Lane 1: molecular weight markers (kDa)

Lane 2: pepsin (15 μM), berberine (15 μM) and CoHA (1 mM), dark control

Lane 3: pepsin (15 μM), berberine (15 μM) and CoHA (1 mM), 345 nm, 10 min

Lane 4: pepsin (15 μM), berberine (15 μM) and CoHA (1 mM), 345 nm, 20 min

Lane 5: pepsin (15 μM), dark control

Lane 6: pepsin (15 μM), 345 nm, 20 min

Lane 7: pepsin (15 μM) and CoHA (1 mM), dark control

Lane 8: pepsin (15 μM) and CoHA (1 mM), 345 nm, 20 min

Lane 9: pepsin (15 μM) and berberine (15 μM), dark control

Lane 10: pepsin (15 μM) and berberine (15 μM), 345 nm, 20 min

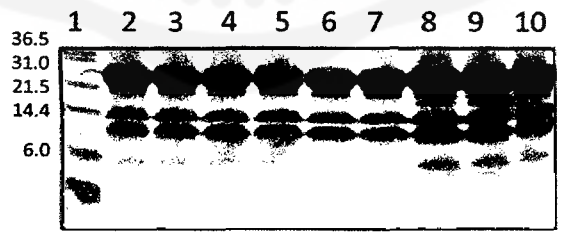


Figure 135 Photocleavage of concanavalin A obtained from the reaction with berberine.

Lane 1: molecular weight markers (kDa)

Lane 2: concanavalin A (15 μM), berberine (15 μM) and CoHA (1 mM), dark control

Lane 3: concanavalin A (15 μM), berberine (15 μM) and CoHA (1 mM), 345 nm, 10 min

Lane 4: concanavalin A (15 μM), berberine (15 μM) and CoHA (1 mM), 345 nm, 20 min

Lane 5: concanavalin A (15 μM), dark control

Lane 6: concanavalin A (15 μM), 345 nm, 20 min

Lane 7: concanavalin A (15 μM) and CoHA (1 mM), dark control

Lane 8: concanavalin A (15 μM) and CoHA (1 mM), 345 nm, 20 min

Lane 9: concanavalin A (15 μM) and berberine (15 μM), dark control

Lane 10: concanavalin A (15 μM) and berberine (15 μM), 345 nm, 20 min

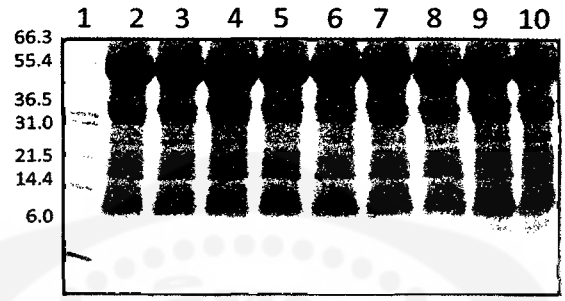


Figure 136 Photocleavage of β-glucosidase obtained from the reaction with berberine.

Lane 1: molecular weight markers (kDa)

Lane 2: β-glucosidase (15 μM), berberine (15 μM) and CoHA (1 mM), dark control

Lane 3: β-glucosidase (15 μM), berberine (15 μM) and CoHA (1 mM), 345 nm, 10 min

Lane 4: β-glucosidase (15 μM), berberine (15 μM) and CoHA (1 mM), 345 nm, 20 min

Lane 5: β-glucosidase (15 μM), dark control

Lane 6: β-glucosidase (15 μM), 345 nm, 20 min

Lane 7: β-glucosidase (15 μM) and CoHA (1 mM), dark control

Lane 8: β-glucosidase (15 μM) and CoHA (1 mM), 345 nm, 20 min

Lane 9: β-glucosidase (15 μM) and berberine (15 μM), dark control

Lane 10: β-glucosidase (15 μM) and berberine (15 μM), 345 nm, 20 min

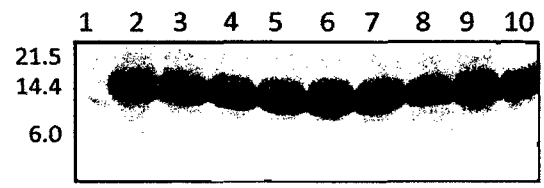


Figure 137 Photocleavage of avidin obtained from the reaction with SST-29.

Lane 1: molecular weight markers (kDa)

Lane 2: avidin (15 μM), SST-29 (15 μM) and CoHA (1 mM), dark control

Lane 3: avidin (15 μM), SST-29 (15 μM) and CoHA (1 mM), 342 nm, 10 min

Lane 4: avidin (15 μM), SST-29 (15 μM) and CoHA (1 mM), 342 nm, 20 min

Lane 5: avidin (15 μM), dark control

Lane 6: avidin (15 μM), 342 nm, 20 min

Lane 7: avidin (15 μM) and CoHA (1 mM), dark control

Lane 8: avidin (15 μM) and CoHA (1 mM), 342 nm, 20 min

Lane 9: avidin (15 μM) and SST-29 (15 μM), dark control

Lane 10: avidin (15 μM) and SST-29 (15 μM), 342 nm, 20 min

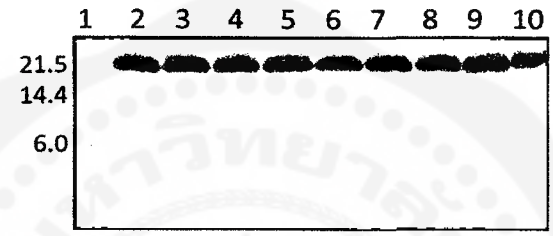


Figure 138 Photocleavage of lysozyme obtained from the reaction with SST-29.

Lane 1: molecular weight markers (kDa)

Lane 2: lysozyme (15 μM), SST-29 (15 μM) and CoHA (1 mM), dark control

Lane 3: lysozyme (15 μM), SST-29 (15 μM) and CoHA (1 mM), 342 nm, 10 min

Lane 4: lysozyme (15 μM), SST-29 (15 μM) and CoHA (1 mM), 342 nm, 20 min

Lane 5: lysozyme (15 μM), dark control

Lane 6: lysozyme (15 μM), 342 nm, 20 min

Lane 7: lysozyme (15 μM) and CoHA (1 mM), dark control

Lane 8: lysozyme (15 μM) and CoHA (1 mM), 342 nm, 20 min

Lane 9: lysozyme (15 μM) and SST-29 (15 μM), dark control

Lane 10: lysozyme (15 μM) and SST-29 (15 μM), 342 nm, 20 min

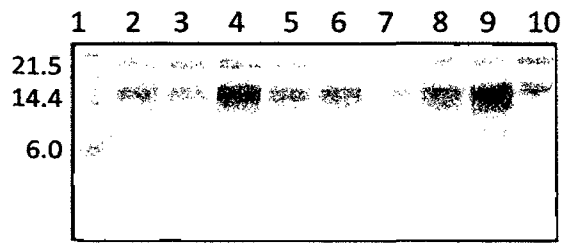


Figure 139 Photocleavage of α-chymotrypsin obtained from the reaction with SST-29.

Lane 1: molecular weight markers (kDa)

Lane 2: α-chymotrypsin (15 μM), SST-29 (15 μM) and CoHA (1 mM), dark control

Lane 3: α-chymotrypsin (15 μM), SST-29 (15 μM) and CoHA (1 mM), 342 nm, 10 min

Lane 4: α-chymotrypsin (15 μM), SST-29 (15 μM) and CoHA (1 mM), 342 nm, 20 min

Lane 5: α-chymotrypsin (15 μM), dark control

Lane 6: α-chymotrypsin (15 μM), 342 nm, 20 min

Lane 7: α-chymotrypsin (15 μM) and CoHA (1 mM), dark control

Lane 8: α-chymotrypsin (15 μM) and CoHA (1 mM), 342 nm, 20 min

Lane 9: α-chymotrypsin (15 μM) and SST-29 (15 μM), dark control

Lane 10: α-chymotrypsin (15 μM) and SST-29 (15 μM), 342 nm, 20 min

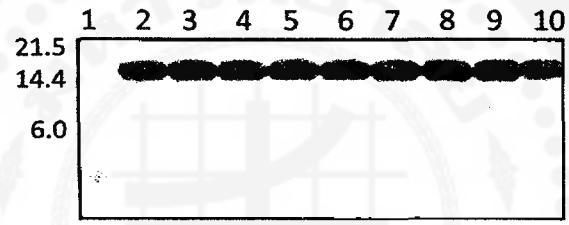


Figure 140 Photocleavage of β-lactoglobulin B obtained from the reaction with SST-29.

Lane 1: molecular weight markers (kDa)

Lane 2: β-lactoglobulin B (15 μM), SST-29 (15 μM) and CoHA (1 mM), dark control

Lane 3: β-lactoglobulin B (15 μM), SST-29 (15 μM) and CoHA (1 mM), 342 nm, 10 min

Lane 4: β-lactoglobulin B (15 μM), SST-29 (15 μM) and CoHA (1 mM), 342 nm, 20 min

Lane 5: β-lactoglobulin B (15 μM), dark control

Lane 6: β-lactoglobulin B (15 μM), 342 nm, 20 min

Lane 7: β-lactoglobulin B (15 μM) and CoHA (1 mM), dark control

Lane 8: β-lactoglobulin B (15 μM) and CoHA (1 mM), 342 nm, 20 min

Lane 9: β-lactoglobulin B (15 μM) and SST-29 (15 μM), dark control

Lane 10: β-lactoglobulin B (15 μM) and SST-29 (15 μM), 342 nm, 20 min

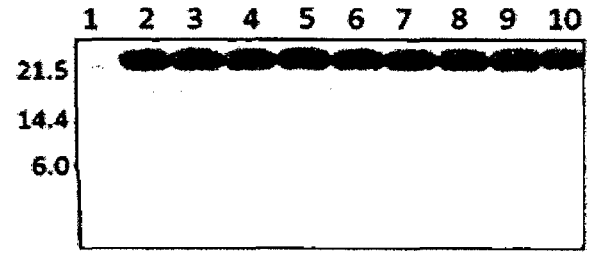


Figure 141 Photocleavage of myoglobin obtained from the reaction with SST-29.

Lane 1: molecular weight markers (kDa)

Lane 2: myoglobin (15 μM), SST-29 (15 μM) and CoHA (1 mM), dark control

Lane 3: myoglobin (15 μM), SST-29 (15 μM) and CoHA (1 mM), 342 nm, 10 min

Lane 4: myoglobin (15 μM), SST-29 (15 μM) and CoHA (1 mM), 342 nm, 20 min

Lane 5: myoglobin (15 μM), dark control

Lane 6: myoglobin (15 μM), 342 nm, 20 min

Lane 7: myoglobin (15 μM) and CoHA (1 mM), dark control

Lane 8: myoglobin (15 μM) and CoHA (1 mM), 342 nm, 20 min

Lane 9: myoglobin (15 μM) and SST-29 (15 μM), dark control

Lane 10: myoglobin (15 μM) and SST-29 (15 μM), 342 nm, 20 min

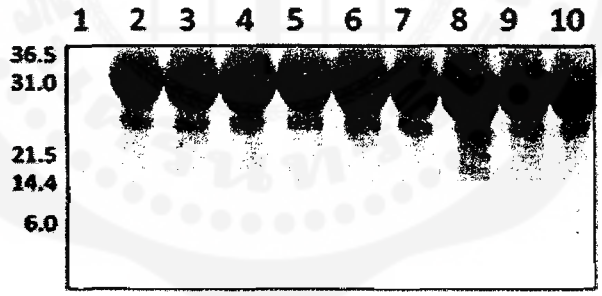


Figure 142 Photocleavage of HSA obtained from the reaction with SST-29.

Lane 1: molecular weight markers (kDa)

Lane 2: HSA (15 μM), SST-29 (15 μM) and CoHA (1 mM), dark control

Lane 3: HSA (15 μM), SST-29 (15 μM) and CoHA (1 mM), 342 nm, 10 min

Lane 4: HSA (15 μM), SST-29 (15 μM) and CoHA (1 mM), 342 nm, 20 min

Lane 5: HSA (15 μM), dark control

Lane 6: HSA (15 μM), 342 nm, 20 min

Lane 7: HSA (15 μM) and CoHA (1 mM), dark control

Lane 8: HSA (15 μM) and CoHA (1 mM), 342 nm, 20 min

Lane 9: HSA (15 μM) and SST-29 (15 μM), dark control

Lane 10: HSA (15 μM) and SST-29 (15 μM), 342 nm, 20 min

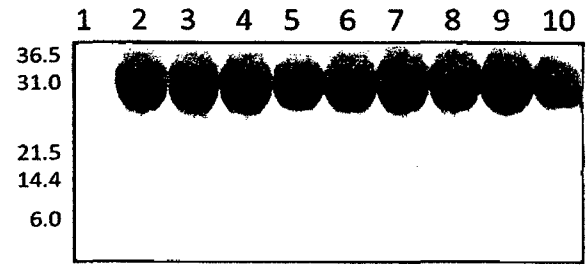


Figure 143 Photocleavage of BSA obtained from the reaction with SST-29.

Lane 1: molecular weight markers (kDa)

Lane 2: BSA (15 μM), SST-29 (15 μM) and CoHA (1 mM), dark control

Lane 3: BSA (15 μM), SST-29 (15 μM) and CoHA (1 mM), 342 nm, 10 min

Lane 4: BSA (15 μM), SST-29 (15 μM) and CoHA (1 mM), 342 nm, 20 min

Lane 5: BSA (15 μM), dark control

Lane 6: BSA (15 μM), 342 nm, 20 min

Lane 7: BSA (15 μM) and CoHA (1 mM), dark control

Lane 8: BSA (15 μM) and CoHA (1 mM), 342 nm, 20 min

Lane 9: BSA (15 μM) and SST-29 (15 μM), dark control

Lane 10: BSA (15 μM) and SST-29 (15 μM), 342 nm, 20 min

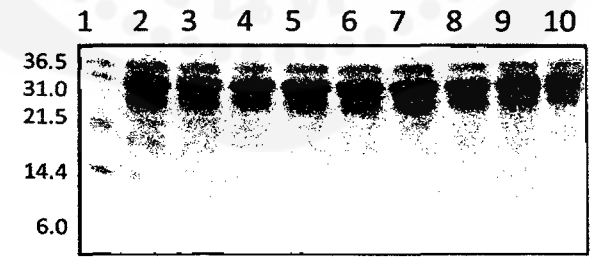


Figure 144 Photocleavage of α-casein obtained from the reaction with SST-29.

Lane 1: molecular weight markers (kDa)

Lane 2: α-casein (15 μM), SST-29 (15 μM) and CoHA (1 mM), dark control

Lane 3: α-casein (15 μM), SST-29 (15 μM) and CoHA (1 mM), 342 nm, 10 min

Lane 4: α-casein (15 μM), SST-29 (15 μM) and CoHA (1 mM), 342 nm, 20 min

Lane 5: α-casein (15 μM), dark control

Lane 6: α-casein (15 μM), 342 nm, 20 min

Lane 7: α-casein (15 μM) and CoHA (1 mM), dark control

Lane 8: α-casein (15 μM) and CoHA (1 mM), 342 nm, 20 min

Lane 9: α-casein (15 μM) and SST-29 (15 μM), dark control

Lane 10: α-casein (15 μM) and SST-29 (15 μM), 342 nm, 20 min

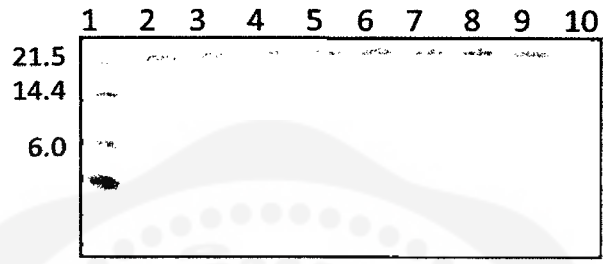


Figure 145 Photocleavage of pepsin obtained from the reaction with SST-29.

Lane 1: molecular weight markers (kDa)

Lane 2: pepsin (15 μM), SST-29 (15 μM) and CoHA (1 mM), dark control

Lane 3: pepsin (15 μM), SST-29 (15 μM) and CoHA (1 mM), 342 nm, 10 min

Lane 4: pepsin (15 μM), SST-29 (15 μM) and CoHA (1 mM), 342 nm, 20 min

Lane 5: pepsin (15 μM), dark control

Lane 6: pepsin (15 μM), 342 nm, 20 min

Lane 7: pepsin (15 μM) and CoHA (1 mM), dark control

Lane 8: pepsin (15 μM) and CoHA (1 mM), 342 nm, 20 min

Lane 9: pepsin (15 μM) and SST-29 (15 μM), dark control

Lane 10: pepsin (15 μM) and SST-29 (15 μM), 342 nm, 20 min

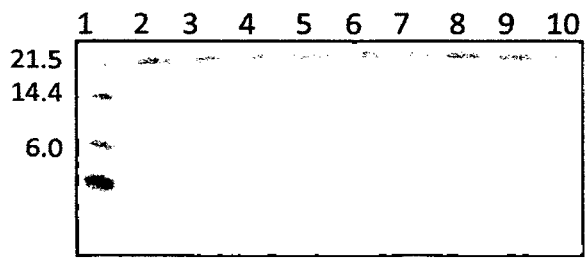


Figure 146 Photocleavage of concanavalin A obtained from the reaction with SST-29.

Lane 1: molecular weight markers (kDa)

Lane 2: concanavalin A (15 μM), SST-29 (15 μM) and CoHA (1 mM), dark control

Lane 3: concanavalin A (15 μM), SST-29 (15 μM) and CoHA (1 mM), 342 nm, 10 min

Lane 4: concanavalin A (15 μM), SST-29 (15 μM) and CoHA (1 mM), 342 nm, 20 min

Lane 5: concanavalin A (15 μM), dark control

Lane 6: concanavalin A (15 μM), 342 nm, 20 min

Lane 7: concanavalin A (15 μM) and CoHA (1 mM), dark control

Lane 8: concanavalin A (15 μM) and CoHA (1 mM), 342 nm, 20 min

Lane 9: concanavalin A (15 μM) and SST-29 (15 μM), dark control

Lane 10: concanavalin A (15 μM) and SST-29 (15 μM), 342 nm, 20 min



Figure 147 Photocleavage of β-glucosidase obtained from the reaction with SST-29.

Lane 1: molecular weight markers (kDa)

Lane 2: β-glucosidase (15 μM), SST-29 (15 μM) and CoHA (1 mM), dark control

Lane 3: β-glucosidase (15 μM), SST-29 (15 μM) and CoHA (1 mM), 342 nm, 10 min

Lane 4: β-glucosidase (15 μM), SST-29 (15 μM) and CoHA (1 mM), 342 nm, 20 min

Lane 5: β-glucosidase (15 μM), dark control

Lane 6: β-glucosidase (15 μM), 342 nm, 20 min

Lane 7: β-glucosidase (15 μM) and CoHA (1 mM), dark control

Lane 8: β-glucosidase (15 μM) and CoHA (1 mM), 342 nm, 20 min

Lane 9: β-glucosidase (15 μM) and SST-29 (15 μM), dark control

Lane 10: β-glucosidase (15 μM) and SST-29 (15 μM), 342 nm, 20 min

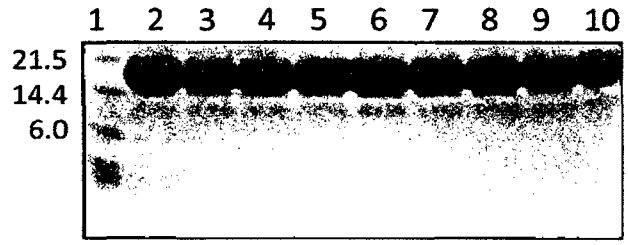


Figure 148 Photocleavage of avidin obtained from the reaction with SST-31.

Lane 1: molecular weight markers (kDa)

Lane 2: avidin (15 μM), SST-31 (15 μM) and CoHA (1 mM), dark control

Lane 3: avidin (15 μM), SST-31 (15 μM) and CoHA (1 mM), 342 nm, 10 min

Lane 4: avidin (15 μM), SST-31 (15 μM) and CoHA (1 mM), 342 nm, 20 min

Lane 5: avidin (15 μM), dark control

Lane 6: avidin (15 μM), 342 nm, 20 min

Lane 7: avidin (15 μM) and CoHA (1 mM), dark control

Lane 8: avidin (15 μM) and CoHA (1 mM), 342 nm, 20 min

Lane 9: avidin (15 μM) and SST-31 (15 μM), dark control

Lane 10: avidin (15 μM) and SST-31 (15 μM), 342 nm, 20 min



Figure 149 Photocleavage of lysozyme obtained from the reaction with SST-31.

Lane 1: molecular weight markers (kDa)

Lane 2: lysozyme (15 μM), SST-31 (15 μM) and CoHA (1 mM), dark control

Lane 3: lysozyme (15 μM), SST-31 (15 μM) and CoHA (1 mM), 342 nm, 10 min

Lane 4: lysozyme (15 μM), SST-31 (15 μM) and CoHA (1 mM), 342 nm, 20 min

Lane 5: lysozyme (15 μM), dark control

Lane 6: lysozyme (15 μM), 342 nm, 20 min

Lane 7: lysozyme (15 μM) and CoHA (1 mM), dark control

Lane 8: lysozyme (15 μM) and CoHA (1 mM), 342 nm, 20 min

Lane 9: lysozyme (15 μM) and SST-31 (15 μM), dark control

Lane 10: lysozyme (15 μM) and SST-31 (15 μM), 342 nm, 20 min

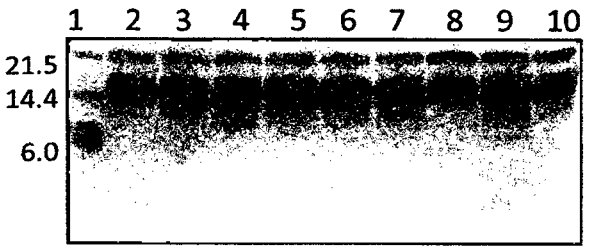


Figure 150 Photocleavage of α-chymotrypsin obtained from the reaction with SST-31.

Lane 1: molecular weight markers (kDa)

Lane 2: α-chymotrypsin (15 μM), SST-31 (15 μM) and CoHA (1 mM), dark control

Lane 3: α-chymotrypsin (15 μM), SST-31 (15 μM) and CoHA (1 mM), 342 nm, 10 min

Lane 4: α-chymotrypsin (15 μM), SST-31 (15 μM) and CoHA (1 mM), 342 nm, 20 min

Lane 5: α-chymotrypsin (15 μM), dark control

Lane 6: α-chymotrypsin (15 μM), 342 nm, 20 min

Lane 7: α-chymotrypsin (15 μM) and CoHA (1 mM), dark control

Lane 8: α-chymotrypsin (15 μM) and CoHA (1 mM), 342 nm, 20 min

Lane 9: α-chymotrypsin (15 μM) and SST-31 (15 μM), dark control

Lane 10: α-chymotrypsin (15 μM) and SST-31 (15 μM), 342 nm, 20 min

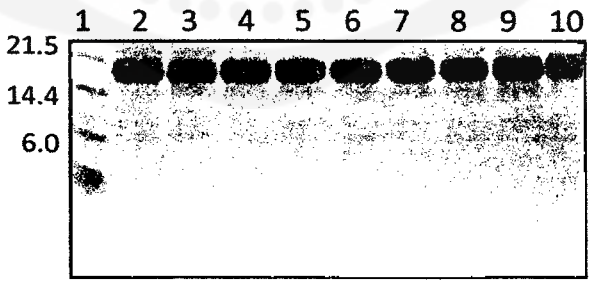


Figure 151 Photocleavage of β-lactoglobulin B obtained from the reaction with SST-31.

Lane 1: molecular weight markers (kDa)

Lane 2: β-lactoglobulin B (15 μM), SST-31 (15 μM) and CoHA (1 mM), dark control

Lane 3: β-lactoglobulin B (15 μM), SST-31 (15 μM) and CoHA (1 mM), 342 nm, 10 min

Lane 4: β-lactoglobulin B (15 μM), SST-31 (15 μM) and CoHA (1 mM), 342 nm, 20 min

Lane 5: β-lactoglobulin B (15 μM), dark control

Lane 6: β-lactoglobulin B (15 μM), 342 nm, 20 min

Lane 7: β-lactoglobulin B (15 μM) and CoHA (1 mM), dark control

Lane 8: β-lactoglobulin B (15 μM) and CoHA (1 mM), 342 nm, 20 min

Lane 9: β-lactoglobulin B (15 μM) and SST-31 (15 μM), dark control

Lane 10: β-lactoglobulin B (15 μM) and SST-31 (15 μM), 342 nm, 20 min

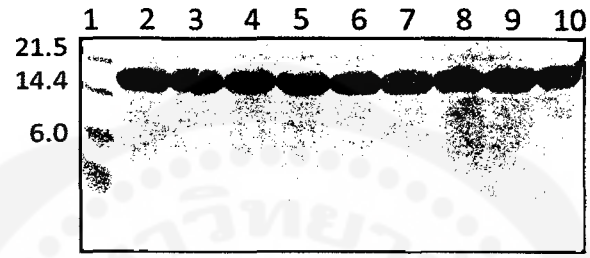


Figure 152 Photocleavage of myoglobin obtained from the reaction with SST-31.

Lane 1: molecular weight markers (kDa)

Lane 2: myoglobin (15 μM), SST-31 (15 μM) and CoHA (1 mM), dark control

Lane 3: myoglobin (15 μM), SST-31 (15 μM) and CoHA (1 mM), 342 nm, 10 min

Lane 4: myoglobin (15 μM), SST-31 (15 μM) and CoHA (1 mM), 342 nm, 20 min

Lane 5: myoglobin (15 μM), dark control

Lane 6: myoglobin (15 μM), 342 nm, 20 min

Lane 7: myoglobin (15 μM) and CoHA (1 mM), dark control

Lane 8: myoglobin (15 μM) and CoHA (1 mM), 342 nm, 20 min

Lane 9: myoglobin (15 μM) and SST-31 (15 μM), dark control

Lane 10: myoglobin (15 μM) and SST-31 (15 μM), 342 nm, 20 min

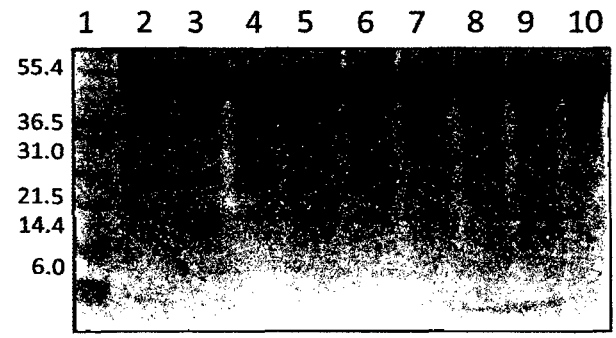


Figure 153 Photocleavage of HSA obtained from the reaction with SST-31.

Lane 1: molecular weight markers (kDa)

Lane 2: HSA (15 μM), SST-31 (15 μM) and CoHA (1 mM), dark control

Lane 3: HSA (15 μM), SST-31 (15 μM) and CoHA (1 mM), 342 nm, 10 min

Lane 4: HSA (15 μM), SST-31 (15 μM) and CoHA (1 mM), 342 nm, 20 min

Lane 5: HSA (15 μM), dark control

Lane 6: HSA (15 μM), 342 nm, 20 min

Lane 7: HSA (15 μM) and CoHA (1 mM), dark control

Lane 8: HSA (15 μM) and CoHA (1 mM), 342 nm, 20 min

Lane 9: HSA (15 μM) and SST-31 (15 μM), dark control

Lane 10: HSA (15 μM) and SST-31 (15 μM), 342 nm, 20 min



Figure 154 Photocleavage of BSA obtained from the reaction with SST-31.

Lane 1: molecular weight markers (kDa)

Lane 2: BSA (15 μM), SST-31 (15 μM) and CoHA (1 mM), dark control

Lane 3: BSA (15 μM), SST-31 (15 μM) and CoHA (1 mM), 342 nm, 10 min

Lane 4: BSA (15 μM), SST-31 (15 μM) and CoHA (1 mM), 342 nm, 20 min

Lane 5: BSA (15 μM), dark control

Lane 6: BSA (15 μM), 342 nm, 20 min

Lane 7: BSA (15 μM) and CoHA (1 mM), dark control

Lane 8: BSA (15 μM) and CoHA (1 mM), 342 nm, 20 min

Lane 9: BSA (15 μM) and SST-31 (15 μM), dark control

Lane 10: BSA (15 μM) and SST-31 (15 μM), 342 nm, 20 min

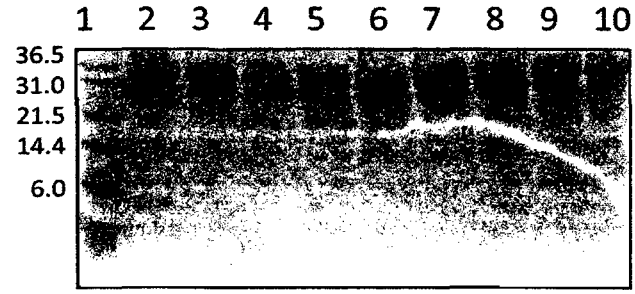


Figure 155 Photocleavage of α-casein obtained from the reaction with SST-31.

Lane 1: molecular weight markers (kDa)

Lane 2: α-casein (15 μM), SST-31 (15 μM) and CoHA (1 mM), dark control

Lane 3: α-casein (15 μM), SST-31 (15 μM) and CoHA (1 mM), 342 nm, 10 min

Lane 4: α-casein (15 μM), SST-31 (15 μM) and CoHA (1 mM), 342 nm, 20 min

Lane 5: α-casein (15 μM), dark control

Lane 6: α-casein (15 μM), 342 nm, 20 min

Lane 7: α-casein (15 μM) and CoHA (1 mM), dark control

Lane 8: α-casein (15 μM) and CoHA (1 mM), 342 nm, 20 min

Lane 9: α-casein (15 μM) and SST-31 (15 μM), dark control

Lane 10: α-casein (15 μM) and SST-31 (15 μM), 342 nm, 20 min

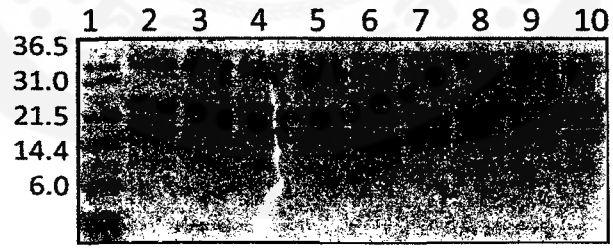


Figure 156 Photocleavage of pepsin obtained from the reaction with SST-31.

Lane 1: molecular weight markers (kDa)

Lane 2: pepsin (15 μM), SST-31 (15 μM) and CoHA (1 mM), dark control

Lane 3: pepsin (15 μM), SST-31 (15 μM) and CoHA (1 mM), 342 nm, 10 min

Lane 4: pepsin (15 μM), SST-31 (15 μM) and CoHA (1 mM), 342 nm, 20 min

Lane 5: pepsin (15 μM), dark control

Lane 6: pepsin (15 μM), 342 nm, 20 min

Lane 7: pepsin (15 μM) and CoHA (1 mM), dark control

Lane 8: pepsin (15 μM) and CoHA (1 mM), 342 nm, 20 min

Lane 9: pepsin (15 μM) and SST-31 (15 μM), dark control

Lane 10: pepsin (15 μM) and SST-31 (15 μM), 342 nm, 20 min



Figure 157 Photocleavage of concanavalin A obtained from the reaction with SST-31.

Lane 1: molecular weight markers (kDa)

Lane 2: concanavalin A (15 μM), SST-31 (15 μM) and CoHA (1 mM), dark control

Lane 3: concanavalin A (15 μM), SST-31 (15 μM) and CoHA (1 mM), 342 nm, 10 min

Lane 4: concanavalin A (15 μM), SST-31 (15 μM) and CoHA (1 mM), 342 nm, 20 min

Lane 5: concanavalin A (15 μM), dark control

Lane 6: concanavalin A (15 μM), 342 nm, 20 min

Lane 7: concanavalin A (15 μM) and CoHA (1 mM), dark control

Lane 8: concanavalin A (15 μM) and CoHA (1 mM), 342 nm, 20 min

Lane 9: concanavalin A (15 μM) and SST-31 (15 μM), dark control

Lane 10: concanavalin A (15 μM) and SST-31 (15 μM), 342 nm, 20 min

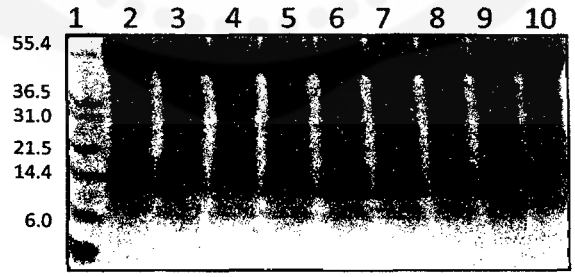


Figure 158 Photocleavage of β-glucosidase obtained from the reaction with SST-31.

Lane 1: molecular weight markers (kDa)

Lane 2: β-glucosidase (15 μM), SST-31 (15 μM) and CoHA (1 mM), dark control

Lane 3: β-glucosidase (15 μM), SST-31 (15 μM) and CoHA (1 mM), 342 nm, 10 min

Lane 4: β-glucosidase (15 μM), SST-31 (15 μM) and CoHA (1 mM), 342 nm, 20 min

Lane 5: β-glucosidase (15 μM), dark control

Lane 6: β-glucosidase (15 μM), 342 nm, 20 min

Lane 7: β-glucosidase (15 μM) and CoHA (1 mM), dark control

Lane 8: β-glucosidase (15 μM) and CoHA (1 mM), 342 nm, 20 min

Lane 9: β-glucosidase (15 μM) and SST-31 (15 μM), dark control

Lane 10: β-glucosidase (15 μM) and SST-31 (15 μM), 342 nm, 20 min

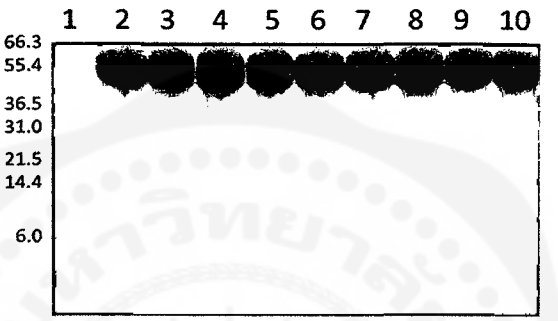


Figure 159 Photocleavage of avidin obtained from the reaction with piperine.

Lane 1: molecular weight markers (kDa)

Lane 2: avidin (15 μM), piperine (15 μM) and CoHA (1 mM), dark control

Lane 3: avidin (15 μM), piperine (15 μM) and CoHA (1 mM), 342 nm, 10 min

Lane 4: avidin (15 μM), piperine (15 μM) and CoHA (1 mM), 342 nm, 20 min

Lane 5: avidin (15 μM), dark control

Lane 6: avidin (15 μM), 342 nm, 20 min

Lane 7: avidin (15 μM) and CoHA (1 mM), dark control

Lane 8: avidin (15 μM) and CoHA (1 mM), 342 nm, 20 min

Lane 9: avidin (15 μM) and piperine (15 μM), dark control

Lane 10: avidin (15 μM) and piperine (15 μM), 342 nm, 20 min

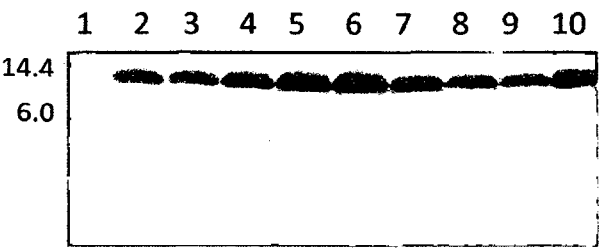


Figure 160 Photocleavage of lysozyme obtained from the reaction with piperine.

Lane 1: molecular weight markers (kDa)

Lane 2: lysozyme (15 μM), piperine (15 μM) and CoHA (1 mM), dark control

Lane 3: lysozyme (15 μM), piperine (15 μM) and CoHA (1 mM), 342 nm, 10 min

Lane 4: lysozyme (15 μM), piperine (15 μM) and CoHA (1 mM), 342 nm, 20 min

Lane 5: lysozyme (15 μM), dark control

Lane 6: lysozyme (15 μM), 342 nm, 20 min

Lane 7: lysozyme (15 μM) and CoHA (1 mM), dark control

Lane 8: lysozyme (15 μM) and CoHA (1 mM), 342 nm, 20 min

Lane 9: lysozyme (15 μM) and piperine (15 μM), dark control

Lane 10: lysozyme (15 μM) and piperine (15 μM), 342 nm, 20 min

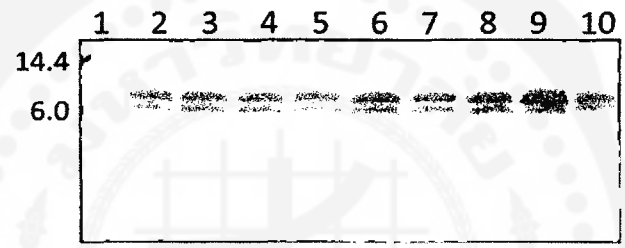


Figure 161 Photocleavage of α-chymotrypsin obtained from the reaction with piperine.

Lane 1: molecular weight markers (kDa)

Lane 2: α-chymotrypsin (15 μM), piperine (15 μM) and CoHA (1 mM), dark control

Lane 3: α-chymotrypsin (15 μM), piperine (15 μM) and CoHA (1 mM), 342 nm, 10 min

Lane 4: α-chymotrypsin (15 μM), piperine (15 μM) and CoHA (1 mM), 342 nm, 20 min

Lane 5: α-chymotrypsin (15 μM), dark control

Lane 6: α-chymotrypsin (15 μM), 342 nm, 20 min

Lane 7: α-chymotrypsin (15 μM) and CoHA (1 mM), dark control

Lane 8: α-chymotrypsin (15 μM) and CoHA (1 mM), 342 nm, 20 min

Lane 9: α-chymotrypsin (15 μM) and piperine (15 μM), dark control

Lane 10: α-chymotrypsin (15 μM) and piperine (15 μM), 342 nm, 20 min

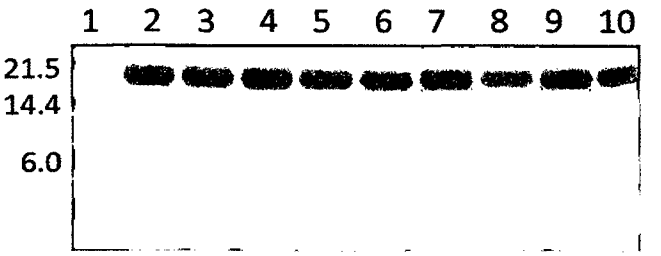


Figure 162 Photocleavage of β-lactoglobulin B obtained from the reaction with piperine.

Lane 1: molecular weight markers (kDa)

Lane 2: β-lactoglobulin B (15 μM), piperine (15 μM) and CoHA (1 mM), dark control

Lane 3: β-lactoglobulin B (15 μM), piperine (15 μM) and CoHA (1 mM), 342 nm, 10 min

Lane 4: β-lactoglobulin B (15 μM), piperine (15 μM) and CoHA (1 mM), 342 nm, 20 min

Lane 5: β-lactoglobulin B (15 μM), dark control

Lane 6: β-lactoglobulin B (15 μM), 342 nm, 20 min

Lane 7: β-lactoglobulin B (15 μM) and CoHA (1 mM), dark control

Lane 8: β-lactoglobulin B (15 μM) and CoHA (1 mM), 342 nm, 20 min

Lane 9: β-lactoglobulin B (15 μM) and piperine (15 μM), dark control

Lane 10: β-lactoglobulin B (15 μM) and piperine (15 μM), 342 nm, 20 min

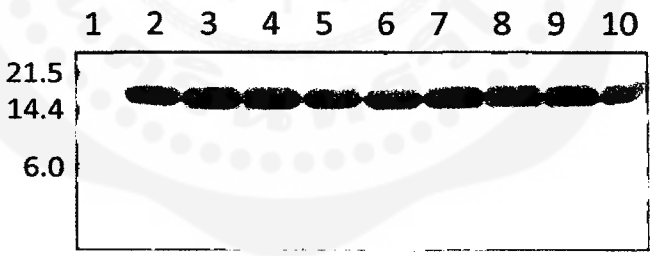


Figure 163 Photocleavage of myoglobin obtained from the reaction with piperine.

Lane 1: molecular weight markers (kDa)

Lane 2: myoglobin (15 μM), piperine (15 μM) and CoHA (1 mM), dark control

Lane 3: myoglobin (15 μM), piperine (15 μM) and CoHA (1 mM), 342 nm, 10 min

Lane 4: myoglobin (15 μM), piperine (15 μM) and CoHA (1 mM), 342 nm, 20 min

Lane 5: myoglobin (15 μM), dark control

Lane 6: myoglobin (15 μM), 342 nm, 20 min

Lane 7: myoglobin (15 μM) and CoHA (1 mM), dark control

Lane 8: myoglobin (15 μM) and CoHA (1 mM), 342 nm, 20 min

Lane 9: myoglobin (15 μM) and piperine (15 μM), dark control

Lane 10: myoglobin (15 μM) and piperine (15 μM), 342 nm, 20 min

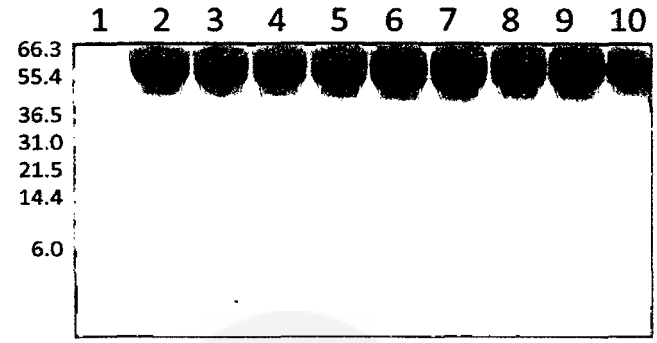


Figure 164 Photocleavage of HSA obtained from the reaction with piperine.

Lane 1: molecular weight markers (kDa)

Lane 2: HSA (15 μM), piperine (15 μM) and CoHA (1 mM), dark control

Lane 3: HSA (15 μM), piperine (15 μM) and CoHA (1 mM), 342 nm, 10 min

Lane 4: HSA (15 μM), piperine (15 μM) and CoHA (1 mM), 342 nm, 20 min

Lane 5: HSA (15 μM), dark control

Lane 6: HSA (15 μM), 342 nm, 20 min

Lane 7: HSA (15 μM) and CoHA (1 mM), dark control

Lane 8: HSA (15 μM) and CoHA (1 mM), 342 nm, 20 min

Lane 9: HSA (15 μM) and piperine (15 μM), dark control

Lane 10: HSA (15 μM) and piperine (15 μM), 342 nm, 20 min

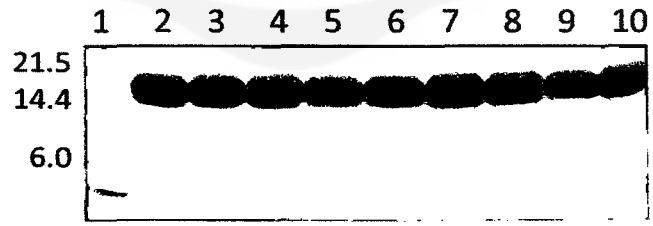


Figure 165 Photocleavage of BSA obtained from the reaction with piperine.

Lane 1: molecular weight markers (kDa)

Lane 2: BSA (15 μM), piperine (15 μM) and CoHA (1 mM), dark control

Lane 3: BSA (15 μM), piperine (15 μM) and CoHA (1 mM), 342 nm, 10 min

Lane 4: BSA (15 μM), piperine (15 μM) and CoHA (1 mM), 342 nm, 20 min

Lane 5: BSA (15 μM), dark control

Lane 6: BSA (15 μM), 342 nm, 20 min

Lane 7: BSA (15 μM) and CoHA (1 mM), dark control

Lane 8: BSA (15 μM) and CoHA (1 mM), 342 nm, 20 min

Lane 9: BSA (15 μM) and piperine (15 μM), dark control

Lane 10: BSA (15 μM) and piperine (15 μM), 342 nm, 20 min



Figure 166 Photocleavage of α-casein obtained from the reaction with piperine.

Lane 1: molecular weight markers (kDa)

Lane 2: α-casein (15 μM), piperine (15 μM) and CoHA (1 mM), dark control

Lane 3: α-casein (15 μM), piperine (15 μM) and CoHA (1 mM), 342 nm, 10 min

Lane 4: α-casein (15 μM), piperine (15 μM) and CoHA (1 mM), 342 nm, 20 min

Lane 5: α-casein (15 μM), dark control

Lane 6: α-casein (15 μM), 342 nm, 20 min

Lane 7: α-casein (15 μM) and CoHA (1 mM), dark control

Lane 8: α-casein (15 μM) and CoHA (1 mM), 342 nm, 20 min

Lane 9: α-casein (15 μM) and piperine (15 μM), dark control

Lane 10: α-casein (15 μM) and piperine (15 μM), 342 nm, 20 min

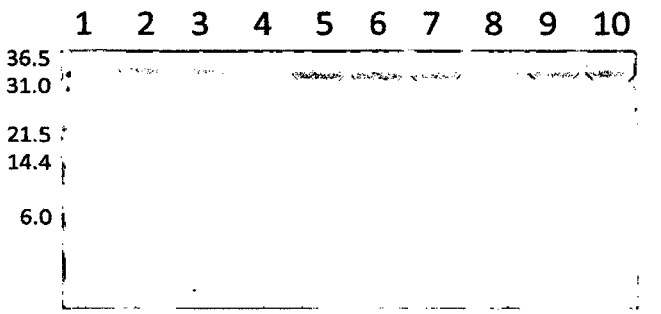


Figure 167 Photocleavage of pepsin obtained from the reaction with piperine.

Lane 1: molecular weight markers (kDa)

Lane 2: pepsin (15 μM), piperine (15 μM) and CoHA (1 mM), dark control

Lane 3: pepsin (15 μM), piperine (15 μM) and CoHA (1 mM), 342 nm, 10 min

Lane 4: pepsin (15 μM), piperine (15 μM) and CoHA (1 mM), 342 nm, 20 min

Lane 5: pepsin (15 μM), dark control

Lane 6: pepsin (15 μM), 342 nm, 20 min

Lane 7: pepsin (15 μM) and CoHA (1 mM), dark control

Lane 8: pepsin (15 μM) and CoHA (1 mM), 342 nm, 20 min

Lane 9: pepsin (15 μM) and piperine (15 μM), dark control

Lane 10: pepsin (15 μM) and piperine (15 μM), 342 nm, 20 min



Figure 168 Photocleavage of concanavalin A obtained from the reaction with piperine.

Lane 1: molecular weight markers (kDa)

Lane 2: concanavalin A (15 μM), piperine (15 μM) and CoHA (1 mM), dark control

Lane 3: concanavalin A (15 μM), piperine (15 μM) and CoHA (1 mM), 342 nm, 10 min

Lane 4: concanavalin A (15 μM), piperine (15 μM) and CoHA (1 mM), 342 nm, 20 min

Lane 5: concanavalin A (15 μM), dark control

Lane 6: concanavalin A (15 μM), 342 nm, 20 min

Lane 7: concanavalin A (15 μM) and CoHA (1 mM), dark control

Lane 8: concanavalin A (15 μM) and CoHA (1 mM), 342 nm, 20 min

Lane 9: concanavalin A (15 μM) and piperine (15 μM), dark control

Lane 10: concanavalin A (15 μM) and piperine (15 μM), 342 nm, 20 min

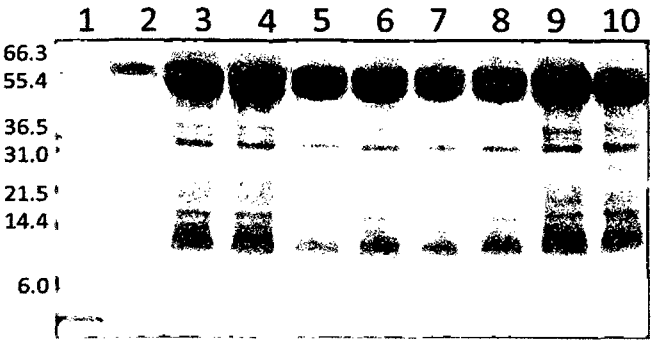


Figure 169 Photocleavage of β-glucosidase obtained from the reaction with piperine.
Lane 1: molecular weight markers (kDa)
Lane 2: β-glucosidase (15 μM), piperine (15 μM) and CoHA (1 mM), dark control
Lane 3: β-glucosidase (15 μM), piperine (15 μM) and CoHA (1 mM), 342 nm, 10 min
Lane 4: β-glucosidase (15 μM), piperine (15 μM) and CoHA (1 mM), 342 nm, 20 min
Lane 5: β-glucosidase (15 μM), dark control
Lane 6: β-glucosidase (15 μM), 342 nm, 20 min
Lane 7: β-glucosidase (15 μM) and CoHA (1 mM), dark control
Lane 8: β-glucosidase (15 μM) and CoHA (1 mM), 342 nm, 20 min
Lane 9: β-glucosidase (15 μM) and piperine (15 μM), dark control
Lane 10: β-glucosidase (15 μM) and piperine (15 μM), 342 nm, 20 min

REFERENCES

REFERENCES

Atkins, P.W. (2001). *The Elements of Physical Chemistry*. 3rd ed. England. Oxford University Press.

Berg, J.M.; Tyymoczko, J.L.; & Stryer, L. (2012). *Biochemistry*. 7th ed. New York. W.H. Freeman and Company.

BIO-RAD Instruction Manual. (2015). Retrieved December 18, 2015, from http://www.bio-rad.com/webroot/web/pdf/lsr/literature/M1703930.pdf

Branden, C.; & Tooze, J. (1999). *Introduction to Protein Structure*. 2nd ed. New York. Garland Publishing.

Burnette, W.N. (1981). Western Botting: Electrophoretic Transfer of Proteins from Sodium Dodecyl Sulfate-Polyacrylamide Gels to Unmmodified Nittrocellulose and Radiographic Detection with Antibody and Radioiodinated Protein A. *Anal. Biochem.* 195-203.

Circular Dichroism Spectrometer Operating Principles. (2012). Retrieved December 13, 2015, from http://www.analyticalchemistrygsu.com/2012/04/circular-dichroism-spectrometer.html

DeLange, R.J.; & Huang, T.S. (1971). Egg White Avidin, 3. Sequence of the 78-Residue Middle Cyanogen Bromide Peptide. Complete Amino Acid Sequence of the Protein Subunit, *J. Biol. Chem.* 246: 698–709.

Discontinous Gel. (2005). Retrieved December 11, 2015, from http://www.siumed.edu/~bbartholomew/course_material/protein_methods.htm

Do, M. T.; et al. (2013). Antitumor Efficacy of Piperine in the Treatment of Human HER2-Overexpressing Breast Cancer Cells. *Food. Chemistry.* 141: 2591–2599.

Drago, R.S. (1992). *Physical Methods for Chemists*. 2nd ed. San Diego. Saunders College Publishing.

Good, N.E.; et al. (1966). Hydrogen Ion Buffers for Biological Research. *Biochemistry*. 5: 467-477.

Grilo, L.S.; Carrupt, P.A.; & Hugues A. (2010). Stereoselective Inhibition of the hERG1 Potassium Channel. *Front. Pharmacol*. 1: 1-11.

Guo, X.J.; et al. (2011). The Investigation of the Interaction Between Ribavirin and Bovine Serum Albumin by Spectroscopic Methods. *Mol. Biol. Rep*. 38: 4185–4192.

Hames, B.D.; & Rickwood, D. (1990). *Gel Electrophoresis of Proteins: A Practical Approach*. 2nd ed. New York. Oxford University Press.

Hegg, E. L.; et al. (1999). Structure-Reactivity Studies in Copper(II)-Catalyzed Phosphodiester Hydrolysis. *Inorg. Chem.* 38: 2961-2968.

Holdgate, G.A.; & Ward, W.H. (2005). Measurements of Binding Thermodynamics in Drug Discovery. *DDT.* 10: 1543-1550.

Jemal, A.; Siegel, R.; Xu, J.; Ward, E. (2010). Cancer Statistics. *CA. Cancer. J. Clin.* 60: 277–300.

Kahne, D.; & Skill, W. C. (1988). Hydrolysis of Peptide Bond in Neutral Water. *J. Am. Chem. Soc.* 110: 7529-7534.

Kumar, C.V.; & Tolosa, L. M. (1993). Interaction of Hydrophobic Probes with Serum Albumin-Influence of the Side Chain and Exciplex Formation at the Binding Site. *J. Phys. Chem.* 97: 13914–13919

Kumar, C.V.; & Buranaprapuk, A. (1997). Site-Specific Photocleavage of Proteins. *Angew. Chem. Int. Ed. Engl.* 36: 2085–2087.

Kumar, C.V.; et al. (1998). Photochemical Protease: Site-Specific Photocleavage of Hen Egg Lysozyme and Bovine Serum Albumin. *Proc. Natl. Acad. Sci.* 95: 10361-10366.

Kumar, C.V.: & Buranaprapuk, A. (1999). Tuning the Selectivity of Protein Photocleavage: Spectroscopic and Photochemical Studies. *J. Am. Chem. Soc.* 121: 4262-4270.

Kumar, C.V.; et al. (2002). Chiral Protein Scissor: High Enantiomeric Selectivity for Binding and its Effect on Protein Photocleavage Efficiency and Specificity. *Proc. Natl. Acad. Sci.* 99: 5810-5815.

Leavitt, S.; & Freire, E. (2001). Direct Measurement of Protein Binding Energetics by Isothermal Titration Calorimetry. USA. Elsevier Science, Ltd.

Lee, S.Y.; et al. (2008). From Genome Sequence to Integrated Bioprocess for Succinic Acid Production by Mannheimia Succiniciproducens. *Appl. Microbiol. Biotechnol.* 79: 11-22.

Malaikaew, P.; et al. (2011). Photocleavage of Avidin by a New Pyrenyl Probe. *J. Photochem. Photobiol. B.* 103: 251-255.

Metia, M.D.; et al. (2015). Multi-Spectroscopic Investigation of the Binding Interaction of Fosfomycin with Bovine Serum Albumin. *J. Pharm. Anal.* 5: 249-255.

Mohind, C. M.; et al. (2017). Identification and Characterization of Berberine in Tinospora cordifolia by Liquid Chromatography Quadrupole Time of Flight Mass Spectrometry (LC MS/MS Q-tof) and Evaluation of its Anti-Inflammatory Potential. *Pharmacogn. J.* 9: 350-355.

Moran, L.A.; et al. (2012). *Principles of Biochemistry*, 5th Ed. Prentice Hall.

Nelson, D.L.; and Cox, M.M. (2013). *Lehninger Principles of Biochemistry*. 6th ed. New York. W.H. Freeman and Company.

Núñez, S.; Venhorst, J.; & Kruse, C.G. (2012). Target–Drug Interactions: First Principles and their Application to Drug Discovery. *DDT*. 17: 10-22.

Polarization. (August 1, 2007). Retrieved December 13, 2015, from http://www.arborsci.com/cool/polarization

Protein Purification. (August 9, 2008). Retrieved December 11, 2015, from http://biochem.co/2008/08/protein-purification/

Protein Structure. (2009). Retrieved December 10, 2015, from http://www.particlesciences.com/news/technical-briefs/2009/protein-structure.html

Radzicka, A.; & Wolfenden, R. (1996). Rates of Uncatalyzed Peptide Bond Hydrolysis in Neutral Solution and the Transition State Affinities of Proteases. *J. Am. Chem. Soc.* 118: 6105–6109.

Rana, T. M.; & Meares, C. F. (1991). Iron Chelate Mediated Proteolysis: Protein Structure Dependence. *J. Am. Chem. Soc.* 113: 1859-1861.

Rickwood, D.; & Hames, B.D. (1990). *Protein Structure a Practical Approach*. 1st ed. England. Oxford University Press.

Robert, J.D.; & Caserio, M.C. (1977). *Basic Principles of Organic Chemistry*. 2nd ed. California. W. A. Benjamin, Inc.

Rub, M.A.; et al. (2014). Study on the Interaction Between Amphiphilic Drug and Bovine Serum Albumin: A Thermodynamic and Spectroscopic Description. *J. Lumin.* 155: 39-46.

Samykutty, A.; et al. (2013). Piperine, a Bioactive Component of Pepper Spice Exerts Therapeutic Effects on Androgen Dependent and Androgen Independent Prostate Cancer Cells. *PLoS. ONE*. 8: e65889.

Schematic illustration of docking. (December 14, 2015). Retrieved December 14, 2015, from https://en.wikipedia.org/wiki/Docking_(molecular)

Shangger, H.; & Jagow, V.G. (1987). Tricine-Sodium Dodecyl Sulfate-Polyacrylamide Gel Electrophoresis for the Separation of Proteins in the Range From 1 to 100 kDa. *Anal. Biochem.* 166: pp. 368-379.

Sheehan, D.; (2000). *Physical Biochemistry: Principles and Applications.* 1st ed. West Sussex. John Wiley & Sons, Ltd.

Song, H.; & Lee, S.Y. (2006). Production of Succinic Acid by Bacterial Fermentation. *Enzyme. Microbial. Technol.* 39: 352-361.

Sriwilaijareon, N.; et al. (2002). Stage Specificity of Plasmodium Falciparum Telomerase and its Inhibition by Berberine. *Parasitol. Int.* 51: 99-103.

Structure of Sodium Dodecyl Sulfate and the SDS Molecules Coat the Protein with Negative Charges. (2015). Retrieved December 11, 2015, from www.nationaldiagnostics.com

The Chemical Structure of Acrylamide, *N,N'*-methylenebisacrylamide and *N,N,N',N'*-tetramethylethylenediamine. (2015). Retrieved December 10, 2015, from http://www.sigmaaldrich.com/

The Chemical Structure of 2-Mercaptoethanol and Dithiothreitol (DTT). (2015). Retrieved December 11, 2015, from http://www.sigmaaldrich.com/

The Nature of Light. (2015). Retrieved December 12, 2015, from http://www.public.asu.edu/~laserweb/woodbury/classes/chm467/bioanalytical/spectroscopy/absflr.html

The Photochemistry Portal. (October 30, 2009). Retrieved December 12, 2015, from https://photochemistry.wordpress.com/2009/10/30/quenching-mechanisms/

Tinoco, J.I.; et al. (2002). *Physical Chemistry: Principles and Applications in Biological Sciences.* 4th ed. New Jersey. Prentice Hall, Inc.

Vasavirama, K.; & Upender, M. (2014). Piperine: A Valuable Alkaloid Form Piper Species. *Int J Pharm Pharm Sci.* 6: 34-38.

Whittaker, A.G.; Mount, A.R.; & Heal, M.R. (2000). *Instant Notes: Physical Chemistry.* New York. Springer-Verlag New York, Inc.

Willard, H.H.; Merritt JR., L.L.; & Dean, J.A. (1965). *Instrumental Methods of Analysis.* 4th ed. New York. USA. D. Van Nostrand Company, Inc.

Young, V.R. (1994). Adult Amino Acid Requirements: The Case for a Major Revision in Current Recommendations. *J. Nutr.* 124: 1517S-1523S.

Zeikus, J.G.; Jain, M.K.; & Elankovan, P. (1999). Biotechnology of Succinic Acid Production and Markets for Derived Industrial Products. *Appl Microbiol Biotechnol.* 51: 545-552.

Zheng, M.; et al. (2013). Computational Methods for Drug Design and Discovery: Focus on China. *Trends Pharmacol Sci.* 34: 549-559.

CURRICULUM VITAE

VITAE

Name: Sudarat Yenjai

Date of Birth: 24 February 1987

Place of Birth: Chonburi province, Thailand

Mail box: sudarat.yenjai@gmail.com

Institutional Affiliation: Department of Chemistry, Faculty of Science, Srinakharinwirot University, Suhhumvit 23, Bangkok, 10110.

Award: Diatinguish Research Award from Graduate School, Srinakharinwirot University, 2013.

Education Background:

2005 – 2008	Bachelor of Science (Major: Chemistry) from Srinakharinwirot University, Bangkok, Thailand.
2009 – 2011	Master of Science (Major: Physical Chemistry) from Srinakharinwirot University, Bangkok, Thailand.
2012 – 2018	Doctor of Philosophy (Major: Applied Chemistry) from Srinakharinwirot University, Bangkok, Thailand.